

Structure and Biochemistry of otoferlin C₂-domains

Dissertation

for the award of the degree

“Doctor rerum naturalium”

Division of Mathematics and Natural Sciences

of the Georg-August-Universität Göttingen

submitted by

Sarah Helfmann

from Munich

Göttingen, 2011

Members of the thesis committee:

Reviewer: Prof. Dr. Tobias Moser
InnerEarLab, Department of Otolaryngology, UMG

Reviewer: Prof. Dr. Ralf Ficner
Department of Molecular Structural Biology, Institute for Microbiology
and Genetics

Prof. Dr. Nils Brose
Department of Molecular Neurobiology, Max-Planck-Institute for
Experimental Medicine

Date of the oral examination: 04.07.2011

Declaration

This thesis has been written independently and with no other sources and aids than quoted.

Sarah Helfmann

Göttingen, 23.05.2011

Publications resulting from this work

- **Helfmann, S.**, Neumann, P., Tittmann, K., Moser, T., Ficner, R., Reisinger, E. (2011) The crystal structure of the C₂A domain of otoferlin reveals an unconventional top loop region. *J Mol Biol.* **406**(3), 479-490.

Table of contents

1. Introduction.....	1
1.1 Anatomy and function of the ear.....	1
1.2 Deafness.....	4
1.3 Otoferlin.....	5
1.4 C ₂ -domains of otoferlin.....	8
1.4.1 C ₂ A.....	9
1.4.2 C ₂ B-C ₂ F.....	9
1.5 Research goals.....	12
1.6 Theory of the experiments.....	13
1.6.1 Crystallography.....	13
1.6.2 Isothermal Titration Calorimetry.....	16
1.6.3 CD-spectroscopy.....	17
1.6.4 Flootation assay.....	18
2. Material.....	20
2.1 Equipment.....	20
2.2 Water and Chemicals.....	21
2.2.1 Water.....	21
2.2.2 Chemicals.....	21
2.3 Consumable material.....	24
2.4 Enzymes.....	24
2.5 Antibodies.....	25
2.6 Kits.....	25
2.7 Vectors.....	25
2.8 Organisms.....	26
2.9 Oligonucleotides.....	26
3. Methods.....	29
3.1 Molecular biology.....	29
3.1.1 Polymerase chain reaction (PCR).....	29
3.1.2 Restriction enzyme digestion.....	31

• Table of contents •

3.1.3 Ligation	31
3.1.4 Transformation and sequencing	31
3.2 Protein overexpression	32
3.3 Protein purification.....	33
3.3.1 Affinity chromatography	34
3.3.2 Ion exchange chromatography	34
3.3.3 Size exclusion chromatography	35
3.4 Protein detection by SDS-PAGE.....	35
3.5 Protein detection by Western Blotting	36
3.6 Crystallization and X-ray data collection.....	37
3.7 Structure solution and refinement	38
3.8 Circular Dichroism Spectroscopy	38
3.9 Isothermal Titration Calorimetry	39
3.10 Liposome Flootation Assay	40
3.11 Purification trials for otoferlin C ₂ -domains besides C ₂ A	41
3.11.1 Solubility problems: purification from inclusion bodies.....	41
3.11.2 Aggregation problems: new constructs and buffers	42
4. Results	43
4.1 Structure and biochemistry of the C ₂ A-domain of rat otoferlin.....	43
4.1.1 Purification	43
4.1.2 Structure	44
4.1.3 Ca ²⁺ binding behavior	50
4.1.4 Binding of small signal molecules	55
4.1.5 Phospholipid binding.....	56
4.1.6 Mutant Otof-C ₂ A.....	59
4.2 Purification of otoferlin's single C ₂ -domains besides Otof-C ₂ A	61
4.2.1 Molecular cloning and preparation	61
4.2.2 Expression and solubility	62
4.2.3 Affinity purification and size exclusion	64
4.2.4 Attempt to solve purification problems: cloning of new constructs	66
4.3 Expression and purification of Otof-tandem/triple-C ₂ -domains	69
4.4 Expression and purification of full length otoferlin without transmembrane domain.....	71

5. Discussion	73
5.1 Otof-C ₂ A	73
5.1.1 Structure of Otof-C ₂ A and Ca ²⁺ -binding behavior.....	73
5.1.2 Phospholipid-binding	74
5.1.3 Biochemistry of Otof-5D-C ₂ A mutant.....	75
5.1.4 Comparison to other proteins: function of Otof-C ₂ A?.....	75
5.2 Purification of otoferlin's single C ₂ -domains besides Otof-C ₂ A.....	76
5.3 Expression and purification of Otof-tandem/triple-C ₂ -domains and full length otoferlin without transmembrane domain	78
6. Summary	79
7. References.....	80

Table of figures and tables

Figure 1: Schematic illustration of the human ear.	1
Figure 2: Illustration of cochlear canals.....	2
Figure 3: The organ of Corti.	2
Figure 4: Uncoiled cochlea	3
Figure 5: Scheme of mouse inner hair cell with ribbon synapse.	4
Figure 6: Pathogenesis of deafness.	5
Figure 7: Protein structure and sites of missense mutations in otoferlin.	6
Figure 8: Otoferlin is located at synaptic vesicles near the ribbon synapse.....	6
Figure 9: Otoferlin knock-out mice are deaf.....	7
Figure 10: Structure of a typical C ₂ domain.....	8
Figure 11: CD-spectroscopy of WT- and Pachanga-Otof-C ₂ F.	11
Figure 12: X-ray beam impinging on two-dimensional periodic lattice	14
Figure 13: ITC curve of GlnK2 of <i>Archaeoglobus fulgidus</i> titrated with adenosine-5'- triphosphate (ATP).....	16
Figure 14: CD-spectra of several types of secondary structures.....	17
Figure 15: Schematic illustration of floatation assay-experiment.....	18
Figure 16: Documentation of purification of His ₆ -Otof-C ₂ A.....	43
Figure 17: Structure of otoferlin C ₂ A solved from a single protein crystal.	44

• **Table of contents** •

Figure 18: Polar contacts in the crystal packing.....	47
Figure 19: The crystal packing of space group $I4_1$	48
Figure 20: Topologies of C_2 -domains.	48
Figure 21: Surface charge illustration of Otof- C_2A and other C_2 -domains.....	50
Figure 22: Detail view on the Ca^{2+} -binding region of Otof- and Syt- C_2A	51
Figure 23: Structure-based sequence alignments of Otof- C_2A with other C_2 -domains.	52
Figure 24: Alignments of the structure of Otof- C_2A with the structures of other C_2 -domains.	52
Figure 25: Isothermal titration calorimetry (ITC) with Otof- C_2A and Ca^{2+}	53
Figure 26: CD-spectroscopy of His ₆ -Otof- C_2A in presence and absence of Ca^{2+}	54
Figure 27: Binding of small signal molecules in ITC experiments.....	55
Figure 28: Floatation assays of Otof- C_2A with Syt1- C_2AB as positive control with three different lipid mixtures.	57
Figure 29: Floatation assays of Otof- C_2A and Syt1- C_2AB with brain total lipid extract.....	59
Figure 30: Biochemical data for Otof-5D- C_2A	60
Figure 31: Floatation assay of Otof-5D- C_2A with three different lipid mixes.	61
Figure 32: Calibration of Superdex 75 10/300 gel filtration column.	62
Figure 33: Expression and solubility tests with the Otof- C_2 -domains.	63
Figure 34: Solubility and purification of Otof- C_2D	64
Figure 35: Purification of Otof-GST- C_2C and Otof- C_2C -His ₆	65
Figure 36: Three examples of purifications of Otof- C_2F	66
Figure 37: Expression and purification of tandem- and triple- C_2 -domains.....	70
Figure 38: Western Blot of expression test of GST-Otof- ΔTM	71
Table 1: Buffers used in purifications.	33
Table 2: Recipe for 12%-acrylamide-SDS-gels.	36
Table 3. Composition of lipids used in floatation assays.....	41
Table 4: Statistics for Otoferlin C_2A crystal structure.....	45
Table 5: Proteins with highest similarity to the structure of Otof- C_2A according to Z -scores.	49
Table 6: Variety of short constructs of Otof- C_2F	67
Table 7: Available constructs of single, tandem- and triple C_2 -domains of otoferlin.	68
Table 8: Summary of the progression of the work with the single Otof- C_2 -domains.	77

List of abbreviations

2YT	2 x YT medium (Yeast-Tryptone)
ADP	Adenosine diphosphate
AMP	Adenosine monophosphate
AP	Alkaline phosphatase
APS	Ammonium persulfate
BCIP	5-Bromo-4-chloro-3-indolyl phosphate
Ca _v 1.3	Voltage-dependent Ca ²⁺ -channel 1.3
cAMP	Cyclic adenosine monophosphate
CD	Circular dichroism
Da	Dalton
ddH ₂ O	Double distilled water
DFN	X-chromosomal linked deafness
DFNA	Deafness type A (dominant)
DFNB	Deafness type B (recessive)
DMSO	Dimethyl sulfoxide
Dysf	Dysferlin
EB	Elution buffer
ECL	Enhanced chemiluminescence
EDTA	Ethylenediaminetetraacetic acid
EGTA	Ethylene glycol tetraacetic acid
E _x /P _x	Embryonal day _x /Postnatal day _x
GSH	γ-L-Glutamyl-L-cysteinylglycin (Glutathione)
GST	Glutathione-S-Transferase
His ₆ -tag	Tag containing six histidines in sequence
HRP	Horseradish peroxidase
IPTG	Isopropyl β-D-1-thiogalactopyranoside
ITC	Isothermal Titration Calorimetry
KO	Knock-out
LB	Lysogeny broth
LiAc	Lithium acetate

• Table of contents •

Myof	Myoferlin
NBT	Nitro blue tetrazolium
NDSB	Non detergent sulfobetaine
PC	Phosphatidylcholine
PCR	Polymerase chain reaction
PE	Phosphatidylethanolamine
PEG	Polyethyleneglycol
PI	Phosphatidylinositol
PIP ₂	Phosphatidylinositol 4,5-bisphosphate
PKC	Protein Kinase C
PLA/C	Phospholipase A/C
PBS	Phosphate buffered saline
PBS-T	Phosphate buffered saline + Tween
PS	Phosphatidylserine
Rpm	Revolutions per minute
Rcf	Relative centrifugal force
RT	Room temperature
RT-PCR	Reverse transcription PCR
SDS-PAGE	Sodium dodecyl sulfate polyacrylamide gel electrophoresis
SPR	Surface plasmon resonance
Stx	Syntaxin
Syt1	Synaptotagmin 1
TB	Terrific broth
TE buffer	Tris-EDTA buffer
TEMED	Tetramethylethylenediamine
TM-domain	Transmembrane domain
WT	Wildtype
YPDA	Yeast peptone dextrose adenine

1. Introduction

1.1 Anatomy and function of the ear

Sound information like language or music enters the human ear through the ear canal as acoustic waves. In the middle ear, sound is transferred as pressure differences over mechanical vibration of the tympanic membrane and the auditory ossicles.

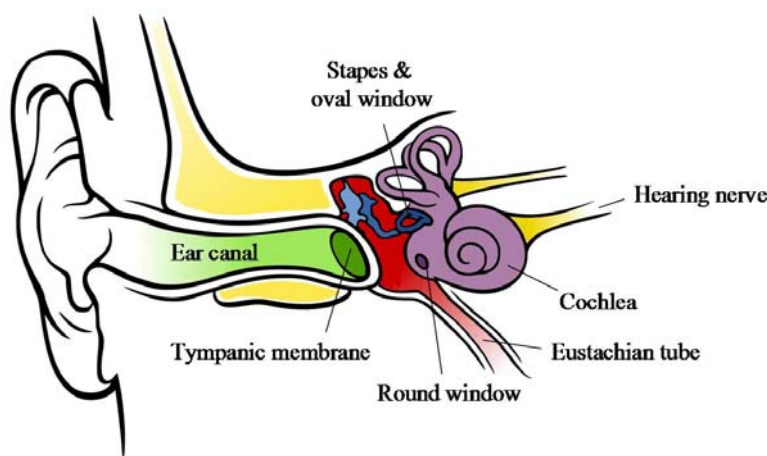


Figure 1: Schematic illustration of the human ear. Chittka L., Brockmann (modified; http://commons.wikimedia.org/wiki/File:Anatomy_of_the_Human_Ear_blank.svg).

The third ossicle, the stapes, contacts the oval window (membrane) of the cochlea and transmits the vibration to the cochlear fluid, which is contained in three scalae: *Scala vestibule*, *scala media* and *scala tympani* (Fig. 2&4). This elicits a traveling wave on the basilar membrane (Fig. 2).

The *Scala media* between *scala vestibuli* and *scala tympani* is separated from the former by the Reissner's and from the latter by the basilar membrane and is filled with endolymph (Fig. 2). The traveling wave moving through *scalae vestibuli* and *tympani* leads to an oscillation of the basilar membrane and the tectorial membrane. Depending on the frequency of the tone entering, the pressure is transferred to the basilar membrane at a specific position in the cochlea. On the basilar membrane sits the sensory epithelium, which holds both outer and inner hair cells (Fig. 3). In

• Introduction •

mammals, only the outer hair cells are in contact with the tectorial membrane via their stereocilia.

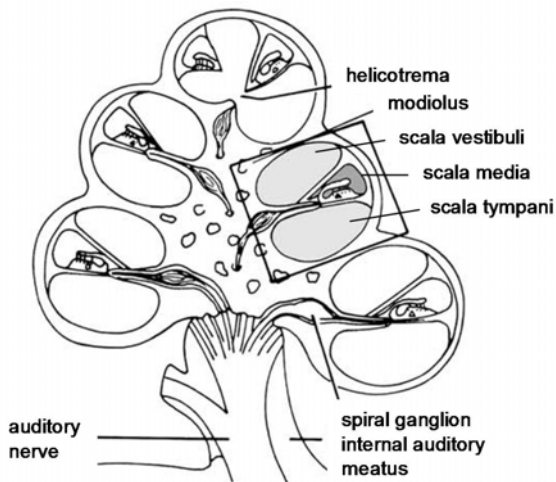


Figure 2: Illustration of cochlear canals. Brugge and Howard, 2002 (modified).

The outer hair cell gets depolarized by the movement and reacts with length alteration caused by piezoelectric properties of the membrane protein called prestin (electromotility). This protein is highly abundant in the lateral membrane of the outer hair cell and undergoes a voltage dependent conformational change. The oscillation of basilar and tectorial membrane is amplified or damped by the movement of the outer hair cells differently: every frequency is amplified at one specific point of the basilar membrane (Fig. 4, base -> apex, high -> low frequencies). Therefore, outer hair cell electromotility enables high sensitivity and frequency specificity of hearing.

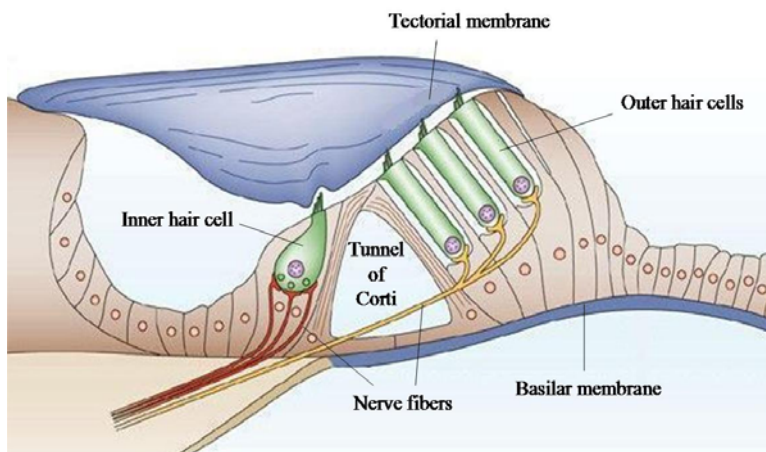


Figure 3: The organ of Corti. Fettiplace and Hackney, 2006 (modified).

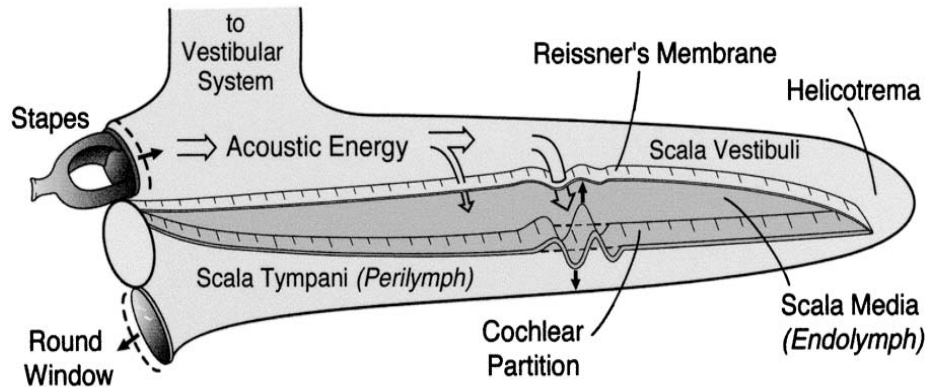


Figure 4: Uncoiled cochlea. Brugge and Howard, 2002.

As the tectorial membrane and the basilar membrane move relative to each other, cation-selective mechanosensitive channels at the stereocilia of the inner hair cells, connected by tip-links. The influx of K^+ , and to a lesser extent Ca^{2+} , depolarizes the cell. Upon depolarization, voltage dependent Ca^{2+} -channels ($Ca_v1.3$) open and the Ca^{2+} -influx leads to Ca^{2+} -dependent exocytosis of glutamate-filled vesicles at the ribbon synapse (Fig. 5). The spiral ganglion neurons, receiving excitatory input via this synapse, produce action potentials and forward the signal to the brain stem, from where it is relayed to the thalamus and auditory cortex, where hearing, as it is perceived, occurs.

The so called ribbon, closely localized to the plasma membrane at the inner hair cell synapse, is an electron dense organelle which has so far been observed in retinal, vestibular and cochlear sensory cells. Wherever found, this special type of synapse upon depolarization leads to graded vesicle release with glutamate as transmitter (for a review see Sterling and Matthews, 2005). It mainly consists of the protein ribeye which can interact with itself in multiple ways (Magupalli *et al.*, 2008). The hair cell ribbon, which tethers hundreds of vesicles through tethers of so far unknown molecular identity, is believed to be responsible for the high speed and temporal resolution of synaptic transmission at these special synapses. The protein bassoon is believed to be part of the anchor that holds the ribbon in place (Khimich *et al.*, 2005; for review see Nouvian *et al.*, 2006). However the machinery of vesicle release at the inner hair cell ribbon synapse is not yet full understood.

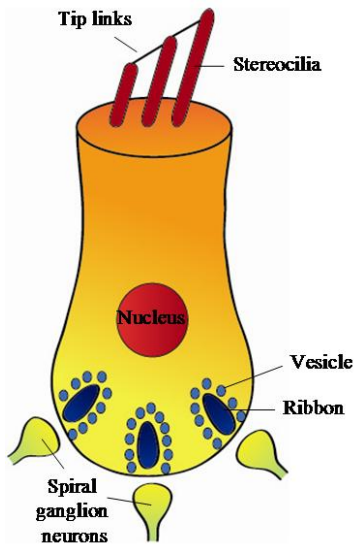


Figure 5: Scheme of mouse inner hair cell with ribbon synapse.

1.2 Deafness

Among 1000 children, one to two suffer from a prelingual deafness (Morton, 1991). Prelingual means that deafness occurs already before children learn to speak. Early deafness is typically acquired through environmental factors like perinatal hypoxia, hyperbilirubinemia or infections, but in ~50% of the cases, it has genetic reasons. Approximately 70% of these genetic cases are non-syndromic, meaning besides deafness no other symptoms occur. Currently, more than 100 loci have been found to be connected to this kind of disease and more than 40 deafness related genes were identified (for a review see Matsunaga, 2009). Four types of genetically inherited deafness are distinguished: type A (deafness type A = DFNA; ~10-15%) has autosomal dominant inheritance, while type B (deafness type B = DFNB) has autosomal recessive inheritance. Rarely, non-syndromic deafness is linked to the X-chromosome (DFN) or inherited with mitochondria (~1-2%). Most cases of non-syndromic deafness occur as DFNB (~75%; Fig. 6) (Robertson and Morton, 1999; Mukherjee *et al.*, 2003).

Most genetic forms of deafness are connected to defects in the genes of connexins (e.g. DFNB1), from which isoforms 26, 29, 30, 31 and 32 are present in the

mammalian cochlea (Forge et al., 2003; López-Bigas et al., 2002). They are gap junction membrane proteins involved in K⁺-recycling, with the most prominent one, connexin 26, being responsible for assumed 50% of nonsyndromic deafness cases with recessive inheritance in some populations (for review see Mukherjee *et al.*, 2003).

Genetic deafness often affects hair cell function, as is the case for the deafness DNB9, in which the protein otoferlin is defect (Yasunaga *et al.*, 1999).

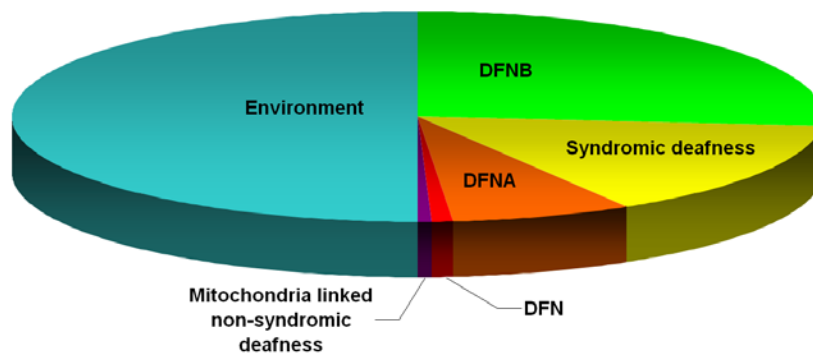


Figure 6: Pathogenesis of deafness. Values for diagram from Robertston and Morton, 1999 and Mukherjee *et al.*, 2003.

1.3 Otoferlin

Otoferlin was discovered in 1999. DFNB9 is a prelingual, non-syndromic deafness (Yasunaga *et al.*, 1999). Otoferlin is a 220 kDa membrane protein with six to seven conserved domains, namely C₂-domains, one coiled coil domain in the middle of the sequence and one transmembrane (TM)-domain in the C-terminus (Fig. 7). It belongs to the ferlin protein family, which was founded by fer-1, a worm protein, and holds five more members in mammals (Fer1L1 (dysferlin), Fer1L3 (myoferlin), Fer1L4, Fer1L5, Fer1L6). Also the other members of the ferlin family contain multiple C₂-domains, which is a particularity of this protein family, setting it apart from other proteins that only have one to three C₂-domains (examples for one C₂-domain: protein kinase C alpha (PKC α), phospholipase A & C (PLA/C); two C₂-domains: synaptotagmin 1 (Syt1); three C₂-domains: Munc13).

• Introduction •

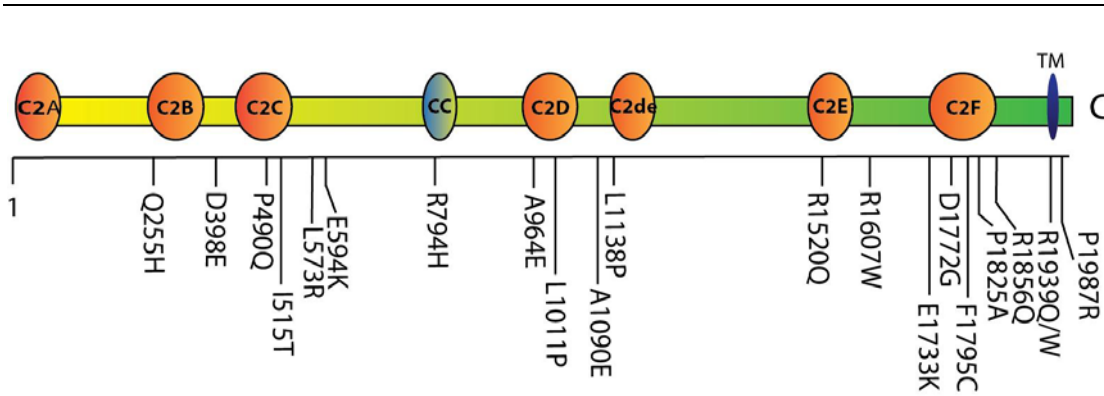


Figure 7: Protein structure and sites of missense mutations in otoferlin.

In 2010: 19 human pathogenic missense mutations were known, mutation D1772G (C₂F) has only been reported in mouse.

Otoferlin was detected in the vestibular system and the inner and outer hair cells of the cochlea with highest expression levels in inner hair cells (Roux *et al.*, 2006, Beurg *et al.*, 2008; Dulon *et al.*, 2009).

Currently, 20 missense mutations in the gene of otoferlin are known to cause deafness with and without temperature sensitivity (Fig 7; Varga *et al.*, 2006; Rodríguez-Ballesteros *et al.*, 2008; Choi *et al.*, 2009; Marlin *et al.*, 2010; Wang *et al.*, 2010). One of them, D1772G, is only known in mouse (Schwander *et al.*, 2007).

While otoferlin was found in mouse outer hair cells only between E18 and P6, it is constantly expressed in inner hair cells (Roux *et al.*, 2006). Using immunogold electron microscopy, otoferlin has been detected at the presynapse of the inner hair cell where it is localized close to the vesicles near the ribbon (Fig 8; Roux *et al.*, 2006).

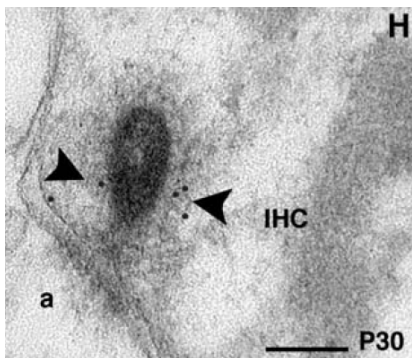


Figure 8: Otoferlin is located at synaptic vesicles near the ribbon synapse. Immunogold electron microscopy. Roux *et al.*, 2006.

• Introduction •

Otoferlin knock-out (KO) mice are profoundly deaf (flat auditory brainstem responses up to 120 db; Fig. 9A, grey traces) and hardly show any increase of membrane capacitance of the cell upon calcium influx, which means exocytosis is almost completely abolished (Fig. 9B, grey trace). Inner hair cell ribbon synapse formation is not affected in otoferlin KO-mice, but synapses undergo rapid degeneration (Roux *et al.*, 2006).

Yasunaga *et al.* (2000) discussed the existence of short and long isoforms of otoferlin. The short isoform contains the three most C-terminal C₂-domains, C₂D-C₂F, and the transmembrane domain. However, as missense mutations in the second and third N-terminal C₂-domains also lead to deafness, the short isoform by itself is not sufficient for hearing (Rodríguez-Ballesteros *et al.*, 2008), and may instead present a cloning artifact.

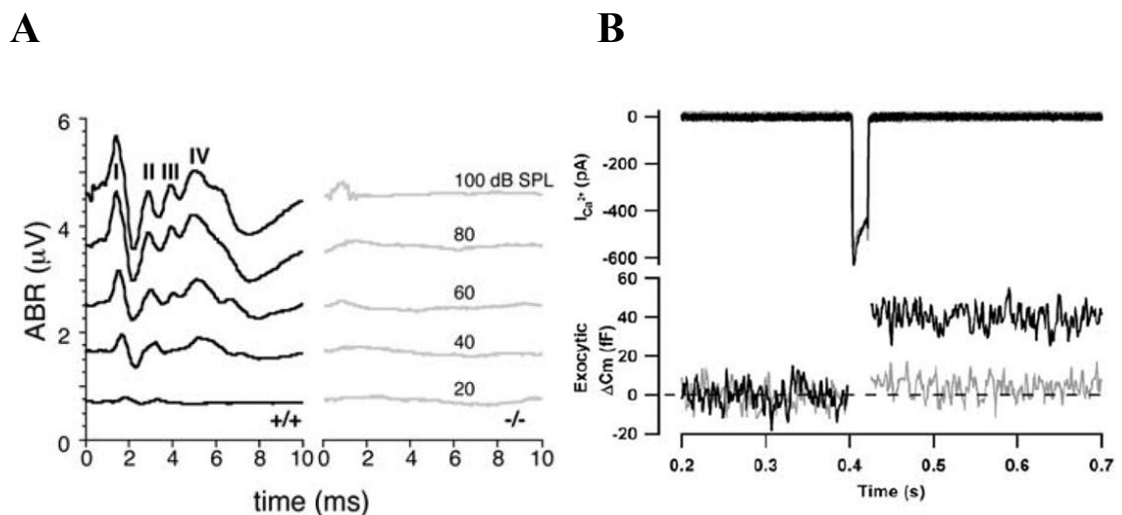


Figure 9: Otoferlin knock-out mice are deaf. Roux *et al.*, 2006.

A: Auditory brainstem response measurements with wildtype (WT) (black, left) and knock-out (KO) mice (grey, right).

B: Capacitance measurements upon Ca^{2+} influx with WT (black) and KO mice (grey). Roux *et al.*, 2006.

The exact role of otoferlin in exocytosis is still unclear. From the presence of C₂-domains in the protein, a Ca^{2+} -dependent membrane interaction was suggested for otoferlin (Yasunaga *et al.*, 1999). Recently, a role for otoferlin in vesicle replenishment was detected (Pangrsic *et al.*, 2010).

1.4 C₂-domains of otoferlin

The first exemplar of C₂-domains was identified in protein kinase C and was termed C₂ for being the second of the two conserved domains of this protein family.



Figure 10: Structure of a typical C₂ domain (Syt1 C₂A, PDB-ID: 1BYN; Shao *et al.*, 1998). Drawing in *Pymol* (DeLano, W.L.).

C₂-domains are best known for their Ca²⁺-dependent phospholipid-binding, though the related domains are quite heterogeneous: there are C₂-domains known that share the structural similarity of this type of domain, but do not bind Ca²⁺; also the phospholipid specificity varies a lot among C₂-domains (for review see Cho and Stahelin, 2006). C₂-domains consist of eight β-strands, four on each side of the protein opposing each other and building four anti-parallel β-sheets in total (Fig. 10). The connections between the β-strands form loops on two sides of the molecule. Typically, C₂-domains bind two to three Ca²⁺-ions with four or five aspartate residues located in the loops facing the same side of the molecule. Depending on the side of the molecule where Ca²⁺-binding occurs (loops 2, 4, 6 or loops 1, 3, 5, 7), the domain is called a type 1 or a type 2 C₂-domain.

Otoferlin contains six or seven C₂-domains, namely C₂A, C₂B, C₂C, C₂D, (C₂de,) C₂E and C₂F.

1.4.1 C₂A

In the most N-terminal C₂ domain of otoferlin, Otof-C₂A, two non-pathogenic mutations have been found in humans (A53V, R82C). Currently, no pathogenic mutations in Otof-C₂A are known.

Prior to this study, it was unclear whether C₂A is a full C₂-domain, as according to predictions (Yasunaga *et al.*, 2000), one β -strand was suggested to be missing. Also, the aspartates believed to be necessary for Ca²⁺-binding could not be found in C₂A with sequence alignments (Yasunaga *et al.*, 2000; Jimenez and Bashir, 2007), assuming that C₂A probably does not bind Ca²⁺-ions. However, for the C₂A-domains of dysferlin (Dysf) and myoferlin (Myof), Ca²⁺-dependent phospholipid-binding was shown (Davis *et al.*, 2002; Doherty *et al.*, 2006) despite the absence of at least two of the five aspartates (Dysf: DDDER; Myof: KDDEK; according to Jimenez and Bashir, 2007). So the question arose whether C₂A is able to bind Ca²⁺-ions in biochemical experiments, and if not, whether the presence of the five aspartates alone would enable this C₂-domain to bind Ca²⁺. Moreover, it was necessary to find out if Otof-C₂A is a phospholipid-binding domain, and if it binds phospholipids dependently or independently from Ca²⁺-ions.

During my thesis work, two studies were published, in neither of which Ca²⁺-binding activity could be detected for this C₂-domain (Ramakrishnan *et al.*, 2009; Johnson and Chapman, 2010). Instead, Ca²⁺-independent phospholipid-binding was reported for Otof-C₂A in floatation assays, while in the same study, turbidity measurements argued against phospholipid-binding (Johnson and Chapman, 2010).

1.4.2 C₂B-C₂F

According to sequence alignments with human otoferlin, in the three most C-terminal domains, C₂D, C₂E and C₂F, the five aspartates in the respective positions are present (Jimenez and Bashir, 2007). C₂C misses two aspartates, which are replaced by asparagine and valine (Jimenez and Bashir, 2007). As an aspartate is the neighbour of the last mentioned valine, possibly the sequence alignment might be

shifted by one amino acid in this region, so that C₂C may even contain four of the five aspartates.

1.4.2.1 Ca²⁺-binding

C₂D was the first C₂-domain for which Ca²⁺ binding has been shown in biochemical assays (Roux *et al.*, 2006). By now, a difference in fluorescence emission spectra in presence of Ca²⁺ has been detected for all C₂-domains except Otof-C₂A (Johnson and Chapman, 2010).

The question if Otof-C₂F, the most C-terminal C₂-domain of otoferlin, binds Ca²⁺-ions has recently been subject of intense studies and discussions. Independently of *in vitro* experiments, the Ca²⁺-binding probability of C₂F was estimated via sequence alignments (Jimenez and Bashir, 2007), from which binding was predicted. Surprisingly, contradicting results have been published about the Ca²⁺-binding behavior of this C₂-domain after biochemical experiments: Ca²⁺-binding was not indicated by autofluorescence and circular dichroism (CD) spectroscopy experiments in presence of Ca²⁺ (Pangrsic *et al.*, 2010), while in another study fluorescence emission spectra of C₂F have shown Ca²⁺-binding (Johnson and Chapman, 2010). Moreover, Ca²⁺-dependent protein-protein-interaction with syntaxin 1A (Stx1A) and SNAP25 has been detected for Otof-C₂F (Ramakrishnan *et al.*, 2009; Johnson and Chapman, 2010). Concluding, it remains unclear up to now if Otof-C₂F does or does not bind Ca²⁺.

In mouse, a mutation in C₂F was found to cause deafness though residual exocytosis could be detected upon Ca²⁺ influx (Pangrsic *et al.*, 2010). In this mutation, called *Pachanga* (D1767G in NP 001093865), one aspartatic acid residue is exchanged by glycine in the C₂F-domain of otoferlin (Schwander *et al.*, 2007). According to folding predictions with *Phyre* (Kelley and Sternberg, 2009), the mutation is located on the opposite side of the putative Ca²⁺ binding loops in the molecule, suggesting to rather not effect a putative Ca²⁺-binding of this domain. The phenomenon of deafness despite exocytosis can be explained by fatigue of vesicle release. The authors proposed a role for otoferlin in vesicle replenishment which is impaired by the *Pachanga* mutation (Pangrsic *et al.*, 2010). Moreover, WT-C₂F and *Pachanga*-C₂F were compared via CD-spectroscopy (Fig. 11) and tryptophane autofluorescence

(Pangrsic *et al.*, 2010). Like WT-C₂F, Pachanga-C₂F did not show a change in its CD- or fluorescence-spectrum in presence of Ca²⁺, indicating no Ca²⁺-binding.

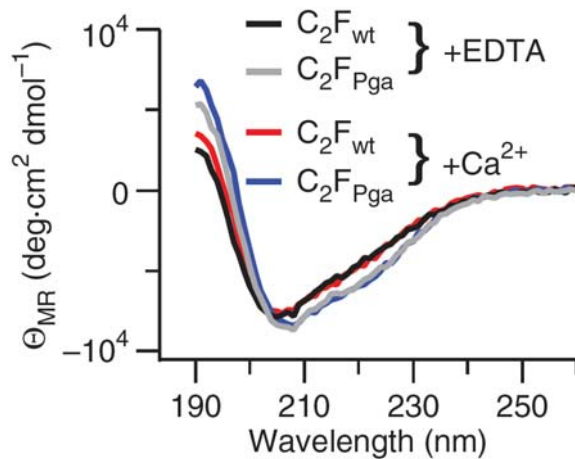


Figure 11: CD-spectroscopy of WT- and Pachanga-Otof-C₂F. Image from Pangrsic *et al.*, 2010.

1.4.2.2 Phospholipid-binding

Phospholipid-binding has been tested for the six C₂-domains with help of two methods with partly inconsistent results: in floatation assays, the binding to phospholipids was independent of Ca²⁺ for C₂A, C₂B and C₂C. However, for C₂B and C₂C, binding occurred only in presence of Ca²⁺ in turbidity measurements. For C₂D, C₂E and C₂F, the results were consistent in both methods: binding occurred only in presence of Ca²⁺ (Johnson and Chapman, 2010).

Phospholipid-binding was tested for WT- and mutant C₂F via flotation assays in another study, too: here, for both proteins, no or only weak binding occurred (Pangrsic *et al.*, 2010).

Together, as results were not consistent for all C₂-domains, the Ca²⁺-dependency of phospholipid-binding is unclear especially for C₂B and C₂C and should be further tested for all Otof-C₂-domains.

1.5 Research goals

One goal in otoferlin research is to identify the effects of mutations on the protein function, especially when Ca^{2+} -binding sites are mutated. Otoferlin's C_2 -domains only show poor sequence similarity with C_2 -domains of other proteins (31% amino acid sequence identity and 51% sequence homology between $\text{PKC}\alpha\text{-C}_2$ and Otof- C_2D as one of the highest similarities), so that for example the exact position of β -strands and the location of Ca^{2+} -binding aspartates can not easily be identified in these C_2 -domains. Structural comparisons with the program *Phyre* (Kelley and Sternberg, 2009), which builds a structure from a model with high sequence similarity, are biased by the model protein and the length of the input sequence. In conclusion, modelling attempts or sequence alignments with C_2 -domains from other proteins are not sufficient to predict the folding of Otof- C_2 -domains and the position of Ca^{2+} -coordinating aspartates.

This study planned to investigate the structure of all six C_2 -domains of otoferlin. With the structures, the surface charges of the C_2 -domains can be calculated to estimate the ability of Ca^{2+} -binding for this domain. Also, the Otof- C_2 -domain-structures can be compared to the structures of other C_2 -domains available on www.pdb.org to study similarities and differences among C_2 -domains.

With the structure, Ca^{2+} -binding sites, presumably aspartates or other acidic amino acids, can be identified by structure based sequence alignments with the structures of other C_2 -domains. Next, the respective amino acids can be mutated on DNA level by mutagenesis. The C_2 -domain-mutant shall then also be crystallized to find differences in folding and surface charge. Moreover, the mutants could be studied biochemically for differences in the Ca^{2+} -binding behavior.

Moreover, the location of known mutations (other than in the Ca^{2+} -binding area) that disturb protein function can be identified within the protein structure. Here, a mutant protein shall be produced to conduct crystallization and biochemical experiments, too. From the WT structure, it can possibly be predicted whether the mutant C_2 -domain will still be able to fold properly (and thus to crystallize) depending on if the mutation lies within a β -strand or a strand-connecting loop and if the concerned amino acid is exposed to the solvent. Thus, the pathogenicity of the mutations can most likely be explained in a better way, once the structure is available.

To address the questions whether there is (still) Ca^{2+} - and/or phospholipid-binding and whether the C_2 -domains fold properly, wildtype and mutant C_2 -domains with either known (Varga *et al.*, 2006; Rodríguez-Ballesteros *et al.*, 2008; Choi *et al.*, 2009; Marlin *et al.*, 2010; Wang *et al.*, 2010) or new mutations (structure-based mutations of Ca^+ -binding-sites) that are introduced into C_2 -domains on DNA level shall be studied biochemically.

1.6 Theory of the experiments

1.6.1 Crystallography

Protein crystallography is one of the available methods which can deliver the three dimensional model of a protein. The prerequisite to use this method is obtaining a protein crystal possessing diffraction properties. In order to obtain a crystal the protein must be expressed, purified, concentrated and incubated in different crystallization conditions which can facilitate crystal growing (so-called crystal screening).

Once a crystal has formed, it is exposed to X-ray radiation in order to collect information about the distribution of electrons within the crystal, hence positions of the atoms. When the X-ray beam collides with the crystal's electrons, they start to oscillate. Through scattering of the beam by the electrons, spherical waves develop which interfere positively or negatively and are thus enhanced or extinguished, depending on the location of the electrons in the crystal. The scattered X-rays originating from a constructive interference hit a detector (CCD or Image Plate) behind the setup, which records a unique for each crystal diffraction pattern which is saved, before the crystal is rotated by a small angle and the next picture is collected. Thus, the location of the crystal's electrons can be studied in 3D-manner.

According to Bragg's law (Bragg, 1913), the path difference of interfering waves has to be a whole-number multiplication of the wavelength used in the experiment, so that the interference from a set of parallel lattice (Bragg) planes is constructive and the resulting enhanced wave (reflection) can be recorded:

• Introduction •

$$n\lambda = 2d \sin \theta \text{ (Figure 8)}$$

In the formula, λ represents the wavelength of the X-ray beam, d stands for the distance between parallel lattice planes in the crystal, n is the order of the diffraction maximum and θ is $\frac{1}{2}$ the angle between the entering and the leaving beam (Fig. 12).

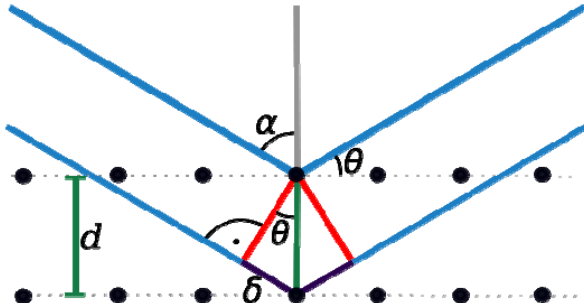


Figure 12: X-ray beam impinging on two-dimensional periodic lattice (<http://upload.wikimedia.org/wikipedia/commons/thumb/c/ca/Bragg.svg/548px-Bragg.svg.png>).

With help of the Miller indices (hkl) , the sets of parallel Bragg planes and originating from those reflections are labeled. The intensity $I(hkl)$ of the spots on the pattern is proportional to the square of the structure factor amplitude $|F(hkl)|$:

$$I(h, k, l) \approx |F(h, k, l)|^2$$

The measured intensities $I(hkl)$ of all diffraction spots are converted to structure factors $F(hkl)$, which are needed by most of the programs used for the structure refinement and calculating the electron density maps:

$$F(h, k, l) = \int V \cdot \rho(x, y, z) \exp[2\pi i(hx + ky + lz)] \cdot dV$$

Here, V is the volume of the unit cell, while $\rho(x,y,z)$ is the electron density, which can be computed from the structure factors $F(hkl)$ by Fourier transformation:

$$\rho(x, y, z) = \frac{1}{V} * \sum_{h,k,l} |F(h, k, l)| \exp[-2\pi i(hx + ky + lz) + i\alpha(h, k, l)]$$

The electron density is the Fourier transform of the amplitudes, this calculation requires the knowledge of the phase angles $\alpha(hkl)$ of each reflection, which can not be measured experimentally. This inability gives rise to the so called “phase problem” of crystallography which can be solved in several ways:

1. Molecular replacement (MR)
2. Single isomorphous replacement with anomalous scattering (SIRAS)
3. Multiple wavelength anomalous dispersion (MAD)
4. Single isomorphous replacement (SIR)
5. Multiple isomorphous replacement (MIR)
6. Multiple isomorphous replacement with anomalous scattering (MIRAS)

In this study, the phase problem was solved by Molecular Replacement (MR). The usage of MR requires a known protein structure sharing high structural similarity to the target protein. This similarity is often assessed based on sequence identity between the model and the target protein (in some cases sequence identity of about 30% allows a successful MR search).

This structure serves as a search model. The MR search is performed in two steps: first, the orientation of the model in a new crystal is determined by calculation a rotation function (overlap between two Patterson functions – one calculated based on the model and the other calculated from the measured intensities), then a translation search is performed to place the properly oriented model in the unit cell.

The success of the MR search can be assessed by calculating the R-Factor, which measures the agreement between the structural model and the experimental diffraction data:

$$R = \frac{\sum_{h,k,l} |F(obs) - k|F(calc)|}{\sum_{h,k,l} |F(obs)|}$$

• Introduction •

The lower the R-factor, the better the agreement between observed and calculated structure factors.

In this formula, k represents a scaling factor, $|F(\text{obs})|$ are the structure factor amplitudes that are experimentally obtained and $|F(\text{calc})|$ are the structure factor amplitudes which are calculated from the model.

1.6.2 Isothermal Titration Calorimetry

The basis of ITC is that in every biochemical reaction such as binding of other molecules by a protein, heat is released or consumed. By measuring the temperature in the sample cell, where the reaction occurs, and a reference cell, heat changes can be detected. The ligand is titrated to the sample protein in small steps. If a reaction occurs, the temperature will change in the sample cell. The water-filled reference cell is then heated or cooled to the same temperature, and the energy released or consumed is recorded. At a certain point, the reaction heat will get weaker and weaker, as the protein gets saturated with ligand molecules (Fig. 13).

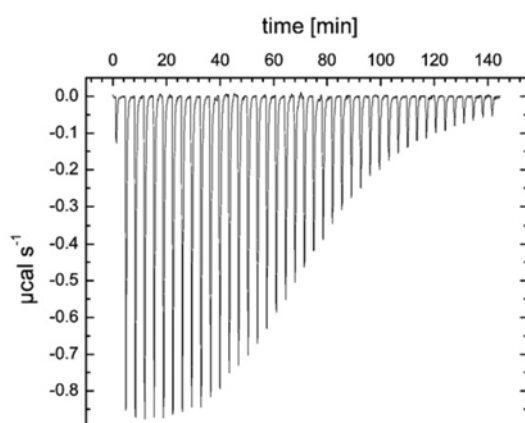


Figure 13: ITC curve of GlnK2 of *Archaeoglobus fulgidus* titrated with adenosine-5'-triphosphate (ATP). Helfmann *et al.*, 2010 (modified).

Feedback power regulation [$\mu\text{cal/s}$] in the reference cell responding to the exothermic reaction in the sample cell.

With heat change information, the slope of the saturation and the given concentrations of protein and binding partner, the enthalpy (ΔH), Gibb's free energy

(ΔG) and entropy (ΔS) of the reaction are calculated with the formula $\Delta G = \Delta H - \Delta S \cdot T$. If $\Delta G \sim 0$, ideally when measured at different temperatures, no binding has occurred.

1.6.3 CD-spectroscopy

In CD-spectroscopy, circularly polarized light is sent through a cuvette containing the diluted protein. Chiral molecules like proteins absorb left- and right-handed circularly polarized light in a different manner.

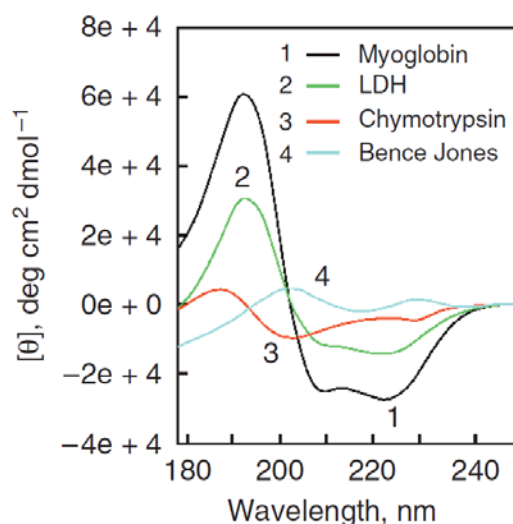


Figure 14: CD-spectra of several types of secondary structures. Greenfield, 2006.

- 1, black trace: CD-spectrum of myoglobin.
- 2, green trace: CD-spectrum of lactate dehydrogenase.
- 3, red trace: CD-spectrum of α -chymotrypsin.
- 4, cyan trace: CD-spectrum of Bence Jones protein REI light chain.

As a phase difference between the left- and right-handed light develops through the interaction with the optically active molecule in the cuvette, the plane of polarization changes. From this change between entering and leaving light, conclusions can be drawn about the protein's secondary structure: for example, for α -helices, characteristic minima appear at 220 nm and 208 nm, while a maximum appears at 193 nm. For β -strands, a minimum at 218 nm and a maximum at 195 nm appear

(examples in Fig. 14; Greenfield, 2006). Thus, from the CD-spectrum of a protein, the amount of α -helices and β -strands can be obtained.

For every protein, an individual ellipticity spectrum can be recorded at wavelengths 180 nm - 260 nm. In this study, CD-spectroscopy was also used to observe differences between WT and mutant proteins.

1.6.4 Flootation assay

With help of floatation assays, binding of protein to liposomes containing several lipids is studied. Liposomes are produced via gel filtration and mixed with the protein at the bottom of a Nycodenz-gradient. As liposomes have low density, they float to the top of the tube during the following long centrifugation.

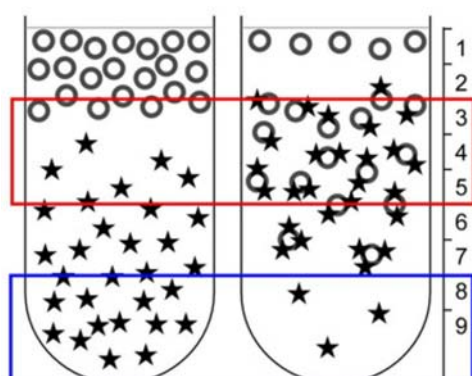


Figure 15: Schematic illustration of floatation assay-experiment. Helfmann *et al.*, 2011.

Stars: Protein. Circles: liposomes. Red box: Middle phase after centrifugation contains bound protein (circles with stars attached). Blue box: Lower phase contains unbound protein.

Proteins that bound to liposomes are found with these in the upper part (Fig. 15, right), while unbound proteins stay in the lower part of the tube (Fig. 15, left). After 90 minutes centrifugation at 197.000 g, the distribution of protein in the tube is investigated by sodium dodecyl sulfate polyacrylamide gel electrophoresis (SDS-PAGE, 2.4). Thus, the amount of liposome-bound protein can be estimated from the intensity of bands on the acrylamide-gel. In this study, the binding behavior of WT

• Introduction •

and mutant protein was tested with different lipids compositions in the liposomes in presence and absence of Ca^{2+} .

2. Material

2.1 Equipment

ÄKTAprime plus	GE Healthcare, Munich, Germany
Allegra X-15R Benchtop centrifuge	Beckman Coulter, Krefeld, Germany
Avanti J-30 I	Beckman Coulter, Krefeld, Germany
Brain total lipid extract	Avanti polar lipids, Alabaster, Alabama, USA
Branson Sonifier 250	Branson, Danbury, CT, USA
Chirascan Circular Dichroism Spectrometer	Applied Photophysics, Leatherhead, UK
Electrophoresis Power Supply EPS 301	GE Healthcare, Munich, Germany
Gene Pulser® Cuvettes	Bio-Rad, Munich, Germany
Heraeus FRESCO 17 centrifuge	Thermo Electron GmbH, Karlsruhe, Germany
HisTrap FF crude column (1 ml)	GE Healthcare, Munich, Germany
HiTrap Desalting column (5 ml)	GE Healthcare, Munich, Germany
JA-18 rotor	Beckman Coulter, Krefeld, Germany
Loop (0.5 ml)	GE Healthcare, Munich, Germany
MAR 345 image plate detector	MarResearch GmbH, Norderstedt, Germany
Sartorius arium® 611 VF	Sartorius, Goettingen, Germany
Mini-PROTEAN Tetra Cell	Bio-Rad, Munich, Germany
Micro Pulser™ Electroporator	Bio-Rad, Munich, Germany
MyCycler PCR machine	Bio-Rad, Munich, Germany
NanoDrop1000 spectrophotometer	Thermo Scientific, Bonn, Germany
Pipettes	Brand, Wertheim, Germany
pipetus®	Hirschmann Laborgeräte, Eberstadt, Germany
Resource Q column (1 ml)	GE Healthcare, Munich, Germany
Rotating-anode MicroMax-007	Rigaku, Tokyo, Japan

• **Material** •

Superdex 75 10/300 (24 ml)	GE Healthcare, Munich, Germany
Superdex 75 16/60 (150 ml)	GE Healthcare, Munich, Germany
Superdex 200 10/300 (24 ml)	GE Healthcare, Munich, Germany
Superloop (50 ml)	GE Healthcare, Munich, Germany
Thermomixer comfort	Eppendorf, Hamburg, Germany
UV-Detection System	Intas, Goettingen, Germany

2.2 Water and Chemicals

2.2.1 Water

For most applications, deionized water, produced by a Sartorius arium® 611 VF, was used (H₂O). Double distilled water (ddH₂O) was only used in PCR, restriction enzyme digestion and ligation.

2.2.2 Chemicals

Acrylamide, 30% solution	Carl Roth, Karlsruhe, Germany
peqGOLD Universal Agarose	PEQLAB Biotechnologie GMBH, Erlangen, Germany
Ampicillin, sodium salt	Carl Roth, Karlsruhe, Germany
Ammonium persulfate (APS)	Sigma-Aldrich, Munich, Germany
AmSO4 Suite screen	Qiagen, Hilden, Germany
Aureobasidin A	Clontech, Saint-Germain-en-Laye, France
Bacto Agar	Becton, Dickinson and Company, Heidelberg, Germany
Bacto Tryptone	Becton, Dickinson and Company, Heidelberg, Germany
Bacto Yeast extract	Becton, Dickinson and Company,

• Material •

	Heidelberg, Germany
Bradford solution	Bio-Rad, Munich, Germany
CaCl ₂	Sigma-Aldrich, Munich, Germany
Carbenicillin	Carl Roth, Karlsruhe, Germany
Casein	Sigma-Aldrich, Munich, Germany
Chelex100®	Sigma-Aldrich, Munich, Germany
Cholesterol (ovine wool, >98%)	Avanti polar lipids, Alabaster, Alabama, USA
Coomassie Brilliant Blue R250	Biomol, Hamburg, Germany
CryoLoops™	Hampton Research, Aliso Viejo, California, USA
Crystal Screen I	Hampton Research, Aliso Viejo, California, USA
Dithiothreitol (DTT)	Biomol GmbH, Hamburg, Germany
dNTPs	Fermentas, St. Leon-Rot, Germany
Ethanol absolute	Merck Biosciences, Schwalbach, Germany
Ethylenediaminetetraacetic acid (EDTA)	SERVA Electrophoresis, Heidelberg, Germany
Ethylene glycol tetraacetic acid (EGTA)	Fluka Biochemika, Buchs, Switzerland
Gel filtration Standard	Bio-Rad, Munich, Germany
Guanidine hydrochloride	Sigma-Aldrich, Munich, Germany
HEPES	Sigma-Aldrich, Munich, Germany
Hydrochloric acid	Merck Biosciences, Schwalbach, Germany
Imidazole	Carl Roth, Karlsruhe, Germany
Isopropyl-β-D-thiogalactopyranosid (IPTG)	Carl Roth, Karlsruhe, Germany
JBScreen Classic 1, 2, 4, 5, 6, 7, 8, 10	Jena Bioscience, Jena, Germany
JCSG Screen	Quiagen, Hilden, Germany
Kanamycine	Carl Roth, Karlsruhe, Germany
KH ₂ PO ₄	Merck Biosciences, Schwalbach,

• Material •

	Germany
L- α -phosphatidylcholine (Brain, Porcine)	Avanti polar lipids, Alabaster, Alabama, USA
L- α -phosphatidylethanolamine (Brain, Porcine)	Avanti polar lipids, Alabaster, Alabama, USA
L- α -phosphatidylinositol (Liver, Bovine) (sodium salt)	Avanti polar lipids, Alabaster, Alabama, USA
L- α -phosphatidylinositol-4,5-bisphosphate (Brain, Porcine) (ammonium salt)	Avanti polar lipids, Alabaster, Alabama, USA
Minstrel™ HT crystallization roboter	Rigaku, Berlin, Germany
Na ₂ HPO ₄	Merck Biosciences, Schwalbach, Germany
Sodium hydroxide	Merck Biosciences, Schwalbach, Germany
NBT/BCIP stock solution	Roche, Grenzach-Wyhlen, Germany
Non detergent sulfobetaine 201 (NDSB 201)	Merck Biosciences, Schwalbach, Germany
Nycodenz®	Nycomed Pharma AS, Oslo, Norway
Phosphatidylserine	Avanti polar lipids, Alabaster, Alabama, USA
ProPlex screen	Molecular Dimensions, Newmarket, UK
Sodium acetate	Sigma-Aldrich, Munich, Germany
Sodium chloride (NaCl)	Carl Roth, Karlsruhe, Germany
Sodium dodecyl sulfate (SDS)	Sigma-Aldrich, Munich, Germany
Tetramethylethyldiamin (TEMED)	Carl Roth, Karlsruhe, Germany
Texas Red DHPE	Invitrogen, Darmstadt, Germany
Tris(hydroxymethyl)-aminomethan (Tris)	Carl Roth, Karlsruhe, Germany
Triton X-100	Merck4Biosciences, Darmstadt, Germany
Tween 20	Carl Roth, Karlsruhe, Germany

• **Material** •

Pierce ECL Detection Reagent 1+2	Thermo Fisher Scientific, Bonn, Germany
----------------------------------	--

2.3 Consumable material

Crychem Plate	Hampton Research, Aliso Viejo, California, USA
Econo columns	Bio-Rad, Munich, Germany
Eppendorf cups 1,5 and 2 ml	Eppendorf AG, Hamburg, Germany
Glass beads (425-600 μm)	Sigma-Aldrich, Munich, Germany
Plastic pipettes	Sarstedt, Nümbrecht, Germany
Plastic tubes 10 ml	Greiner Bio-One GmbH, Frickenhausen, Germany
Prestained Protein Molecular Weight Marker SM0441	Fermentas, St. Leon-Rot, Germany
Prestained Protein Molecular Weight Marker SM1811	Fermentas, St. Leon-Rot, Germany
Immun-Blot™ PVDF membrane	Bio-Rad, Munich, Germany
Shark Tape	Henkel, Düsseldorf, Germany
Unstained Protein Molecular Weight Marker SM0431	Fermentas, St. Leon-Rot, Germany
Vivaspin 20 MW cutoff 10 kDa	GE Healthcare, Munich, Germany
Amersham Hyperfilm™ ECL High performance chemiluminescence film	GE Healthcare, Munich, Germany
CD-spectroscopy-cuvette	Hellma Analytics, Muellheim, Germany

2.4 Enzymes

DreamTaq DNA Polymerase + buffer	Fermentas, St. Leon-Rot, Germany
BamHI + buffer	Fermentas, St. Leon-Rot, Germany

• **Material** •

EcoRI + buffer	Fermentas, St. Leon-Rot, Germany
NdeI + buffer	Fermentas, St. Leon-Rot, Germany
PreScission Protease	GE Healthcare, Munich, Germany
Pfu DNA Polymerase + buffer	Fermentas, St. Leon-Rot, Germany
T4 DNA Ligase + buffer	Fermentas, St. Leon-Rot, Germany

2.5 Antibodies

Anti-GST antibody (host: goat)	GE Healthcare, Munich, Germany
Anti-His ₅ antibody (host: mouse)	Qiagen, Hilden, Germany
Anti-otoferlin (N-terminus) (host: mouse)	Abcam plc, Cambridge, UK
Mouse Kappa Light Chain Antibody, Alkaline Phosphatase-conjugated	Bethyl Laboratories, Montgomery, USA
Anti-goat antibody, AP-linked (host: donkey)	DIANOVA GmbH, Hamburg, Germany

2.6 Kits

DNA Clean & Concentrator TM -5 Kit	Zymo Research, Freiburg, Germany
Zymoclean TM Gel DNA Recovery Kit	Zymo Research, Freiburg, Germany
GeneJET TM Plasmid Minprep Kit	Fermentas, St. Leon-Rot, Germany
Gel filtration standard	Bio-Rad, Munich, Germany

2.7 Vectors

pET21a	Merck Biosciences, Schwalbach, Germany
--------	--

• Material •

pET28a	Merck Biosciences, Schwalbach, Germany
pGEX-6P-3	GE Healthcare, München, Germany

2.8 Organisms

Molecular cloning	XL1 Blue	Agilent Technologies, Böblingen, Germany
Protein expression	BL21(DE3)	Merck Biosciences, Schwalbach, Germany
	BL21(DE3)Star	Merck Biosciences, Schwalbach, Germany
	Rosetta2	Merck Biosciences, Schwalbach, Germany
	Rosetta2 Star	Merck Biosciences, Schwalbach, Germany Produced from BL21(DE3) by Molecular Structural Biology laboratory, Goettingen

2.9 Oligonucleotides

11442	5'-GAGACATATGGCCCTGATCGTCCACCT-3'
11443	5'-GAGAGAATTCTCATGTGCCATCTGCGGCTTGATAC-3'
14188	5'-CTATCGAGCTGGACCTGAACC-3'
14894	5'-GAGAGGATCCATGGCCCTGATTGTTACCTCAAG-3'
14895	5'-GAGAGAATTCTAGTCGTCCTCATCCGTCTCGTTG-3'
14896	5'-GAGAGAATTCTACTCCGAGACAGGCGTGGC-3'
14897	5'-GAGAGGATCCAAGCTGGAGCTCTACCTGTG-3'
14899	5'-GAGAGAATTCTAATCAGGTTTCATTGCGAGCCAG-3'
15220	5'-AGCTTCATCATCATCATCACGC-3'
15490	5'-GGCCGCGTGATGATGATGATGATGA-3'
15717	5'-AGCTTCCAGCATCACACCACCACCACCACCACCA CCCAGCATCAGC-3'

• Material •

C ₂ B-BamHI_for ¹	5'-ATATGGATCCATGGAGGACCTGGACCACC-3'
C ₂ B-EcoRI_rev ¹	5'-ATATGAATTCTAGTCATCCTCATCTGTCTCGTTG-3'
C ₂ C-BamHI_for ¹	5'-ATATGGATCCACAGATGAGGATGACATTGAAGG-3'
C ₂ C-EcoRI_rev ¹	5'-ATATGAATTCTACTCTGAGACAGGTGTGGCCTG-3'
C ₂ D-BamHI_for ¹	5'-ATATGGATCCAAGCTGGAACCTACCTG-3'
C ₂ D-EcoRI_rev ¹	5'-ATATGAATTCTACTCCACTCTGTACTTGCTGAG-3'
C ₂ E-BamHI_for ¹	5'-ATATGGATCCGATGAGGATGGCTCCACAG-3'
C ₂ E-EcoRI_rev ¹	5'-ATATGAATTCTACTCATCTGTGGGCTTCCTCTG-3'
C ₂ F-BamHI_for ¹	5'-ATATGGATCCAACCCTGACAAGCCAGGC-3'
C ₂ F-EcoRI_rev ¹	5'-ATATGAATTCTAGTCAGGTTTCATTGCGAGCCAG-3'

Mutation sites indicated in italic letters

¹Designed by Kirsten Reuter

3. Methods

3.1 Molecular biology

3.1.1 Polymerase chain reaction (PCR)

Standard PCRs were conducted in 100 μ l total volume with 0.15 mM dNTPs, 4% (v/v) dimethyl sulfoxide (DMSO), 0.5 μ M of each oligonucleotide, 0.001 μ g template-DNA and 2.5 u of Pfu-polymerase in its provided buffer in a MyCycler PCR machine.

The following program was used for standard PCR:

94°C	1 minute	
94°C	20 seconds	} 30x
Annealing temperature	30 seconds	
72°C	1 min/kb	
72°C	4 minutes	
10°C	∞	

To test a lysogeny broth (LB)-agar-plate for positive clones after ligation and transformation, colony PCRs were performed on single colonies. For this, a colony was picked with a tooth pick which was then put into a PCR tube filled with 10 μ l of ddH₂O for one minute. Subsequently, the tooth pick was moved to LB-medium (Bertani, 1951) with the appropriate antibiotic (for pGEX-6P-3: ampicillin; pET28a: kanamycine) and shaken at 37°C, 250 rpm. In parallel, a PCR reaction with the appropriate oligonucleotides was done to detect the desired DNA fragment in the plasmid DNA. Colony PCRs were performed with 20 μ l total volume containing 0.125 mM dNTPs, 0.5 μ M of each oligonucleotide and 5 u Dream Taq-polymerase in its provided buffer. 1% agarose gels were run to find positive clones, these samples were further shaken at 37°C, 250 rpm over night to prepare plasmids.

• Methods •

The following program was used for colony PCR:

95°C	3 minutes	
95°C	20 seconds	} 20x
Annealing temperature	45 seconds	
72°C	1 min/kb	
72°C	2 minutes	
10°C	∞	

In most of the cases, the annealing temperature was 58°C. It was slightly changed to higher or lower values when the first PCR did not show a band on the test agarose gel.

To mutate Otof-C₂A (A17D, N68D, S70D and K76D), two mutagenesis steps were performed. First, the N-terminal mutation A17D was inserted by amplifying the whole plasmid with mutated oligonucleotides (16961; 16962). The initial plasmid was digested with DpnI, and the newly synthesized plasmid was electroporated into the *E. coli* XL1Blue strain. Next, the other three mutations were inserted with help of overlap PCR. Here, two PCRs were done using forward WT oligonucleotide and reverse mutant oligonucleotide (11443 + 17855) for the first PCR, and forward mutant oligonucleotide and reverse WT oligonucleotide (11442 + 17854) for the second PCR. Oligonucleotides were removed afterwards by extracting the PCR products from a 1% agarose gel (3.1.2). The overlapping dsDNA pieces were annealed in an overlap PCR and amplified using the oligonucleotides situated at the ends of the new DNA fragment with the standard PCR protocol. The overlap PCR was conducted in 98 µl total volume with each 10 µl of the two gel eluates, 0.1 mM dNTPs and 2.5 u Pfu-polymerase in its provided buffer.

The following PCR program was used for overlap PCRs:

94°C	5 minutes	} 2x
37°C	5 minutes	
72°C	5 minutes	
94°C	1 minute	

0.5 μ M of each oligonucleotide were added for the standard PCR afterwards.

3.1.2 Restriction enzyme digestion

Prior to restriction enzyme digestions, PCR products were purified with the DNA Clean & ConcentratorTM-5 Kit. Digestions were done in 20-30 μ l total volume with 1 μ l of each restriction enzyme and 1x appropriate buffer for 1-3 hours at 37°C. After restriction enzyme digestion, the products were loaded on a 1% agarose gel and, after 30 min at 100 V, extracted from the gel with help of ZymocleanTM Gel DNA Recovery Kit.

For Syt1-C₂A-WT, which was kindly provided by Alexander Stein (Max-Planck-Institute for Biophysical Chemistry, Goettingen, Germany), NdeI and XhoI were used. For all other constructs, the enzymes indicated in Table 1 were used.

3.1.3 Ligation

Ligations were conducted in 10-20 μ l total volume with 0.25-0.5 u/ μ l T4 DNA Ligase in its supplied buffer at 16°C over night. The molar amount of insert was chosen 4-5 fold higher than that of the vector, according to 1% test agarose gels which were done prior to ligation.

Before transformation, an ethanol precipitation was performed. For this, 3 M sodium acetate (1/10 of the ligation volume) and 100% ethanol (3x the total volume) were added. The mixture was incubated at -20°C for at least 12 hours, then centrifuged for 60 min at 17.000 rcf. The pellet was washed with 70-75% ethanol and centrifuged again for 10 min at 17.000 rcf. The pellet was air dried at 37°C and resuspended in 10 μ l ddH₂O.

3.1.4 Transformation and sequencing

When cloning plasmid DNA, *Escherichia (E.) coli* XL1Blue cells were transformed with ligation products (3.1.3) to grow single colonies containing only one specific

DNA plasmid. 50 µl of bacterial suspension were transformed with 1-5 µl of DNA solution in a Micro Pulser™ electroporator with Gene Pulser® Cuvettes at 1.8 kV. The cells were diluted in 350 µl LB medium (10 g NaCl, 5 g Bacto Yeast extract, 10 g Bacto Tryptone per one Liter medium) and incubated for 60 minutes at 37°C in an Eppendorf-Thermomixer with 750 rpm. After centrifugation for 1 minute at 17.000 rcf, the cells were resuspended in a small volume (~50 µl) of LB medium and plated on LB agar plates (LB medium with 12 g/L Bacto Agar). The plates contained 25 µg/ml kanamycine when pET28a or pGBK-T7 were used in the transformation, and 100 µg/ml ampicillin/carbenicillin when pGEX-6P-3 or pGAD-T7 were used. The plates were incubated over night at 37°C. Whenever possible, colonies were tested with colony PCR (3.1.1) for the correct insert. Over night cultures were prepared with 5 ml of LB liquid medium containing the appropriate antibiotic and incubated over night at 37° and 250 rpm. The DNA was extracted from the cells with help of the GeneJET™ Plasmid Minprep Kit.

DNA samples were given to the sequencing service in the Department of Molecular Neurobiology in Max-Planck-Institute for Experimental Medicine, Goettingen, Germany. Sequencing results were evaluated using *Chromas Lite* (Technelysium Pty Ltd).

Table 7 shows the otoferlin constructs for *E. coli* expression that have been produced for the project so far.

3.2 Protein overexpression

Prior to expression, *E. coli* strain BL21(DE3) was transformed (see 3.1.4) with pET28a or pGEX-6P-3 vectors containing target cDNA and grown on LB-Agar-plates containing 25 µg/ml kanamycine (pET28a) or 100 µg/ml ampicillin/carbenicillin (pGEX-6P-3). 50 ml of LB medium containing 20 µg/ml kanamycine or 100 µg/ml ampicillin/carbenicillin were inoculated with few colonies and grown over night at 37°C. This bacterial suspension was distributed to five liters of 2YT medium (16 g tryptone, 10 g yeast extract, 5 g sodium chloride/liter medium) with 20 µg/ml kanamycine in 2 L erlenmeyer flasks and grown at 30°C. Overexpression was induced by addition of 1 mM IPTG at an OD₆₀₀ of ~0.6 and

carried out for 15-20 hours at 16°C. Cells were harvested at 5,250 rcf for 15 minutes and resuspended in appropriate buffers: mostly, buffer A (Table 1) was used; for resuspension of cells expressing His₆-Syt1-C₂A, buffer B (Table 1) was used. The cell-suspensions were either directly used or frozen at -20°C or -80°C.

3.3 Protein purification

To obtain pure protein for biochemical experiments and crystallography, several purification steps have to be performed to separate *E. coli* proteins from the target protein. First, proteins can be separated from each other by their affinity to bind to certain materials (affinity chromatography, 3.3.1). Second, proteins can be purified by their charge (ion exchange chromatography, 3.3.2). Third, proteins are separated by their size (size exclusion or gel filtration chromatography, 3.3.3). Several combinations of purification steps were performed for the proteins in this work.

Prior to purification, the harvested cells were broken in a Branson Sonifier 250 with 3 times 45 seconds sonication at 50% duty cycle and output control 4-5. The suspension was centrifuged at 21.280 rcf for 60 minutes. The supernatant containing cytosolic proteins was further used in the purification protocol.

Table 1: Buffers used in purifications.

Buffer A	150 mM NaCl, 20 mM Tris pH 7.4
Buffer B	50 mM NaCl, 20 mM Tris pH 7.4
Buffer C	500 mM NaCl, 20 mM Tris pH 7.4
Buffer D	50 mM Hepes-NaOH pH 7.5, 6 M Guanidine HCl, 25 mM DTT
Buffer E	50 mM Hepes-NaOH pH 7.5, 0.2 M NaCl, 1 mM DTT, 1 M non detergent sulfobetaine 201 (NDSB 201)
PBS	8 g NaCl, 0.2 g KCl, 1.44 g Na ₂ HPO ₄ , 0.24 g KH ₂ PO ₄ /L
PBS-T	8 g NaCl, 0.2 g KCl, 1.44 g Na ₂ HPO ₄ , 0.24 g KH ₂ PO ₄ , 2 ml Tween 20/L

3.3.1 Affinity chromatography

In affinity purification, different covalently bound tags were used in order to separate the target protein from impurities.

In first case, an N-terminal His₆-tag was used to bind the desired protein to Ni²⁺ beads on a gel matrix. The HisTrap FF crude columns (1 to 4 times 1 ml-column in row) were run on the ÄKTAprime plus system at 1 ml/min. Mostly, the column was equilibrated in buffer A. For His₆-Syt1-C₂A, it was equilibrated in buffer B. The protein was injected to the column with a 50 ml-Superloop. The column was washed with the appropriate buffer until a steady baseline of the 280 nm UV measurement was reached. The protein was eluted and collected from the column with the same buffer containing imidazole. Proteins leaving the column were detected with 280 nm UV light. In successful purifications, 25 mM (His₆-Otof-5D-C₂A), 25-100 mM (His₆-Otof-C₂A) or 500 mM (His₆-Syt1-C₂A) imidazole were used in elution. For other C₂-domains of otoferlin, elution was mostly done with buffer A containing 500 mM imidazole.

As alternative to the His₆-tag, an N-terminal GST-tag was used to bind the target protein to GSH-sepharose. The GSTrapTM 4B columns (5 ml column) were run on the ÄKTAprime plus system at 1 ml/min. The column was equilibrated in buffer A. The protein was injected to the column with a 50 ml-Superloop. The column was washed with the appropriate buffer until a steady baseline of the 280 nm UV measurement was reached. The protein was eluted and collected from the column with the same buffer containing 30 mM glutathione. Proteins leaving the column were detected with 280 nm UV light.

3.3.2 Ion exchange chromatography

His₆-Syt1-C₂A was further purified using ion exchange chromatography. Here, the protein was loaded on a 1 ml Resource Q column after equilibration with buffer B (Table 1). After reaching a steady baseline at 280 nm, a 20 ml salt gradient from 50 mM NaCl to 500 mM NaCl (Buffer B & Buffer C; Table 1) was applied. The elution fraction was collected. The column was run on the ÄKTAprime plus system at 1-2

ml/min. When necessary, the volume of the protein solution was reduced in a Vivaspin 20 MW cutoff 10 kDa concentrator prior to the experiment.

3.3.3 Size exclusion chromatography

The monomeric state of His₆-Otof-C₂A, His₆-Otof-5D-C₂A and His₆-Syt1-C₂A was verified via size exclusion chromatography using a Superdex 75 10/300 with 24 ml bed volume or a Superdex 75 16/60 with 120 ml bed volume. The proteins were injected into the columns using 0.5 ml loops (5 ml loops for Superdex 75 16/60) after equilibration with buffer A. The columns were run on the ÄKTAprime plus system at 0.5 ml/min (up to 1 ml/min for Superdex 75 16/60). Fractions were collected. When necessary, the volume of the protein solution was reduced in a Vivaspin 20 MW cutoff 10 kDa concentrator prior to the experiment.

Before analyzing the proteins in flotation assays, the His₆-tag was cut off prior to size exclusion chromatography using 2 u PreScission Protease and slow shaking at 4°C over night. Also, the His₆-tag was removed in one control experiment prior to circular dichroism spectra measurement.

To test with size exclusion chromatography whether the other C₂-domains of otoferlin (C₂B-C₂F) are in a non-aggregated, monomeric state, mostly buffer A was used. If a domain was GST-tagged, the GST-tag was removed prior to gel filtration.

3.4 Protein detection by SDS-PAGE

Sodium dodecyl sulphate (SDS) gels containing poly-acrylamide were used to study the composition of protein samples and to detect and identify particular proteins by their size.

Mostly, proteins were loaded on 12% poly-acrylamide gels (Table 2) and run at 25 mA for ~45 min in the Mini-PROTEAN Tetra Cell system.

For 7.5% gels, the amounts of acrylamide and water were adjusted. On every gel, 5 µl of a molecular weight marker (SM0441, SM0431 or SM1811) were loaded as control.

• **Methods** •

Table 2: Recipe for 12%-acrylamide-SDS-gels. Amounts are for two gels.

	Resolving gel	Stacking gel
H₂O	2.72 ml	1.36 ml
30% acrylamide	3.2 ml	1.6 ml
1.5 M Tris pH 8.8	2 ml	-
0.5 M Tris pH 6.8	-	1 ml
10% SDS	80 μ l	40 μ l
APS	40 μ l	20 μ l
Temed	4 μ l	4 μ l

SDS-gels were stained with ~50 ml of Coomassie Brilliant Blue staining solution (2.5 g Coomassie Brilliant Blue R-250, 450 ml ethanol, 100 ml acetic acid, 400 ml H₂O) and destained with 50% ethanol/10% acetic acid destaining solution. Gels were either photographed or scanned.

3.5 Protein detection by Western Blotting

SDS-PAGE gels (see 3.4) were blotted onto a membrane for immunostaining to perform “Western Blots”. For blots with full length otoferlin without transmembrane domain (Otof- Δ TM) constructs, 7.5%-gels were prepared. The gels were run as described (see 3.4). Next, the bands on the SDS-gel were transferred to a PVDF-membrane (pre-incubation with methanol) with electrophoresis at 25 V and 400 mA for 90 minutes. The membrane was blocked in 1% casein diluted in phosphate buffered saline (PBS) buffer (Table 1) for one hour. The membrane was washed two times for 10 minutes in PBS buffer containing 0.05% Tween 20 (PBS-T, Table 1), then for 10 minutes in PBS buffer. Next, it was exposed to the primary antibody diluted 1:1,000 in PBS for one hour at room temperature or 4°C over night. After another two washes in PBS-T and one wash in PBS, the membrane was exposed to the secondary antibody diluted 1:10,000 in PBS for another hour. After four 10-minutes washing steps in PBS-T, the membrane was either stained with the NBT/BCIP-system when using alkaline phosphatase-linked secondary antibodies, or

with a chemiluminescence-system when using horseradish peroxidase-linked secondary antibodies.

In the NBT/BCIP-system, the membrane is stained directly with a colour reaction. BCIP is the substrate for alkaline phosphatase and is finally converted to an indigo dye with help of NBT. For this reaction, 200 μ l of NBT/BCIP stock solution were diluted in 10 ml of 0.1 M Tris-HCl pH 9.5, 0.1 M NaCl, 0.05 M MgCl₂. The blot was incubated in this solution for 10-60 min.

In the chemiluminescence-system, the protein bands are exposed to ECL buffer (1 ml of Pierce ECL Detection Reagent 1 + 1 ml of Pierce ECL Detection Reagent 2) containing luminol, a substrate of horseradish peroxidase. After one minute of incubation time, the bands are transferred to an Amersham HyperfilmTM ECL high performance chemiluminescence film, where the chemiluminescence can be made visible to the eye.

3.6 Crystallization and X-ray data collection

Prior to crystallization, size exclusion chromatography (3.3.3) was performed to assure the monomeric folded state of the protein.

To obtain the molecular structure of His₆-Otof-C₂A via X-ray crystallography, crystallization trials were done with pure His₆-Otof-C₂A protein using Cryschem plates and the sitting drop vapor diffusion technique. The plates were sealed with Shark Tape. His₆-Otof-C₂A crystallized with 40 mg/ml concentration (determined with Bradford solution) in 2 μ l drops containing 1:1 protein and reservoir solution at 20°C. The crystallization condition contained 16% w/v PEG 4000, 100 mM Tris/HCl pH 8.5 and 200 mM magnesium chloride (JB2-screen condition 9) with reservoir size 200 μ l. Final crystals for data collection were grown at 4°C with micro-seedings from the initial condition. For this, a crystal was destroyed in its drop and a cat whisker was pulled through it. Then, the whisker was pulled through a fresh drop containing fresh protein.

From one single crystal, a dataset was collected at the home source machine (rotating-anode Xray source MM007, MAR 345 image plate detector) in the Department of Molecular Structural Biology, Goettingen, Germany. The crystal

diffracted up to 1.95 Å with Cu K α radiation ($\lambda = 1.54179$ Å). The resulting diffraction images were integrated, merged and scaled with the *XDS package* (Kabsch, 2010).

For His₆-1-C₂F-short and His₆-C₂AB, the following crystallization trials with the sitting drop vapour diffusion technique and 1:1 ratio of reservoir to protein were conducted: for C₂F, crystal screens ProPlex screen, JCSG screen, AmSO₄ screen, and JB screens 1, 2, 4, 5, 6, 7, 8 and 10 were used, for C₂AB, Crystal Screen I was used. The crystallization trials were performed at 20°C with sitting drop vapour diffusion as for Otof-C₂A with a MinstrelTM HT crystallization roboter.

3.7 Structure solution and refinement

Running *Phaser* (McCoy *et al.*, 2007) with a truncated version of the structure of PKC α (1DSY; Verdaguer *et al.*, 1999) as search model and a resolution limit of 2.0 Å, the structure of Otof-C₂A could be solved by Molecular Replacement. The initial R-factor was 0.57, after the first refinement with *Refmac5* (Murshudov *et al.*, 1997) the R-factor was 0.432 and R_{free}-factor was 0.555.

Next, the structure was alternately refined manually with help of *Coot* (Emsley *et al.*, 2010) and automatically with *Refmac5*. The last refinement was done in *PHENIX* (Adams *et al.*, 2010). The final R-factor was 0.181, R_{free}-factor was 0.229.

3.8 Circular Dichroism Spectroscopy

Prior to circular dichroism (CD) spectroscopy, proteins were brought into buffer C (2 mM Tris pH 7.4, treated with Chelex100®) using a 5 ml HiTrap Desalting column or gel filtration. The column was run on the ÄKTAprime plus system with 1 ml/min. Proteins were diluted to 5-8.5 μ M concentration with 2 mM Tris pH 7.4 Chelex100®-treated buffer in 200 μ l total volume. To produce this buffer, 50 g of Chelex100® in 1 L buffer were stirred for one hour. Chelex100® was separated from the buffer by filtering. The concentration of protein was determined using the absorbance at 280 nm.

100 μM CaCl_2 or EDTA were contained in the 200 μl total volume to study the calcium binding behavior of His₆-Otof-C₂A and His₆-Otof-5D-C₂A. His₆-Syt1-C₂A was used as a positive control. Spectra were measured in a special 200 μl CD-spectroscopy-cuvette at 180 to 260 nm with 5 seconds of measurement per point (1 nm) using a Chirascan circular dichroism spectrometer. All experiments were performed at 25°C. Data points with high tension voltage (HTV)-values above 600 V were discarded. A test whether or not the His₆-tag has influence on the spectra was performed. A titration with ligand to buffer without protein was subtracted from all experiments to exclude dilution effects from the evaluation.

3.9 Isothermal Titration Calorimetry

Prior to isothermal titration calorimetry (ITC), proteins were dissolved in buffer A, treated with Chelex100®, using gel filtration (3.3.3). The reference cell was filled with ddH₂O. The protein concentration was determined with help of Bradford solution.

For His₆-Otof-C₂A, His₆-Otof-5D-C₂A and His₆-Syt1-C₂A, Ca²⁺-binding studies were performed. For this, proteins were diluted to 80 μM concentration in 2 ml total volume with titration buffer and injected into the sample cell using a 2 ml syringe. 282 μl of 5 mM CaCl_2 (in titration buffer) were loaded into the titration syringe. The titration was performed with one injection of 2 μl injection volume and 56 further injections with 5 μl injection volume.

In addition, for His₆-Otof-C₂A, titrations with 3'-5'-cyclic adenosine monophosphate (cAMP), adenosine monophosphate (AMP), adenosine-5'-triphosphate (ATP) or inositol 1,4,5-trisphosphate (IP₃) were performed. Here, protein was diluted to 17-25 μM in 2 ml total volume with titration buffer. 282 μl of 500 μM ligand solution were loaded into the titration syringe. First, 3 μl were injected. Then, in 28 further injections, 10 μl were titrated in each step.

A spacing time of 210 seconds between two injections gave the cell time to re-equilibrate to a stable baseline. All experiments were performed at 25°C and 300 rpm stirring. For every type of experiment, a “blank run” was done with titration of ligand solution to protein-free titration buffer. This blank run was subtracted from the

experimental data to correct for the dilution heat of the ligand. The Ca²⁺-binding experiments were repeated once for every protein.

3.10 Liposome Flootation Assay

Prior to the experiment, proteins were brought into buffer A using gel filtration. Protein concentrations were determined using the NanoDrop1000 spectrophotometer. Liposomes were prepared freshly for each experiment from lipid mixtures containing different lipid compositions (Table 3). For one additional experiment with His₆-Otof-C₂A and His₆-Syt1-C₂A, a total brain lipid extract mixture was used for liposome production. In both cases, the lipids were dissolved in trichloromethane from their stock solutions, mixed and dried in a rotation evaporator under nitrogen atmosphere, and finally dissolved in 20 mM HEPES pH 7.5, 150 mM KCl, 2 mM DTT, and 5% cholate at 33.5 mM concentration. The mixture was diluted 1:3 in 20 mM Hepes pH 7.5, 150 mM KCl, and 1.5% cholate, injected to an Econo column filled with Sephadex G-50 superfine and run in buffer A. Contained detergents, prohibiting spontaneous liposome-formation, were thus removed from the lipids by size-exclusion chromatography.

In 100 µl total volume, proteins were diluted to 15 µM concentration in buffer A and mixed with 20 µl of liposomes and 40% Nycodenz containing 1 mM CaCl₂/EGTA. 50 µl of 30% Nycodenz buffer containing 1 mM CaCl₂ or EGTA were carefully added, followed by 50 µl of buffer A containing 1 mM CaCl₂ or EGTA.

This gradient was centrifuged at 197,000g for 90 min in an S55S rotor. Carefully, eight fractions of 20 µl volume were pipetted from top to bottom of the tube and collected in Eppendorf tubes. The remaining 40 µl from the bottom of the tube were collected in the ninth fraction. From each fraction, 10 µl were loaded on a 12% acrylamide SDS gel and stained with Coomassie blue (2.4). With help of ImageJ, the intensity of the every single band was quantified for the evaluation. Every floatation assay was done three times with independent batches of protein.

Table 3. Composition of lipids used in floatation assays. Helfmann *et al.*, 2011.
PC: phosphatidylcholine; PS: phosphatidylserine; PE: phosphatidylethanolamine; PI: phosphatidylinositol; Chol: cholesterol, PIP₂: phosphatidylinositol 4,5-bisphosphate; PA: phosphatidic acid.

	PC [%]	PS [%]	PE [%]	PI [%]	Chol [%]	PIP ₂ [%]	Texas red [%]	PA [%]	Unknown [%]
+PS -PIP ₂	43.4	16	20	10	10	0	0.6		
-PS -PIP ₂	59.4	0	20	10	10	0	0.6		
+PS +PIP ₂	43.3	16	20	8.4	10	1.6	0.6		
Brain total lipid extract	9.5	10.5	16.5	1.6			1	2.8	58.1

3.11 Purification trials for otoferlin C₂-domains besides C₂A

For the expression and purification of otoferlin C₂-domains besides C₂A, several different protocols were tested.

First, the standard purification protocol (3.3) was used including affinity purification and gel filtration. To solve the problem of aggregation, a lot of constructs were cloned and tested (Table 7). Especially for Otof-C₂F, several longer and shorter versions were produced to obtain non-aggregated protein (Table 6). Again for Otof-C₂F, several *E. coli* strains have been tested for better solubility of the initial GST-construct.

3.11.1 Solubility problems: purification from inclusion bodies

For purification of proteins from inclusion bodies, a protocol from the internet (<http://www.bmsc.washington.edu/people/kumar/PEX/refold.html>) was used:

BL21(DE3) cells expressing GST-Otof-C₂D on 5 L 2YT-medium were resuspended in buffer C and broken by sonication with a Branson Sonifier 250 with 3 times 45 seconds sonication at 50% duty cycle and output control 4-5. While the supernatant

was discarded, the pellet was washed with PBS buffer containing 1% Triton X-100. The suspension was centrifuged at 30,000 rcf for 30 min at 4°C twice, the supernatants were discarded. The pellet (containing inclusion bodies) was solubilized in 2 ml of buffer D (Table 1). This was incubated for 60 min at 4°C. After 10 min of centrifugation at 100,000 rcf, the protein concentration was reduced to 1 mg/ml (monitored with the quick Bradford-test) with help of buffer D. Then, the solution was quickly added to 10 times the volume of buffer E (Table 1) under constant fast stirring. The resulting solution was stirred for 2 more minutes, then incubated for 1 hour at 4°C. In a Vivaspin 20 MW cutoff 10 kDa concentrator, the Guanidine HCl and non detergent sulfobetaine 201 (NDSB 201) were removed from the solution. Then, the folding of the protein was studied by gel filtration under standard conditions (buffer A, 3.3.3).

3.11.2 Aggregation problems: new constructs and buffers

To solve the aggregation problems, several things differing from the standard protocol (3.3.1 + 3.3.3) were tried: 20 mM Tris pH 7.4 buffers containing 0, 150, 200, 300 or 500 mM NaCl were tested for differences in the aggregation behaviour of GST-C₂F after cut-off of the GST-tag. 5% ethanol and 10 μM ATP were added to the buffers in GST-C₂F purification, 20 mM CaCl₂ and/or 5% ethanol in the buffers were added in GST-C₂C purification to improve the behavior on the gel filtration column.

With the His₆-tagged construct His₆-1-C₂F-short, a degradation product seemed to be sticking to the full length C₂F, according to the retention volume on gel filtration and the corresponding SDS-gel. Here, besides the standard protocol (3.3.1 + 3.3.3), a protocol described in Gaffaney *et al.* (2008) was used. This included washing steps with a buffer containing 1% Triton X-100 and a buffer containing 1% *n*-octylglucoside in the affinity purification step.

4. Results

4.1 Structure and biochemistry of the C₂A-domain of rat otoferlin

4.1.1 Purification

Amino acids 1 to 124 of the sequence of *rat* otoferlin were subcloned into pET28a with restriction enzymes NdeI and XhoI. This led to an N-terminal His₆-tag to facilitate purification. On gel filtration columns, His₆-Otof-C₂A eluted at the appropriate retention volume for its expected monomeric size of 16.4 kDa (14.5 kDa plus 1.9 kDa for the His₆-tag) (Fig. 16C). Accordingly, a relatively pure protein band was detected at this size on 12%-SDS-gels (Fig. 16B).

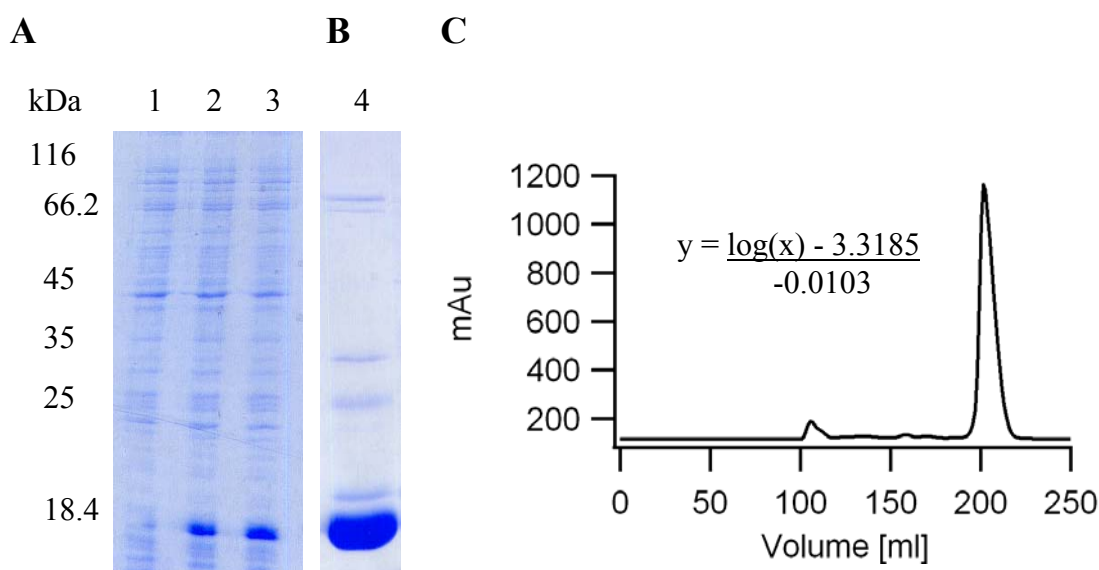


Figure 16: Documentation of purification of His₆-Otof-C₂A.

A: SDS-PAGE documentation of His₆-Otof-C₂A overexpression in *E. coli* BL21(DE3) cells grown on LB liquid medium at 16°C. 1: sample prior to induction of expression. 2: sample 12 hours after induction. 3: sample 13 hours after induction.

B: SDS-PAGE documentation of successful affinity purification of His₆-Otof-C₂A. 4: sample after elution from HisTrap FF crude column.

C: Gel filtration chromatogram of His₆-Otof-C₂A on a Superdex 75 16/60 column: elution at ~201-205 ml, corresponding to the range of 16.1-17.7 kDa.

His₆-Otof-C₂A was successfully overexpressed in *E. coli* BL21(DE3) cells (Fig. 16A), affinity purified via its N-terminal His₆-tag (Fig. 16B) and run over a gel filtration column (Superdex 75 16/60; calibration curve was produced by the Department for Molecular Structural Biology, Goettingen) to assure its monomeric state and to bring it in its storage buffer containing 150 mM NaCl and 20 mM Tris pH 7.4 (Fig. 16C).

4.1.2 Structure

Initial crystals were obtained in JB2-screen condition 9, but not as single crystals. By micro-seeding with a cat whisker, a single crystal was grown in a fresh drop containing concentrated protein. The oscillation photographs were collected in house from a single crystal at -180°C diffracting up to 1.95 \AA with Cu K α radiation ($\lambda = 1.54179 \text{ \AA}$) by using a rotating-anode source (RA Micro 007) and an image plate detector (MAR 345) in the Department of Molecular Structural Biology, Goettingen, Germany. Oscillation photographs were processed (integrated, merged, and scaled) using the *XDS package* (Kabsch, 2010).

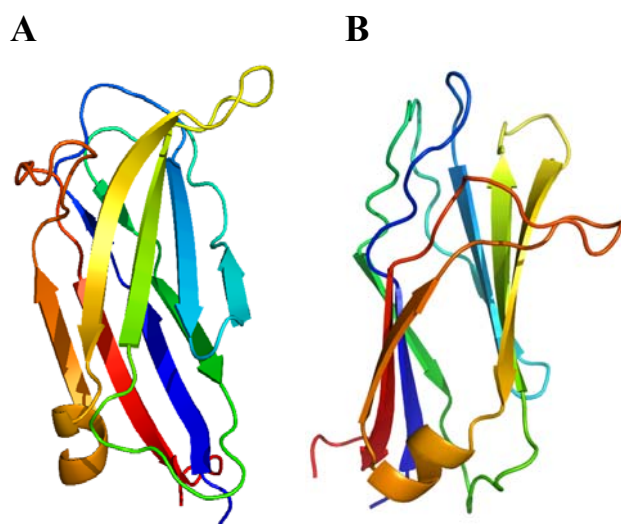


Figure 17: Structure of otoferlin C₂A solved from a single protein crystal.

Cartoon representation of monomeric C₂A coloured rainbow from N-terminus to C-terminus = Blue to red. Picture was done in *Pymol* (DeLano, W.L., www.pymol.org).

A: View on a beta-sheet comprised of four β -strands.

B: Side view perpendicular to β -strands.

• Results •

With the dataset of one single crystal of Otof-C₂A, the structure was solved by Molecular Replacement using the data up to 2.0 Å resolution. The MR search was performed in *Phaser* (McCoy *et al.*, 2007), the search model was the PKC α -C₂ (1DSY). Prior to the MR operation, the amino acid chain of the search model was truncated according to sequence alignments (Schwarzenbacher *et al.*, 2004) with help of *Chainsaw* (Stein, 2008).

The R-factor calculated based on the structure resulting from the Molecular Replacement search was very high (0.57) and suggested the existence of quite big differences between the used model and the target structure. Based on a good packing of the molecules in the unit cell, this structure was further refined and manually rebuild using *Refmac5* (Murshudov *et al.*, 1997) and *Coot* (Emsley *et al.*, 2010) alternately. The final model has been refined at resolution 1.95 Å to an R-factor of 0.181 and R_{free}-factor of 0.229. The final model consists of amino acid residues 1-124 of rat otoferlin plus two N-terminal amino acids resulting from molecular cloning. Due to the quality of electron density maps the 18 other amino acids from the N-terminus including the His₆-tag were not included in the final model and are most likely disordered.

Table 4 shows the statistics for the His₆-Otof-C₂A-crystal (Helfmann *et al.*, 2011).

Table 4: Statistics for Otoferlin C₂A crystal structure. Helfmann *et al.*, 2011.

Values in parentheses correspond to the highest-resolution shell for data scaling (1.95–2.05 Å) and refinement (1.95–2.15 Å). $R_{\text{cryst}} = \frac{||F_{\text{obs}}| - |F_{\text{calc}}||}{|F_{\text{obs}}|}$. R_{free} was calculated as for R_{cryst} , but for a test set comprising reflections not used in the refinement (5.0%).

Data collection	
Space group	I4 ₁
Cell dimensions	
a, b, c (Å)	100.3, 100.3, 30.0
α , β , γ (°)	90.0, 90.0, 90.0
Wavelength (Å)	1.54179
Rmerge (%)	6.0 (47.3)
I/ σ I	15.0 (2.6)
Completeness (%)	98.3 (99.3)
Reflections (observed)	33,068 (4473)

• Results •

Reflections (unique)	10,992 (1522)
Multiplicity	3.0 (2.9)
Wilson B (\AA^2)	24.4
Mosaicity ($^\circ$)	0.47
Refinement	
Resolution (\AA)	24.93–1.95
Number of reflections	10,990
Rcryst/Rfree	18.1 (23.6)/22.9 (30.0)
Number of atoms	
Protein	1042
Mg ²⁺	1
Water	143
B-factors (\AA^2)	
Protein	32.01
Ligand/Ion	16.28
Water	39.27
RMSD	
Bond lengths (\AA)	0.006
Bond angles ($^\circ$)	0.981
Dihedral ($^\circ$)	17.99
Ramachandran statistics	
Favored (%)	96.8
Allowed (%)	2.4
Outliers (%)	0.8

The obtained crystal structure of His₆-Otof-C₂A reveals a typical C₂-domain with two β -sheets consisting of four antiparallel β -strands, one on each side of the molecule, opposing each other. Between β -strand 6 and 7, there is a short alpha-helical region (Fig. 17).

In the solved crystal structure, the C₂A-monomers are in contact with symmetry related molecules in two directions (Fig. 18): in one direction, loops 5 and 7 (counted from N-terminus) interact through the polar contact of Asn105 with Ser74 and Lys76 (Fig. 18, yellow and orange loops in box). On the other side of the molecule, β -strand 4 (counted from N-terminus) makes polar interactions with the equivalent strand of

the neighbor molecule involving Arg49 of one molecule and Glu46 and Thr47 of the neighboring one (Fig.18, green β -strands in box).

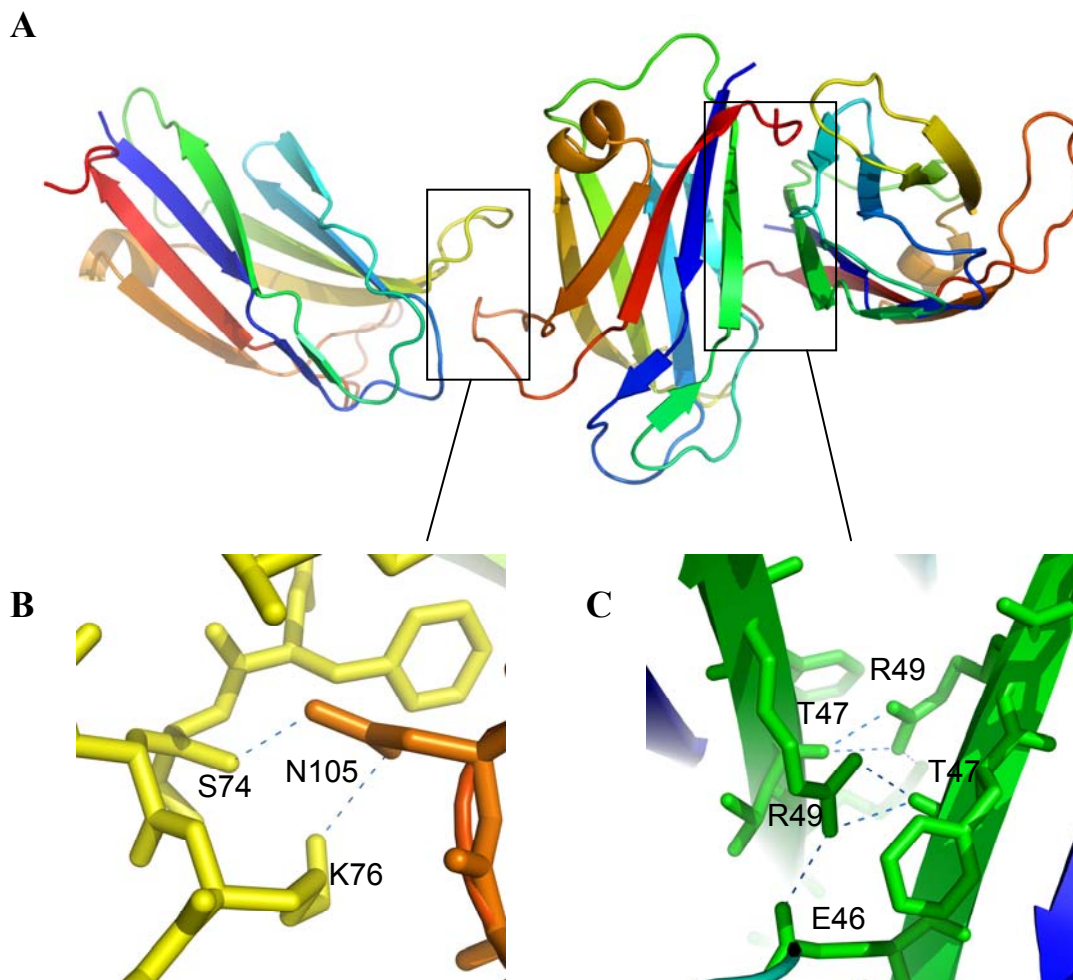


Figure 18: Polar contacts in the crystal packing.

A: Arrangement of monomers in the Otof- C_2A -crystal. Boxes: enlargements in B and C.

B: Polar contacts between left and middle monomer in A: K76 and N105.

C: Polar contacts between middle and right monomer in A: T47 and R49.

The space group in which the crystal developed is defined by the arrangement of molecules, the crystal packing. In this case, the crystal grew in the tetragonal body-centered space group $I4_1$ with a fourfold screw-axis and translation of one quarter of the Z-axis around the screw-axis (Fig. 19).

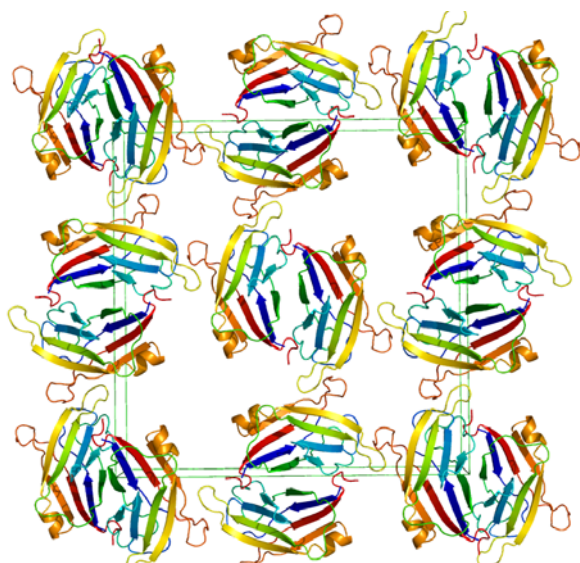


Figure 19: The crystal packing of space group $I4_1$. Crystal packing of the $I4_1$ symmetry shown with symmetry mates in 50 Å diameter. Only first layer of molecules is shown for clarity.

Among C_2 -domains, two different topologies exist: type I and type II C_2 -domains differ in the localization of their Ca^{2+} -binding region (Fig. 20, Jimenez and Bashir, 2007). In type I C_2 -domains, Ca^{2+} is bound with loop 2, 4 and 6, while in type II C_2 -domains, it is bound with loops 1, 3 and 5 (counted from N-terminus). By aligning Otof- C_2A with the structures of PKC α (Verdaguer *et al.*, 1999) and PLA2 (Perisic *et al.*, 1998) in *Pymol* (DeLano, W.L.), Otof- C_2A was identified as type II- C_2 -domain (alignment not shown). This revealed the position of the putative Ca^{2+} -binding site in Otof- C_2A (Figure 17: upper end of molecule).

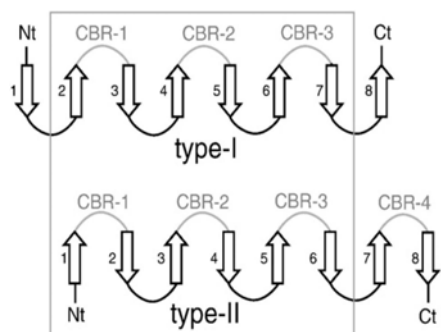


Figure 20: Topologies of C_2 -domains. Jimenez and Bashir, 2007. Type I and Type II C_2 -domains differ in the localization of the Ca^{2+} -binding region.

• Results •

Comparing the structure of Otof-C₂A to the structures of other C₂-domains with *DaliLite* (Holm and Park, 2000; Table 5), Myof-C₂A shows the highest similarity to Otof-C₂A with a Z-score (strength of structural similarity) of 16.0. The highest similarity to a protein known to be involved in the presynaptic machinery is found for Munc13-1-C₂B with a Z-score of 15.8. The similarity of the structure of Otof-C₂A to that of Syt1-C₂A, on the contrary, is relatively low (Z-score of 11.9).

The structure was deposited at www.pdb.org with accession number 3L9B.

Table 5: Proteins with highest similarity to the structure of Otof-C₂A according to Z-scores. Helfmann *et al.*, 2011.

Similarity search was performed with *DaliLite* (Holm and Park, 2000). RMSD: root mean square deviations; Z-score: strength of structural similarity.

Proteins with C ₂ -domains similar to Otof-C ₂ A	PDB-ID	RMSD-value	Z-Score	Reference
Myoferlin C ₂ A	2DMH	2.0	16.0	Nagashima <i>et al.</i> , 2006
Phospholipase Cδ-1 C ₂	1DJH	2.0	15.9	Essen <i>et al.</i> , 1997
Munc13-1 C ₂ B	3KWT	2.1	15.8	Shin <i>et al.</i> , 2010
Intersectin 2 C ₂	3JZY	2.4	15.4	Shen <i>et al.</i> , 2009
MCTP2 C ₂ B	2EP6	2.3	14.9	Nagashima <i>et al.</i> , 2007
Itchy Homolog E3 Ubiquitin Protein Ligase C ₂	2NQ3	2.3	14.4	Walker <i>et al.</i> , 2006
Phospholipase Cβ 2 C ₂	2ZKM	2.2	14.3	Hicks <i>et al.</i> , 2008
Munc-13-1 C ₂ A	2CJS	2.1	14.4	Lu <i>et al.</i> , 2006
Phospholipase A2 C ₂	1RLW	2.6	14.3	Perisic <i>et al.</i> , 1998
Protein Kinase Cε C ₂	1GMI	2.1	14.0	Ochoa <i>et al.</i> , 2001
E3 Ubiquitin-Protein Ligase NEDD4-like protein C ₂	2NSQ	2.1	13.8	Walker <i>et al.</i> , 2006
Protein Kinase Cη C ₂	2FK9	2.2	13.4	Littler <i>et al.</i> , 2006
Axin Interactor “Aida”, C-terminus	2QZQ	2.7	12.6	Zheng, 2007
Synaptotagmin-like protein 4 C ₂	3FDW	1.9	12.0	Bonanno <i>et al.</i> , 2008
Synaptotagmin IV C ₂ B	1W15	1.7	12.0	Dai <i>et al.</i> , 2004
Phosphatidylinositol-4,5-bisphosphate 3-kinase C ₂	2WXO	2.6	12.0	Berndt <i>et al.</i> , 2010
Smurf2 C ₂	2JQZ	2.6	11.9	Wiesner <i>et al.</i> , 2007
Synaptotagmin I C ₂ A	1RSY	1.8	11.9	Sutton <i>et al.</i> , 1995

4.1.3 Ca²⁺ binding behavior

C₂-domains are known as Ca²⁺-binding or -sensing domains, but not all of them bind Ca²⁺-ions (Cho and Stahelin, 2006). To reveal the role of otoferlin at the ribbon synapse, it is important to know which of its C₂-domains do or do not bind Ca²⁺-ions. The structure of Otof-C₂A already gives information: with help of *Pymol* (DeLano, W.L. www.pymol.org), the surface charge of the molecule was calculated and compared to the surface charges of other C₂-domain structures.

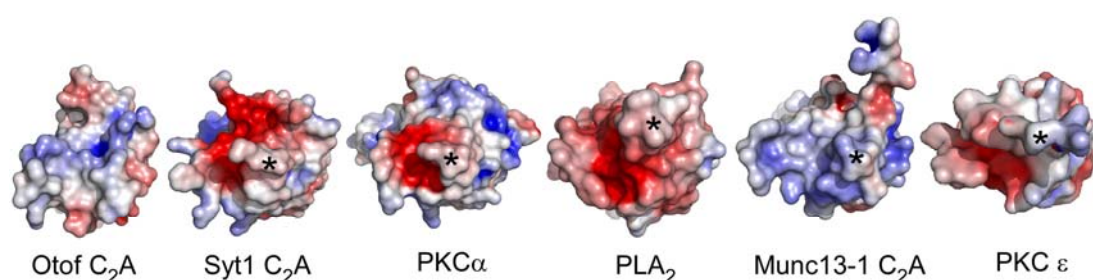


Figure 21: Surface charge illustration of Otof-C₂A and other C₂-domains.

Helfmann *et al.*, 2011. Red -> blue corresponds to negative -> positive charge. Picture was done in *Pymol*.

Otof-C₂A: 3L9B (Helfmann *et al.*, 2011). Syt1-C₂A: 1BYN (Shao *et al.*, 1998), PKCα-C₂: 1DSY (Verdaguer *et al.*, 1999), PLA2-C₂: 1RLW (Perisic *et al.*, 1998), Munc13-1-C₂A: 2CJS (Lu *et al.*, 2006), PKCε-C₂: 1GMI (Ochoa *et al.*, 2001).

Figure 21 shows a view on top of the Ca²⁺-binding region. As Ca²⁺ is a positively charged ion, its binding region should be negatively charged for best binding conditions. While Syt1-C₂A (Shao *et al.*, 1998), PKCα-C₂, PLA2-C₂, and PKCε-C₂ (Ochoa *et al.*, 2001) are negatively charged in the area where Ca²⁺ would be bound, Otof-C₂A and Munc13-1-C₂A (Lu *et al.*, 2006) show rather positive or no charge (Fig. 21). The negative surface charge in the putative Ca²⁺-binding region of a C₂-domain is due to the special position of negatively charged amino acids, especially aspartates in this area. Alignments of the structure of Otof-C₂A with those of other C₂-domains in *Pymol* (DeLano, W.L.) served as control for previous sequence alignments (Jimenez and Bashir, 2007). According to the structure-based sequence alignments with Munc13-1-C₂A, Munc13-1-C₂B (Shin *et al.*, 2010), Myof-C₂A, PLA2-C₂, PKCε-C₂, Syt1-C₂A and PKCα-C₂, Otof-C₂A has one of the five

• Results •

aspartates in the respective position (D18), while three aspartates are replaced by asparagine (N68), serine (S70) and lysine (K76) (Fig. 22&23). The fifth aspartate is completely missing (Fig. 22), as the extension of the corresponding loop (loop 1) where the fifth aspartate would be is missing in Otof-C₂A (Fig. 22&23).

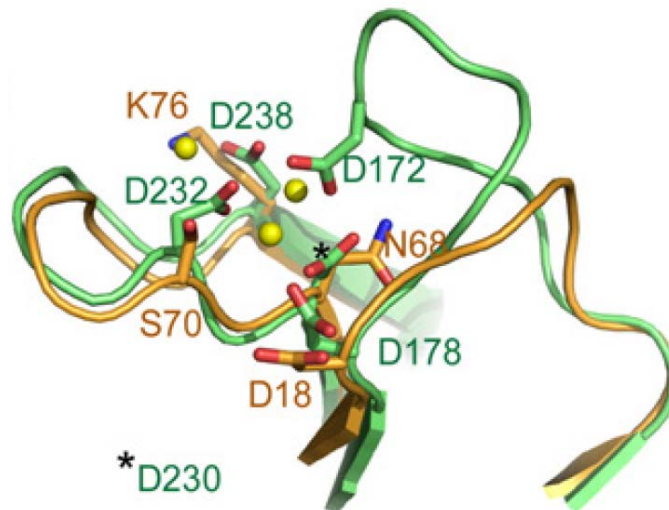


Figure 22: Detail view on the Ca²⁺-binding region of Otof- and Syt-C₂A. Helfmann *et al.*, 2011.
Orange: Otof-C₂A (3L9B).
Green: Syt1-C₂A (1BYN).

In contrast, PKC α -C₂, Myof-C₂A, Munc-13-1-C₂B and PKC ϵ -C₂ show an extended loop at this position (Fig. 24, arrows). Only Munc-13-1-C₂A shows a similarly short loop as Otof-C₂A (Fig. 23 and 24).

Together, three aspects in the structure of Otof-C₂A indicate rather no Ca²⁺-binding for this C₂-domain: first, the surface charge in the putative Ca²⁺-binding area is rather positive. Second, only one of the five aspartates believed to be necessary for Ca²⁺-binding was found in structure-based sequence alignments. Third, the extension of loop 1, which might be required to bring the fifth aspartate in the correct position, is missing in Otof-C₂A.

The Ca²⁺-binding ability of Otof-C₂A was also tested with biochemical assays. First, binding was investigated via isothermal titration calorimetry (ITC). In this method, a ligand is titrated to the sample protein in order to sense heat changes when a reaction between the two occurs.

• Results •

				18					
Otof C2A	1	-----MAL-IVHLKTVSELRG-----	-----RADRIAKVTFR-----						
Munc C2A	1	-----MSLL-CVGVKKAQF-DCAQF-----	-----KFNITYVTLKVG-----						
Munc C2B	687	-----WSAKL-SITVCAQGLQ-AKDKT-----	-----GSSDPYVTVQVG-----						
Myof C2A	1	-----ML-RVIVESASNIPK-----TKF-----	-----GKDPPIVSVIFK-----						
PLA2 C2	17	-----SH-KFTVVVLRATKVTKCAFGLMI-----	-----DTPDPYVELFIS-TT-PDSRKRTRHFNNDI-NPVWNETFEPIL--DP-NQE						
PKCε C2	1	-----MVFNGLL-KIKICEAVSLKPTAWLRDAVGRPQTFLDPYIALNVD-----	-----DSRIGQTATKQRTNSPAWHDEFVIVV--CN-G--						
SytI C2A	142	LGLQYSLDYDFQNNQLLVGIIQAALP--ALDMG-----	-----GTSDPYVKVFLPDK--KKKFETKVRKTL-NPVFNEQFTFKVP--YSELGG						
PKCα C2	159	RGRIYLKAEVTD--EKLHVIVRDAKNLI--PMDPN-----	-----GLSDPYVKLKLIPDPKNEKQKTKTIRSTL-NPQWNESTFKL--KPSDKD						
		68 70	76						
Otof C2A	60	EVLEIQIFNYSKVF-----	SNKLIQTFRMVLQKVVVE-E-NRVE-V-SDTLIDD-----						
Munc C2A	58	LGLTVEVWNGK-LI-----	WDTMVCTVWIPLRTRQ-SNEEGPGE-WLTLDS-QAIMADSEICCTKDPFHRILLDAHFE-----						
Munc C2B	749	DRIKVRVLDDEDDLKSRVQRFKRESDDFLGQTIIEVRTL--S-GEMD-V-WYNLDKR-----	TDKSAVSGAIRLHISVEI----						
Myof C2A	63	SSLGIIIVKDFEITIG-----	QNKLIQTATVALKDI TGDQSRSLP-YKLISLINE-----						
PLA2 C2	85	NVLEITLMDAN-YV-----	MDELGTATFTVSSMK--VGEKKE-V-P-FIE-----						
PKCε C2	77	RKIELAVFHDAPIG-----	YDDFVANCTIQSEELLQNGSRHFE-D-WIDLE-----						
SytI C2A	222	KTLVMAVYDFDRFS-----	KHDIIGEFKVPMTVDF-G-HVTE-E-WRDLQSA-----						
PKCα C2	238	RRLSVEIWDRTT-----	RNDFMGSLSFGVSELMK--MPASG-WYKLL-----						

Figure 23: Structure-based sequence alignments of Otof-C₂A with other C₂-domains. Helfmann *et al.*, 2011.

Red letters mark positions for aspartates. Yellow labeling marks β-strands. Green labeling marks alpha-helical structure. Grey color marks sequence missing in the structure. Munc13-1-C₂B: 3KWU (Shin *et al.*, 2010). Myof-C₂A: 2DMH (Nagashima *et al.*, www.pdb.org).

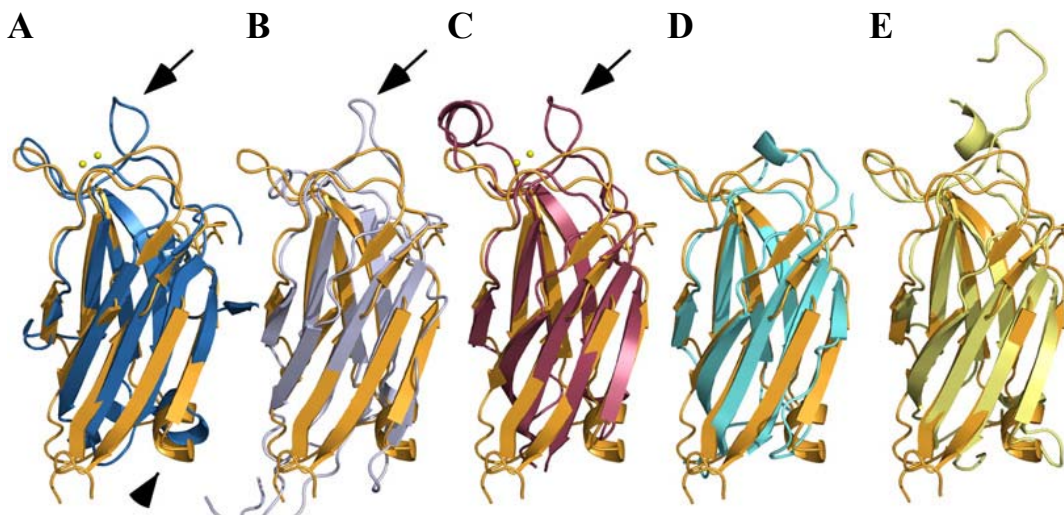


Figure 24: Alignments of the structure of Otof-C₂A with the structures of other C₂-domains. Helfmann *et al.*, 2011.

The arrows point at the extended loop in the Ca²⁺-binding region of the respective C₂-domain.

A: Alignment of structures of Otof-C₂A (orange) with PKCα-C₂ (dark blue).

B: Alignment of structures of Otof-C₂A (orange) with Myof-C₂A (pale blue).

C: Alignment of structures of Otof-C₂A (orange) with Munc13-1-C₂B (red).

D: Alignment of structures of Otof-C₂A (orange) with Munc13-1-C₂A (turquoise).

E: Alignment of structures of Otof-C₂A (orange) with PKCε-C₂ (yellow).

• Results •

For titration with CaCl_2 (5 mM in Chelex100®-treated buffer A), Syt1- C_2A (80 μM) was used as positive control: with every injection of CaCl_2 to the sample of Syt1- C_2A , heat is consumed (endothermic reaction; Fig. 25A).

The reaction becomes stronger with the first few injections and then gets weaker, until saturation begins (Fig. 25A). Otof- C_2A was titrated with the same parameters. In contrast to the experiment with Syt1- C_2A , in the titration of Otof- C_2A no heat is released or consumed (Fig. 25B). Prior to this study, the titration of Otof- C_2A was done once by Anand Radhakrishnan with the same result.

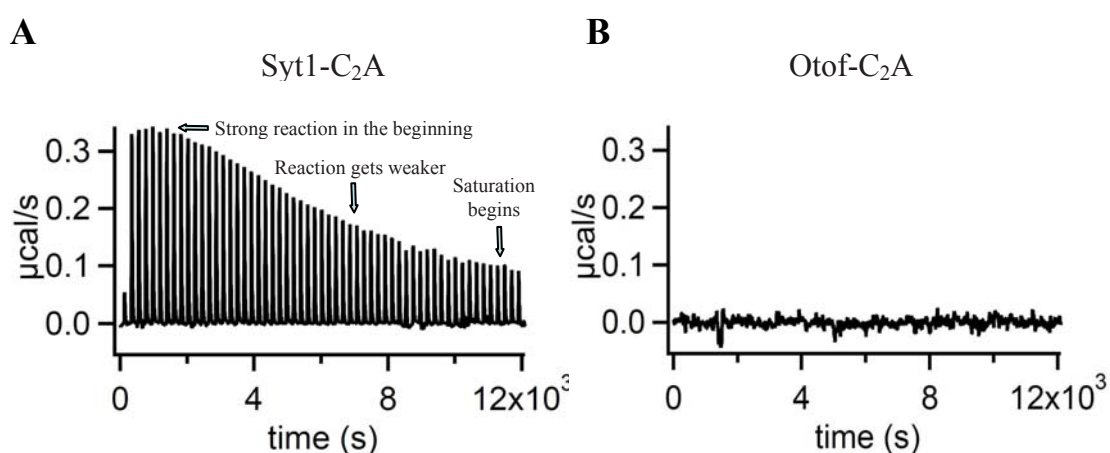


Figure 25: Isothermal titration calorimetry (ITC) with Otof- C_2A and Ca^{2+} . Helfmann *et al.*, 2011.

A: Titration curve for Syt1- C_2A (80 μM) with 5 mM CaCl_2 . 2 μl in first injection, 5 μl in 56 further injections.

B: Titration curve for Otof- C_2A (80 μM) with 5 mM CaCl_2 , injections as in A.

Another biochemical assay was used to study the Ca^{2+} -binding ability of Otof- C_2A : in CD-spectroscopy, the behavior of a protein to absorb circularly polarized light in the UV-range is studied. Here, protein was diluted to $\sim 5 \mu\text{M}$ concentration in 200 μl total volume of Chelex100®-treated buffer A in absence (+ 100 μM EDTA) or presence (+ 100 μM CaCl_2) of Ca^{2+} -ions. In a 200 μl cuvette, an ellipticity spectrum was recorded and plotted between 180 nm and 260 nm (Fig. 26). Syt1- C_2A was used as a positive control to test changed in the CD-spectrum upon Ca^{2+} -binding (Fig. 26A). The spectra of Syt1- C_2A show a minimum at about 220 nm and one around 195 nm, while there is a relative maximum of the curve at about 205 nm. At this point, a difference between the spectra with and without Ca^{2+} is visible: in absence of

• Results •

Ca²⁺-ions, the maximum at 205 nm is significantly lower (paired T-Test resulted in p-values below 0.005 between 201 nm and 214 nm).

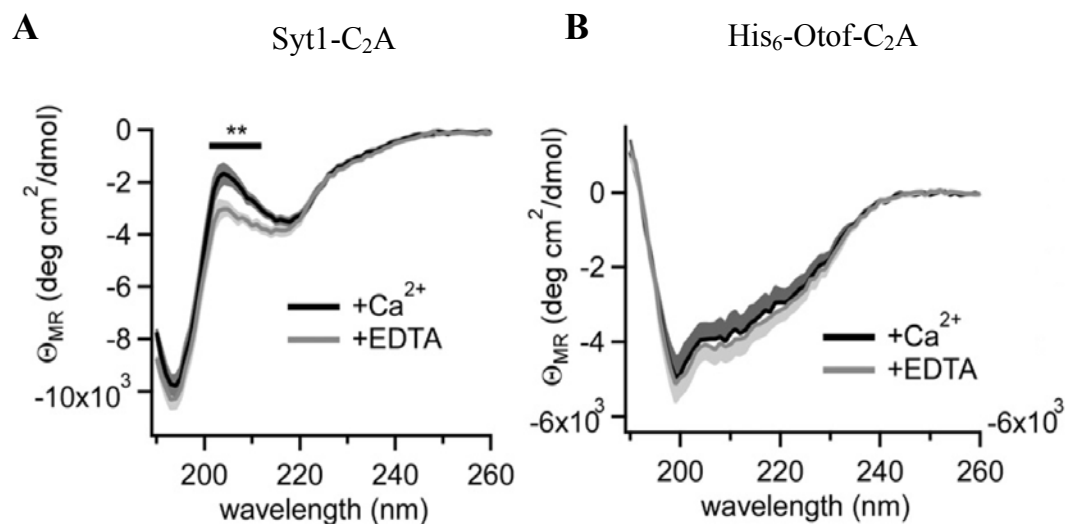


Figure 26: CD-spectroscopy of His₆-Otof-C₂A in presence and absence of Ca²⁺.

Helfmann *et al.*, 2011.

A: Syt1-C₂A spectra +Ca²⁺/+EDTA. Error bars marked in grey behind continuous lines. **B:** Otof-C₂A spectra +Ca²⁺/+EDTA. Error bars marked in grey behind continuous lines.

By contrast, His₆-Otof-C₂A shows similar traces for the experiments in the presence and absence of Ca²⁺-ions. In general, the spectra look different from those of Syt1-C₂A: there is one minimum at ~200 nm, and no maximum similar to the one in the Syt1-C₂A-domain (Fig. 26B). Evaluation of the His₆-Otof-C₂A data with *CDNN* (Böhm *et al.*, 1992) gave the following ratios of secondary structure in solution: ~45-50% β-sheet, ~10-15% alpha-helix and ~25-30% random coil. Analysis of the crystal structure of His₆-Otof-C₂A with *Promotif* (Hutchinson and Thornton, 1996) led to slightly different results: 63.50% β-sheet, 4.80% alpha-helix and 31.70% other (random coil, turns etc.). Possibly, one or more β-strands are to some extent unfolded in solution, while in the crystal structure they are stabilized via polar contacts between the molecules (3.1.1, Fig. 18). Here, especially the closer interaction of T47 and R49 in β-strand 4 with β-strand 4 of the neighbor molecule could play an important role in stabilization of the crystal packing.

Two conclusions can be drawn from the biochemical data: first, ITC and CD-spectroscopy indicate that Otof-C₂A does not bind to Ca²⁺. Second, CD-spectroscopy shows that Otof-C₂A and Syt1-C₂A, though both are from the same family of domains, differ in their CD-spectrum in solution.

4.1.4 Binding of small signal molecules

As Otof-C₂A is positively charged in its putative Ca²⁺-binding region, it was tested whether it could bind to small negatively charged signal molecules. For this test, AMP, cAMP, ATP and IP₃ were chosen.

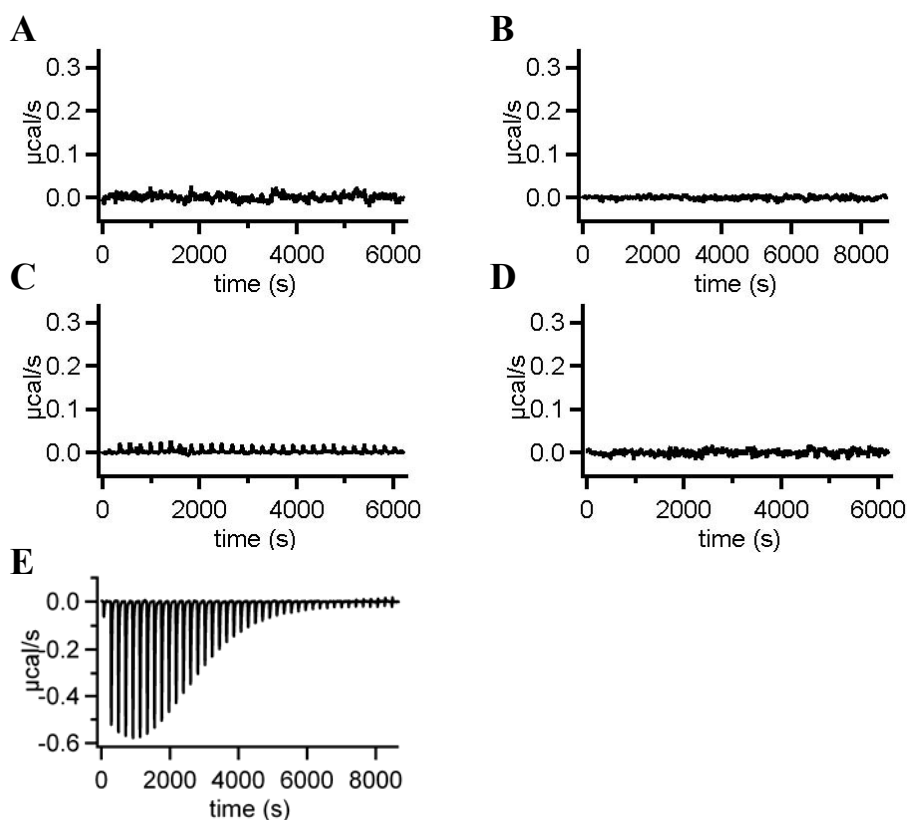


Figure 27: Binding of small signal molecules in ITC experiments.

A: Titration of 17-12 μM Otof-C₂A with 500 μM IP₃.

B: Titration of 17-12 μM Otof-C₂A with 500 μM cAMP.

C: Titration of 17-12 μM Otof-C₂A with 500 μM ATP.

D: Titration of 17-12 μM Otof-C₂A with 500 μM AMP.

E: Titration of 0.25 μM *Archaeoglobus fulgidus*-GlnK2 with 1.5 mM ADP (positive control; Helfmann *et al.*, 2010).

17-25 μM of Otof-C₂A and 500 μM of ligand molecule were used to detect a binding event via ITC. Under the tested conditions, none of the mentioned molecules was able to bind to Otof-C₂A (Fig. 27 A-D). As a reference for a protein that binds to ADP, *Archaeoglobus fulgidus*-GlnK2 was chosen (Helfmann *et al.*, 2010).

4.1.5 Phospholipid binding

The phospholipid-binding behavior of Otof-C₂A was tested using floatation assays. For this, liposomes are produced from defined lipid mixtures via gel filtration and added to protein solution. After a long, fast centrifugation in a Nycodenz-gradient, the liposomes float to the upper phase of the experimental tube and take potentially bound protein with them.

To test phospholipid-binding for Otof-C₂A, several lipid mixes were used (Table 4). Three of them were artificially produced and contain

1. 0% PS and 0% PIP₂
2. 16% PS and 0% PIP₂
3. 16% PS and 1.6% PIP₂.

Experiments with liposomes formed from the first three mixtures were done to clarify the question whether Otof-C₂A binds to liposomes (only) in presence of the anionic phospholipid PS, like for other C₂-domains like Syt1-C₂A or PKC γ -C₂. Also, it needed to be clarified whether binding is enhanced in presence of PIP₂, which was found for example for Syt1-C₂B (for review see Cho and Stahelin, 2006).

As a fourth lipid mixture, a natural total brain lipid extract was used. It was used to study Otof-C₂A's phospholipid-binding behavior also under more natural conditions, though the brain total lipid extract does not necessarily represent the lipid composition of the inner hair cell plasma membrane. All experiments were done in presence (+ 1 mM CaCl₂) and absence (+ 1 mM EGTA) of Ca²⁺-ions.

In contrast to the previously described ITC- and CD-spectroscopy-experiments, this time also the C₂B-domain of Syt1 was part of the construct of the positive/negative control besides Syt1-C₂A. This was done because Syt1-C₂B is known for Ca²⁺-

• Results •

independent PIP₂-binding with its so called “β-groove” (Schiavo *et al.*, 1996), a positively charged region at the concave face of the β-sandwich (Fukuda *et al.*, 1994) that has been found in many C₂-domains (for review see Cho and Stahelin, 2006). As Syt1-C₂B is known to be hard to purify on its own, it was not used separately but in combination with Syt1-C₂A as Syt1-C₂AB tandem domain.

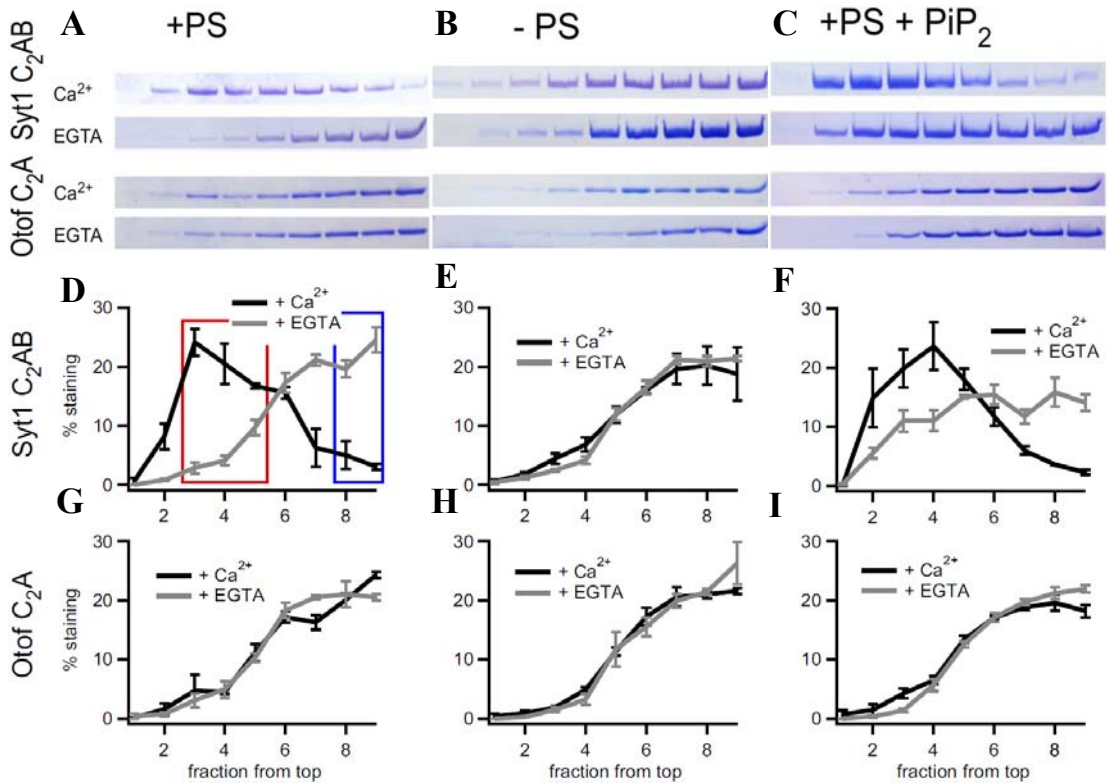


Figure 28: Floatation assays of Otof-C₂A with Syt1-C₂AB as positive control with three different lipid mixtures. Helfmann *et al.*, 2011. Gel pictures: lanes from left to right are the collected fractions from top to bottom of the tube. Graphs show band staining intensities from top to bottom of the tube with mean +/- standard error of the mean (SEM; n=3).

A: SDS-Gel of experiment with liposomes containing PS.

B: SDS-Gel of experiment with liposomes containing no PS.

C: SDS-Gel of experiment with liposomes containing PS and PIP₂.

D+G: Experiment with liposomes containing PS. Syt1-C₂AB (D) and Otof-C₂A (G).

E+H: Experiment with liposomes containing no PS for Syt1-C₂AB (E) and Otof-C₂A (H).

F+I: Graph of experiment with liposomes containing PS and PIP₂ for Syt1-C₂AB (F) and Otof-C₂A (I).

• Results •

For each floatation assay, one 12%-SDS-gel was prepared with the lanes 1-9 containing 10 μ l of the 20 μ l-fractions 1-8 and 10 μ l of the 40 μ l-fraction 9 from top to bottom of the reaction tube.

In presence of PS and Ca^{2+} , Syt1-C₂AB was mainly found in the middle of the gradient (Fig. 28A, first line of gel; Fig. 28D, black trace), while in absence of Ca^{2+} it accumulated in the bottom of the tube (Fig. 28A, second line of gel; Fig. 28D, grey trace). Thus, the Ca^{2+} -dependency of phospholipid-binding of Syt1-C₂AB is confirmed.

In contrast, Otof-C₂A is mainly found in the lower part of the gradient independently of the presence or absence of Ca^{2+} , and was hardly detected in the highest fractions (Fig. 28A, third and fourth line of gel; Fig. 28G).

When liposomes without PS were used, the amount of protein in the upper fractions in Syt1-C₂AB in presence of Ca^{2+} was reduced compared to experiments with PS (Fig. 28B, first and second line of gel; Fig. 28E), so that no difference between the Ca^{2+} - and EGTA-trace was detectable anymore. This means, in absence of PS Syt1-C₂AB does not bind to the liposomes anymore. For Otof-C₂A, the experiment without PS showed no binding of liposomes (Fig. 28B, third and fourth line of gel; Fig. 28H).

Figure 28C displays the results for the experiments with PS and PIP₂: Syt1-C₂AB accumulates in the middle part of the tube in presence of Ca^{2+} (Fig. 28C, first line of gel; Fig. 28F, black trace), but also in absence of Ca^{2+} some protein is detected in the low density fractions (Fig. 28C, second line of gel; Fig. 28F, grey trace). This was expected as Syt1-C₂B was shown to bind to PIP₂ independently of Ca^{2+} with its β -groove. In contrast, Otof-C₂A is found in the bottom of the tube in both experiments (Fig. 28C, third and fourth line of gel; Fig. 28I).

When brain total lipid extract was used in the floatation, both proteins accumulated in the lower fractions (Fig. 29). In presence of Ca^{2+} , around 5% of Syt1-C₂AB appeared in fraction 1, while in presence of EGTA there was no protein at all (Fig. 29A). Brain total lipid extract contains only about two thirds of the amount of PS (10.5%) compared to the 16%-PS-mixtures. As Syt1-C₂AB preferentially binds to the anionic phospholipid PS, this could be a reason for the little binding of the protein. The distribution of Otof-C₂A in the gradient shows no difference in presence and absence of Ca^{2+} (Fig. 29B).

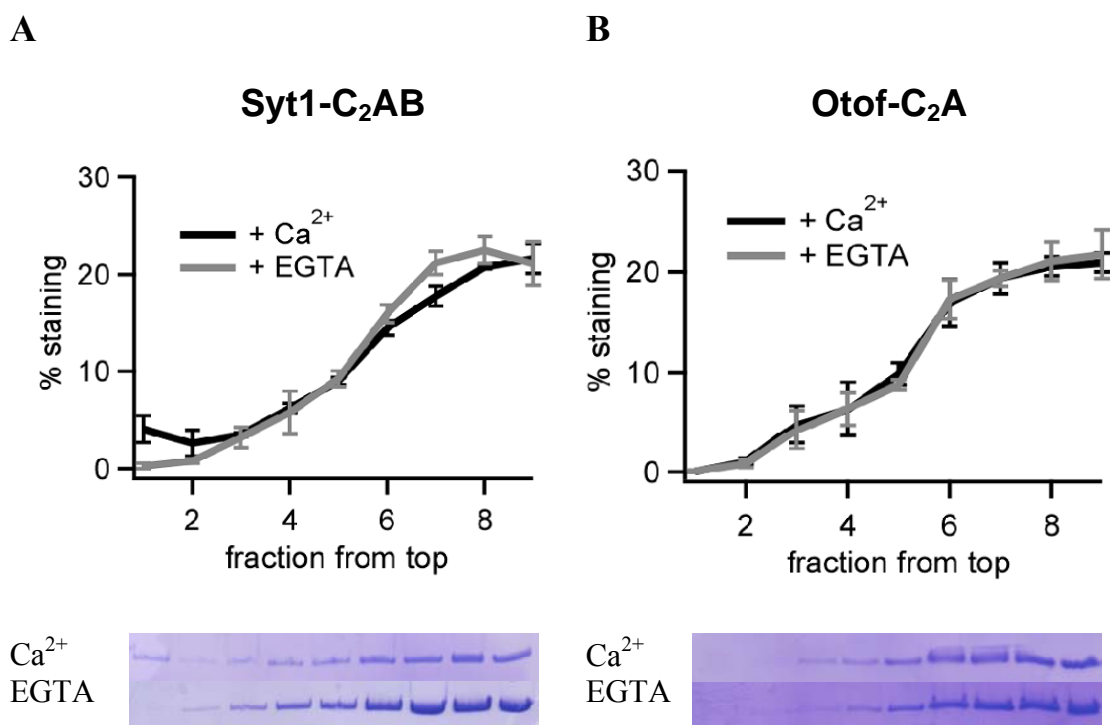


Figure 29: Flootation assays of Otof-C₂A and Syt1-C₂AB with brain total lipid extract. Helfmann *et al.*, 2011. Graph shows band staining intensities from top to bottom of the tube with mean +/- SEM (three experiments). Gel shows distribution of protein in the tube from left to right = top to bottom.
A: Syt1-C₂AB.
B: Otof-C₂A.

Summarizing, Otof-C₂A did not bind to liposomes with four different lipid compositions, independently from the presence or absence of Ca²⁺-ions. Presence of PS or PIP₂ in the liposomes, which enhanced the lipid-binding affinity of Syt1-C₂AB, could not render Otof-C₂A phospholipid-binding.

4.1.6 Mutant Otof-C₂A

As mentioned in chapter 4.1.3, Otof-C₂A has contains only one of the five aspartates believed to be involved in Ca²⁺-binding. Instead, three aspartates are replaced by asparagine (N68), serine (S70) and lysine (K76), while the fifth aspartate misses an equivalent as the extension of loop 1 where it would be positioned is not present in Otof-C₂A. To study the question whether Otof-C₂A would bind to Ca²⁺-ions if the

• Results •

five aspartates were present, the three amino acids N68, S70 and K76 were mutated to aspartates D68, D70 and D76 via mutagenesis (3.1.1). A17 is located close to the missing loop-extension and pointing towards the putative binding pocket. To compensate for the fifth aspartate, it was mutated to aspartate D17.

ITC-measurements with CaCl_2 titration were repeated for Otof-5D-C₂A with the same parameters as for WT protein. The mutant was not binding Ca^{2+} -ions under the tested conditions (Fig. 30A). CD-spectroscopy was done as for WT protein. The spectra of WT and mutant did not significantly differ. Also, the curve of Otof-5D-C₂A recorded in the presence of Ca^{2+} looked the same as the in absence of Ca^{2+} (Fig. 30B). Together, the biochemical data reveal that Otof-5D-C₂A is unable to bind Ca^{2+} .

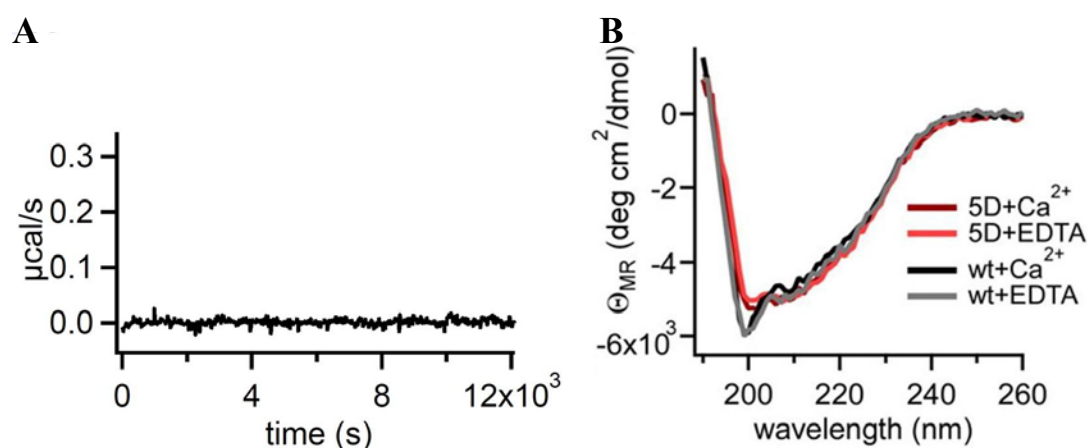


Figure 30: Biochemical data for Otof-5D-C₂A. Helfmann *et al.*, 2011.

A: ITC titration of Otof-5D-C₂A with CaCl_2 .

B: CD-spectra of Otof-5D-C₂A (dark red/bright red) +/- Ca^{2+} , overlay with Otof-WT-C₂A (black/grey).

To clarify the question whether Otof-5D-C₂A binds to phospholipids, the floatation assay experiments were repeated for this protein.

The result resembles that of Otof-WT-C₂A (Fig. 31): no or only little binding to phospholipids was detected. The presence or absence of PS/PIP₂/ Ca^{2+} did not make any difference in the phospholipid-binding affinity of Otof-5D-C₂A.

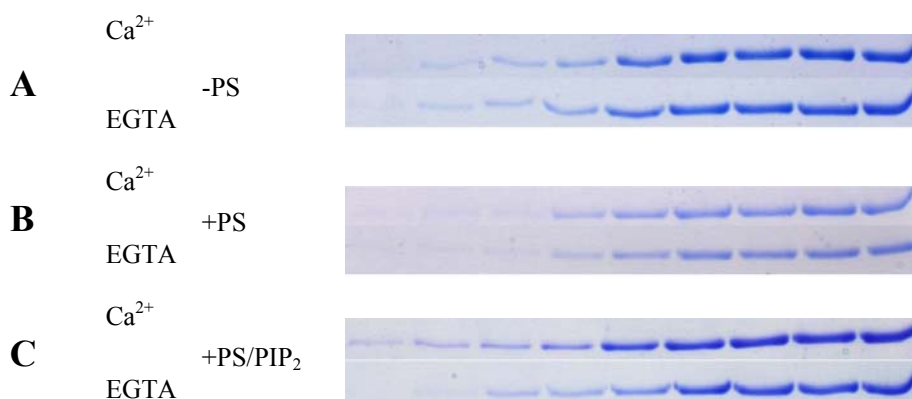


Figure 31: Flootation assay of Otof-5D-C₂A with three different lipid mixes.

Lanes from left to right: fractions from top to bottom of the reaction tube.

A: SDS-gels with Ca²⁺/EGTA in absence of PS.

B: SDS-gels with Ca²⁺/EGTA in presence of PS.

C: SDS-gels with Ca²⁺/EGTA in presence of PS and PIP₂.

4.2 Purification of otoferlin's single C₂-domains besides Otof-C₂A

4.2.1 Molecular cloning and preparation

Prior to this study, several different constructs have been prepared and tested in different vectors: first, the five C₂-domains (C₂B-C₂F) were subcloned to pET28a-vector (His₆-tagged) by Astrid Zeuch and Nina Dankenbrink-Werder (Max-Planck-Institute for Experimental Medicine, Goettingen, Germany). The constructs were tested by Kirsten Reuter (Otorhinolaryngology, Georg-August-University Goettingen, Germany) and Anand Radhakrishnan (Max-Planck-Institute for Biophysical Chemistry, Goettingen, Germany). The C₂-domains were expressed in small scale by *E. coli* BL21(DE3) cells, but could not be purified sufficiently. Kirsten Reuter further subcloned C₂B and C₂F to pET44a (Nus-tagged) to improve solubility of the domains. She did expression and purification tests in *E. coli* BL21(DE3) cells. It was not possible to purify the proteins sufficiently from background impurities.

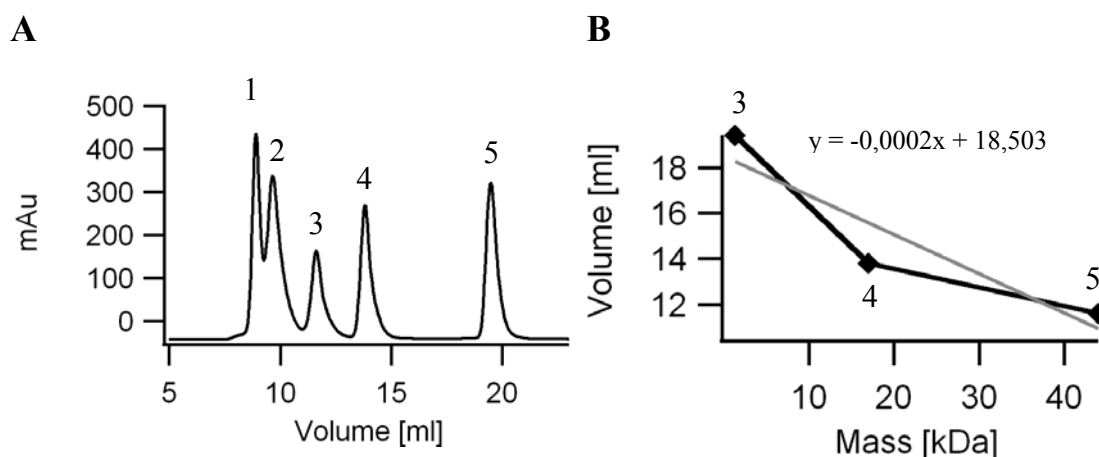


Figure 32: Calibration of Superdex 75 10/300 gel filtration column.

A: Chromatogram of gel filtration standard eluting from Superdex 75 10/300.

1: thyroglobulin (bovine); 670 kDa.

2: γ -globulin (bovine); 158 kDa.

3: ovalbumin (chicken); 44 kDa.

4: myoglobin (horse); 17 kDa.

5: vitamin B12; 1,35 kDa.

B: Calibration curve with trendline for ovalbumin, myoglobin and vitamin B12.

In the beginning of this study, the five C₂-domains had been subcloned to pGEX-6P-3-vector (GST-tagged). This was done because the GST-tag produced from the vector DNA N-terminal to the target protein was believed to improve overexpression, solubility and purification of the latter.

Prior to the experiments, a calibration curve was produced for the Superdex 75 10/300 gel filtration column (Fig. 32) to obtain the retention volumes for C₂-domains expected to elute as monomers from the column. Besides this column, also a Superdex 75 16/60 was used, for which a calibration curve already existed (produced by the Department for Molecular Structural Biology, Goettingen).

4.2.2 Expression and solubility

Expression tests with the five GST-tagged C₂-domains were done in *E. coli* BL21(DE3) cells on LB liquid medium (Bertani, 1951) with good success (Fig. 33A). Several media were tested for best expression results for Otof-GST-Otof-C₂F

• Results •

(LB-medium, TB-medium (Sambrook *et al.*, 1989), 2YT-medium (Sambrook *et al.*, 1989), auto-induction medium (Studier, 2005)).

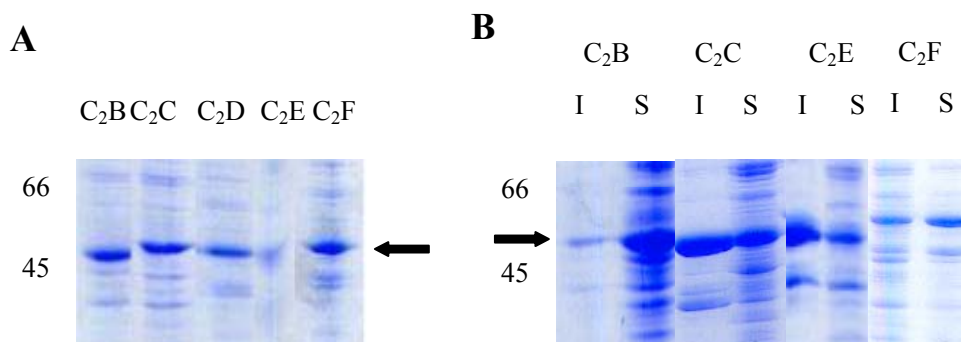


Figure 33: Expression and solubility tests with the Otof-C₂-domains.

A: SDS-gel showing the results of the expression tests in *E. coli* BL21(DE3) cells on LB liquid medium with the GST-tagged C₂-domains. The pellet of 1 ml of culture 12-16 hours after induction was resuspended in 20*(OD₆₀₀/0.1) μ l water. 20 μ l were loaded on the gel. Sizes of GST-tagged C₂-domains vary between 49 kDa and 55 kDa.

B: SDS-gel showing the results of the solubility test with GST-Otof-C₂B, GST-Otof-C₂C, GST-Otof-C₂E and GST-Otof-C₂F. Cells were resuspended in the purification buffer, broken by sonication and centrifuged for 5 minutes. The resulting pellet and supernatant were loaded on an SDS-gel, where supernatant represents the soluble part.

I = insoluble. S = soluble. Sizes vary between 49 kDa and 55 kDa.

Here, the 2YT-medium was found to be the best medium (data not shown), which was used for all overexpressions with the five C₂-domains from that time on. Next, the solubility of all C₂-domains was tested via centrifugation after cell disruption. For the GST-Otof-C₂B-, GST-Otof-C₂C-, GST-Otof-C₂E and GST-Otof-C₂F-domains, at least partial solubility was detected (Fig. 33B), so that the purification could be proceeded with them.

After cell destruction and centrifugation at 21.280 g, GST-Otof-C₂D remained in the pellet under the conditions tested (buffer: 150 mM NaCl, 20 mM Tris pH 7.4). No GST-Otof-C₂D was detected in the supernatant containing the soluble protein fraction via SDS-PAGE (Fig. 34C). This indicates that GST-Otof-C₂D is most likely un- or misfolded. To solve this problem, a purification protocol from inclusion bodies including unfolding with 6 M guanidine hydrochloride and fast refolding with

• Results •

1 M NDSB 201 was performed. However, this did not yield in functional monomeric protein (as monitored by gel filtration, Fig. 34A&B).

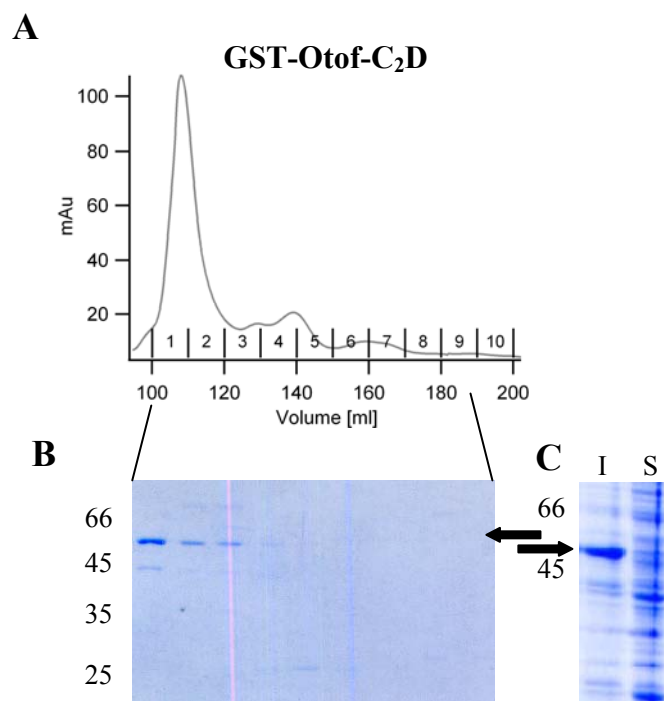


Figure 34: Solubility and purification of Otof-C₂D.

A: Gel filtration of GST-Otof-C₂D after unfolding with 6 M Guanidine HCl and refolding with NDSB 201.

B: SDS-gel of C₂D from A: the nine lanes correspond to the nine fractions in A.

C: Solubility test with GST-C₂D (done as described in Fig.33B). I = insoluble. S = soluble.

4.2.3 Affinity purification and size exclusion

For three soluble C₂-domains, GST-Otof-C₂B, -C₂C and -C₂F, affinity purification was performed using 5 ml GSTrapTM 4B columns. The protein amounts eluting from the column after washing with 30 mM glutathione-buffer were as high as that of His₆-Otof-C₂A on HisTrap FF crude columns, meaning the yield was more than sufficient to proceed with the protocol. Over night at 4°C, the GST-tag was cut off with help of PreScission Protease.

• Results •

Next, correct folding, required for a monomeric protein to be soluble, was tested by gel filtration. The three domains eluted with the exclusion volume of Superdex 75 16/60 and Superdex 75 10/300 columns when using standard conditions with buffers containing 150 mM NaCl and 20 mM Tris pH 7.4 (Fig. 36A&C, example of C₂F). This means, the C₂-domains were at least partly not properly folding and thus aggregated. Several different conditions (buffer: 0/300/500 mM NaCl, 20 mM Tris pH 7.4; +5% ethanol; +20 mM CaCl₂; +10 μM ATP) were tried with no better result (Fig. 35A&C, example of Otof-C₂C purified with 500 mM NaCl in the buffer). For none of the three C₂-domains, sufficient purity could be achieved (Fig. 35B&C, example of Otof-C₂C) to start biochemical experiments.

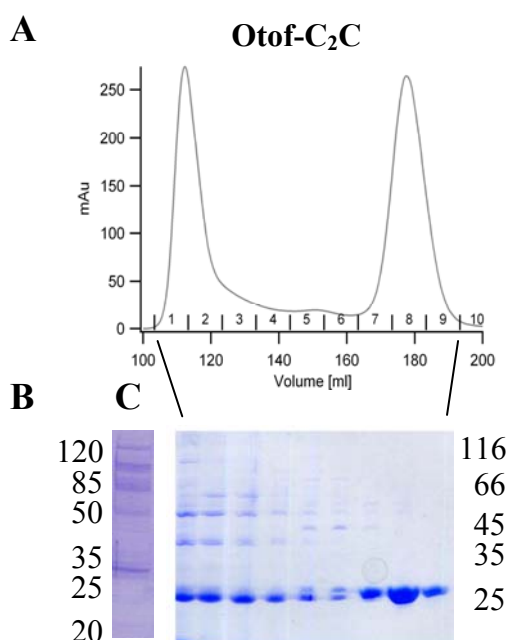


Figure 35: Purification of Otof-GST-C₂C and Otof-C₂C-His₆.

A: Gel filtration (equilibration in buffer A) with C₂C after cut-off of GST-tag. Column: Superdex 75 16/60.

B: SDS-gel of C₂C (pET21a) after affinity purification and gel filtration.

C: SDS-gel of C₂C from A: nine lanes correspond to nine fractions in A. Arrow points to double-band: meant is lower band.

4.2.4 Attempt to solve purification problems: cloning of new constructs

To solve the purification problems of the C₂-domains of otoferlin, more constructs were subcloned into pET28a, pET21a and pGEX-6P-3 (Table 1). The theory behind this is that a few amino acids shorter or longer in N- or C-terminus of a C₂-domain might make a difference for its folding. As C₂B, C₂C and C₂F were not folding properly, preparing new constructs was the strategy of choice.

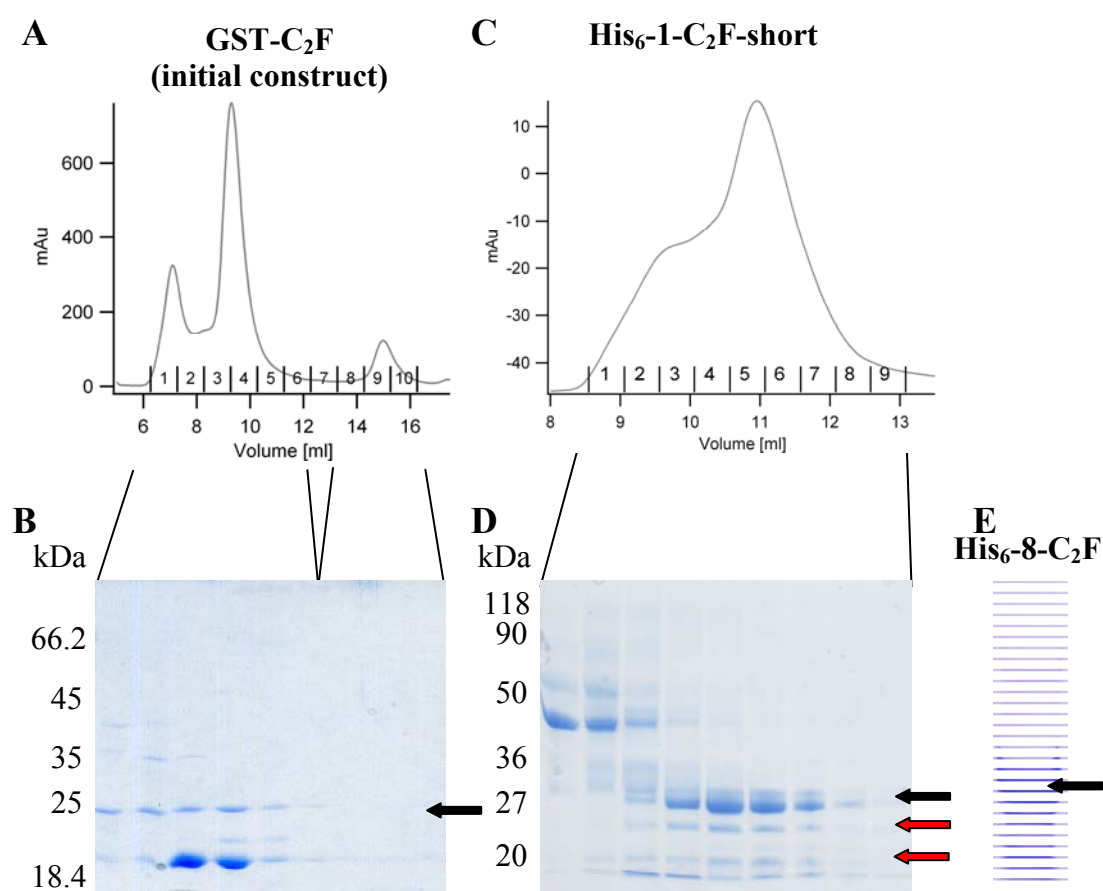


Figure 36: Three examples of purifications of Otof-C₂F.

A: Gel filtration (equilibration in buffer A) with C₂F after cut-off of GST-tag. Column: Superdex 75 10/300.

B: SDS-gel of C₂F: nine lanes correspond to nine fractions in A. Arrow points to full length Otof-C₂F.

C: Gel filtration (equilibration in buffer A) with His₆-1-C₂F-short. Column: Superdex 75 10/300.

D: SDS-gel of His₆-1-C₂F-short: nine lanes correspond to nine fractions in C. Black arrow points to full length Otof-C₂F. Red arrows point to C₂F-fragments.

E: SDS-gel of His₆-8-C₂F after gel filtration. Arrow points to full length Otof-C₂F.

• Results •

In detail, for Otof-C₂F, seven new constructs differing in lengths were subcloned into pGEX-6P-3-vector, two of them also in pET28a-vector (His₆-tagged) (Table 5&6). For all constructs tested, shorter fragments than expected appeared on SDS-PAGE in addition to the full domain (Fig. 36D, example of His₆-1-C₂F-short), independently of the tag used. They have been identified as short C₂F-fragments by mass spectroscopy in the laboratory of Dr. Olaf Jahn, MPI for experimental Medicine, Goettingen. These fragments could match degradation products or result from incomplete translation processes. As revealed by gel filtration, the size of the C₂F-molecules identified on SDS-PAGE (Fig. 36D) relate to a higher molecular weight than expected for a monomer (Fig. 36C, ~37.5 kDa instead of 22.6 kDa). This is compatible with the size of one full length C₂F-monomer plus one degradation product sticking to it.

Nevertheless, as the Otof-His₆-1-C₂F accounted for majority of protein in solution, crystallization was tried with the crystal screens JB 1, 2, 4, 5, 6, 7, 8 and 10. The same was done for Otof-His₆-1-C₂F-short with the crystal screens ProPlex screen, JCSG screen, Ammonium sulphate screen, and JB screens 1, 2, 4, 5, 6, 7, 8 and 10. No crystal developed in any of the conditions.

Table 6: Variety of short constructs of Otof-C₂F. Numbers 1-8 correspond to construct-numbering for C₂F-constructs in Table 7. Affinity tags are specified in Table 7. Yellow marks β-strand.

	1.Strand	2.-8.Strand
1:	EQGRLELWVDMFPMDMPAPGT...P	-----LNRFPFGAKTAKQCTMEMATGEV
2:	EQGRLELWVDMFPMDMPAPGT...P	-----LNRFPFGAKTAKQCTMEM
3:	EQGRLELWVDMFPMDMPAPGT...P	-----LNRFPFGAKTAKQCTMEMATGEVDVPLVSI FKQKR VKGWWPLLA
4:	NPKPGIEQGRLELWVDMFPMDMPAPGT...P	-----LNRFPFGAKTAKQCTMEMATGEV
5:	NPKPGIEQGRLELWVDMFPMDMPAPGT...P	-----LNRFPFGAKTAKQCTMEM
6:	PAPGT...P	-----LNRFPFGAKTAKQCTMEM
7:	PAPGT...P	-----LNRFPFGAKTAKQCTMEMATGEVDVPLVSI FKQKR VKGWWPLLA
8:	T...P	-----LNRFPFGAKTAKQCTMEMATGEVDVPLVSI FKQKR

... = PLDISPRK

For Otof-C₂C, two new constructs were subcloned into pGEX-6P-3: one of them shorter and one of them longer than the initial construct (Table 7). Both were not expressed in *E. coli* BL21(DE3) cells. One construct was prepared with the same oligonucleotides that had been used for pGEX-6P-3-vector, but in pET21a. This construct was expressed by bacteria in low amounts, but purity could not be achieved (Fig. 35B).

• Results •

Besides cloning new constructs and using the standard purification protocol which was also used for Otof-His₆-C₂A (3.3.1 + 3.3.3), also other buffer components were used in the purification (see 3.11) with no difference in the behavior of the C₂-domains on gel filtration columns.

Table 7: Available constructs of single, tandem- and triple C₂-domains of otoferlin.

Cloned by Kirsten Reuter*, Astrid Zeuch & Nina Dankenbrink-Werder^o, Nina Dankenbrink-Werder[†].

Name	Plasmid	Otof amino acid sequence	Organisms	Restriction enzymes	Primer
His ₆ -C ₂ A ^o	pET28a	1-124	Rat	NdeI/EcoRI	11442/11443
GST-C ₂ B*	pGEX-6P-3	216-414	Rat	SmaI/XhoI	C ₂ B-BamHI_for/C ₂ B-EcoRI_rev
GST-C ₂ C	pGEX-6P-3	409-572	Rat	BamHI/EcoRI	C ₂ C-BamHI_for/C ₂ C-EcoRI_rev
GST-C ₂ C short	pGEX-6P-3	424-561	Mouse	BamHI/EcoRI	15763/15764
GST-C ₂ C long	pGEX-6P-3	377-601	Mouse	BamHI/EcoRI	15765/15766
C ₂ C-His ₆	pET21a	BL21(DE3)	Mouse	NdeI/XhoI	16029/16030
His ₆ -C ₂ C2-His ₆	pET28a	BL21(DE3)	Mouse	NdeI/XhoI	18982/18983
GST-C ₂ D*	pGEX-6P-3	923-1151	Rat	BamHI/EcoRI	C ₂ D-BamHI_for/C ₂ D-EcoRI_rev
GST-C ₂ de short	pGEX-6P-3	1148-1251	Mouse	BamHI/EcoRI	17064/17065
His ₆ -C ₂ de short	pET28a	1148-1251	Mouse	NdeI/EcoRI	19055/20689
His ₆ -C ₂ de long	pET28a	1135-1264	Mouse	NdeI/EcoRI	20976/20977
GST-C ₂ E*	pGEX-6P-3	1434-1657	Rat	BamHI/EcoRI	C ₂ E-BamHI_for/C ₂ E-EcoRI_rev
His ₆ -C ₂ A-C ₂ B	pET28a	1-413	Mouse	NdeI/EcoRI	14894/14895
GST-C ₂ A-C ₂ C	pGEX-6P-3	1-600	Mouse	BamHI/EcoRI	14894/14896
GST-C ₂ A-C ₂ C-His ₆	pGEX-6P-3	1-600	Mouse	BamHI/EcoRI	16028/15733
GST-C ₂ D-C ₂ F	pGEX-6P-3	908-1932	Mouse	BamHI/EcoRI	14897/14899
GST-C ₂ E-C ₂ F	pGEX-6P-3	1433-1927	Mouse	BamHI/EcoRI	C ₂ E-BamHI_for/14899
GST-C ₂ E-C ₂ F-His ₆	pGEX-6P-3	1433-1927	Mouse	BamHI/EcoRI	14188/15969
GST-C ₂ F*	pGEX-6P-3	1689-1928	Rat	BamHI/EcoRI	C ₂ F-BamHI_for/C ₂ F-EcoRI_rev
GST-1-C ₂ F [†]	pGEX-6P-3	1700-1873	Mouse	BamHI/EcoRI	16783/16786
His ₆ -1-C ₂ F-short	pET28a	1700-1873	Mouse	NdeI/EcoRI	19807/16786
His ₆ -1-C ₂ F	pET28a	1700-1873	Mouse	BamH/EcoRI	16783/16786
GST-2-C ₂ F [†]	pGEX-6P-3	1700-1868	Mouse	BamHI/EcoRI	16783/16787
GST-3-C ₂ F [†]	pGEX-6P-3	1700-1894	Mouse	BamHI/EcoRI	16783/16788
GST-4-C ₂ F [†]	pGEX-6P-3	1693-1873	Mouse	BamHI/EcoRI	16784/16786
GST-5-C ₂ F [†]	pGEX-6P-3	1693-1868	Mouse	BamHI/EcoRI	16784/16787
GST-6-C ₂ F [†]	pGEX-6P-3	1716-1868	Mouse	BamHI/EcoRI	16785/16787
GST-7-C ₂ F [†]	pGEX-6P-3	1716-1894	Mouse	BamHI/EcoRI	16785/16788

• Results •

His ₆ -8-C ₂ F	pET28a	1720-1885	Mouse	NdeI/EcoRI	22140/22141
GST-Otof-minusTM	pGEX-6P-3	1-1953	Mouse	EcoRI/NotI	14188/14189
GST-Otof-minusTM- His ₆	pGEX-6P-3	1-1953	Mouse	HindIII/NotI	15220/15490
GST-Otof-minusTM- Linker-His ₈	pGEX-6P-3	1-1953	Mouse	HindIII/NotI	15717/15718

4.3 Expression and purification of Otof-tandem/triple-C₂-domains

For Syt1-C₂B, purification problems because of sticky impurities had been observed earlier (Ubach *et al.*, 2001). This problem could be overcome by using the Syt1-C₂AB-tandem-domain, like in this study. Hoping that also Otof-C₂-domains would fold better, longer constructs containing two or three C₂-domains were produced for overexpression and purification.

After small scale expression in 2YT-medium, GST-Otof-C₂ABC, GST-Otof-C₂EF and GST-Otof-C₂DEF (the latter including two mutations: I949N, L1913Q; Table 7) were loaded on 12%-SDS-gels and transferred to PVDF-membranes for expression tests. Using the Anti-GST-tag antibody for GST-Otof-C₂EF and GST-Otof-C₂DEF and the Anti-otoferlin antibody (N-terminus of otoferlin) for GST-Otof-C₂ABC, the expression products were detected on Western Blots with the NBT/BCIP method (Fig. 37D). His₆-Otof-C₂AB was not blotted but just detected on a 12%-SDS-gel (Fig. 37B).

His₆-Otof-C₂AB could be purified with its N-terminal His₆-tag on a HisTrap FF crude column (Fig. 37B), but was completely accumulating in the exclusion volume of the Superdex 200 10/300 gel filtration column (Fig. 37A&C), meaning the protein was not properly folded. Still, crystallization of His₆-Otof-C₂AB was tried with Crystal Screen I, but no crystals developed.

For GST-Otof-C₂ABC, GST-Otof-C₂EF and GST-Otof-C₂DEF, affinity purifications were performed with the appropriate GSTrapTM 4B columns. All of them precipitated at some point during the purification protocol. However, this has only been tried once and might have to be repeated with different conditions.

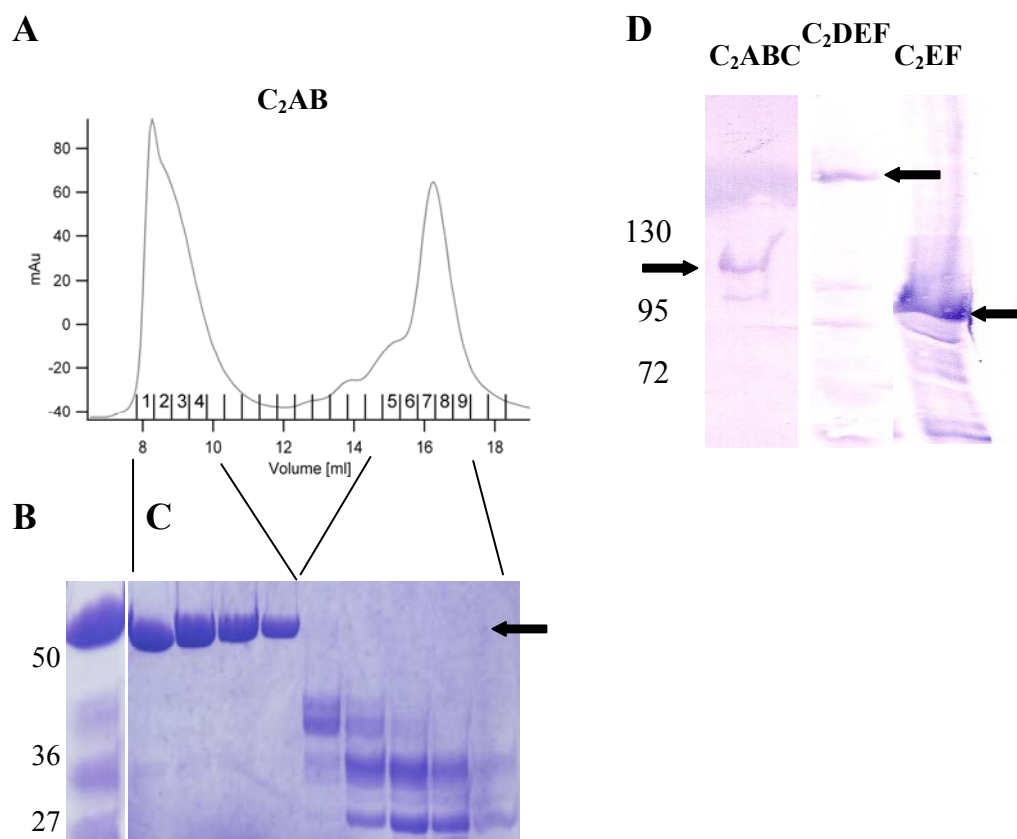


Figure 37: Expression and purification of tandem- and triple-C₂-domains.

A: Gel filtration (equilibration in buffer A) with His₆-C₂AB. Column: Superdex 200 10/300.

B: SDS-gel of crude lysate of His₆-C₂AB after overexpression in *E. coli*.

C: SDS-gel of His₆-C₂AB: nine lanes correspond to nine fractions in A.

D: Western Blot of expression tests of GST-C₂ABC (Anti-otoferin antibody), GST-C₂DEF and GST-C₂EF (both Anti-GST-tag antibody).

As during this purification it was hardly possible to identify the tandem- and triple-domains on SDS-gels, a His₆-tag was cloned to the C-terminus of GST-Otof-C₂ABC and GST-Otof-C₂EF to further facilitate purification. Both tags were used for purification in sequence, meaning first it was taken advantage of the C-terminal His₆-tag using HisTrap FF crude columns, afterwards the proteins were supposed to be further purified via the N-terminal GST-tag. For GST-Otof-C₂EF-His₆, this did not yield in success, the protein still precipitated. The work with GST-Otof-C₂ABC-His₆ is currently continued.

4.4 Expression and purification of full length otoferlin without transmembrane domain

In order to study the Ca^{2+} - and phospholipid-binding behavior of whole otoferlin, constructs of the full length protein missing the transmembrane (TM)-domain (Otof- Δ TM) were prepared for overexpression in *E. coli* (Table 7).

Expression tests with full length protein in pGEX-6P-3, with and without C-terminal His₆-tag, were conducted in *E. coli* BL21(DE3), BL21(DE3)Star and Rosetta2 cells. The success was monitored by Western Blot (Anti-GST-tag and Anti-His₅-tag antibodies). With the Anti-GST-tag antibody, GST-Otof- Δ TM could be detected in various sizes up to 250 kDa (Fig. 38), meaning either *E. coli* was able to produce fragments of the protein, but stopped translation at many points in the amino acid sequence, or the protein was degraded after expression very fast.

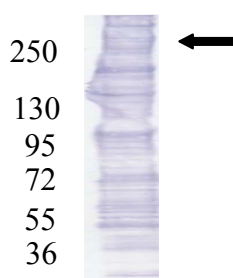


Figure 38: Western Blot of expression test of GST-Otof- Δ TM (Anti-otoferlin antibody).

After expression tests with Rosetta2 cells on 2YT medium with another construct, GST-Otof- Δ TM-His₆, the Anti-His₅-tag antibody was used to find out whether besides truncated versions of the protein also full length protein is produced until the C-terminus. Western Blots did not show any staining with this antibody, indicating that no full length protein was produced until the C-terminal His₆-tag (data not shown).

To reduce the probability that the C-terminal His₆-tag is forming hairpin loops and is thus not properly folding, another construct with a short linker sequence N- and C-terminal to the His₆-tag, including the amino acids proline, alanine and serine, was cloned. However, this did not yield in staining on Western Blots when the Anti-His₅-

• Results •

tag antibody was used (data not shown). For none of the three constructs the Anti-otoferlin antibody showed any staining on a Western Blot.

5. Discussion

5.1 Otof-C₂A

5.1.1 Structure of Otof-C₂A and Ca²⁺-binding behavior

In this study, the most N-terminal C₂-domain of otoferlin, Otof-C₂A, was studied structurally and biochemically.

The overexpression, purification and crystallization of Otof-C₂A worked out reliably/successfully without the need to optimize the strategy/protocols. The protein was produced by the bacteria in amounts sufficient for biochemical experiments. After breaking the cells in the buffer used for purification, the protein accumulated in the fraction representing the cytosolic proteins, as expected. Affinity purification resulted in sufficient protein purity for crystallization. Gel filtration and appropriate SDS-gels showed completely monomeric Otof-C₂A without protein in the exclusion volume, meaning that the purified Otof-C₂A was most likely folded. These evidences for pure and folded protein support the biochemical and structural data measured consecutively.

The structure of Otof-C₂A is the first of an otoferlin C₂-domain that has been solved and studied. Among the ferlin family, only one other structure was solved so far, the one of the C₂A-domain of myoferlin. We found that Otof-C₂A is a full C₂-domain with eight β -strands, contradicting previous predictions (Yasunaga *et al.*, 2000). In agreement with the predictions of Jimenez and Bashir (2007), Otof-C₂A folds as a type II-C₂-domain. This was determined by structural alignments with other C₂-domains (PKC α & PLA2). Otof-C₂A has a positive surface charge in the putative Ca²⁺-binding region and misses four of the five aspartates necessary for Ca²⁺-binding. Overall, the structure does not support Ca²⁺-binding. However, PKC ϵ -C₂ has a negatively charged Ca²⁺-binding region but binds to phospholipids in a Ca²⁺-independent manner (Ochoa *et al.*, 2001), meaning that negative surface charge alone is not a reliable indicator for Ca²⁺-binding.

However, biochemical data collected with ITC and CD-spectroscopy did not show binding of Otof-C₂A to Ca²⁺-ions under the tested conditions and thus confirm the

indications from the structural data. These results match the fluorescence emission spectra presented by Johnson and Chapman (2010), showing also no Ca^{2+} -binding for Otof-C₂A.

Overall, Otof-C₂A is suggested not to be a Ca^{2+} -binding C₂-domain, which is not a rare case: also other non- Ca^{2+} -binding C₂-domains are known (see Cho and Stahelin, 2006 for review). Many of them, like for example PTEN (Lee *et al.*, 1999) or PKC ϵ and η (Sossin and Schwartz, 1993), bind to phospholipids independently from Ca^{2+} . As also signaling, lipid modification, regulation of GTPases, protein phosphorylation and protein-protein interaction are functions attributed to C₂-domains (see Nalefski and Falke, 1996 for review), it might be that Otof-C₂A has another task than Ca^{2+} -sensing or Ca^{2+} -dependent phospholipid-binding.

Otoferlin is commonly believed to be the main Ca^{2+} -sensor in inner hair cells during exocytosis, however acting in a different way than synaptotagmins, which contain only two C₂-domains. Four of the six (or seven) C₂-domains of otoferlin were predicted to be Ca^{2+} -binding (Jimenez and Bashir, 2007), so that it is possible that the Ca^{2+} -sensing function does not involve all C₂-domains in this protein. As stated above, the none- Ca^{2+} -binding domains may fulfill other functions. These might be for example protein-protein interactions, or the domains were developed by domain-duplication and have lost their function by mutations during evolution.

5.1.2 Phospholipid-binding

As C₂-domains are phospholipid-binding domains, the phospholipid-binding behavior of Otof-C₂A was studied with floatation assays using lipid mixes and brain total lipid extract. Under all conditions tested, there was no binding detectable compared to the positive control Syt1-C₂AB. These results contradict the results from a similar experimental approach of Johnson and Chapman (2010) who found Ca^{2+} -independent phospholipid-binding for Otof-C₂A. However, turbidity measurements in the same publication showed no binding of phospholipids to Otof-C₂A in presence and absence of Ca^{2+} -ions. This discrepancy was not further discussed in the study of Johnson and Chapman (2010). As the here presented study consistently shows no binding to phospholipids in presence and absence of Ca^{2+} and

agrees with the turbidity measurements of Johnson and Chapman (2010), it is proposed that the read out of their floatation assays was not reliable. Thus, we assume that the Otof-C₂A-domain does not bind to phospholipids.

5.1.3 Biochemistry of Otof-5D-C₂A mutant

The mutant Otof-5D-C₂A did not behave differently than the WT protein, meaning neither Ca²⁺ - nor phospholipid-binding was restored by replacing four amino acids with aspartates. Thus, providing five aspartates in the Ca²⁺-binding region alone does not suffice to make a C₂-domain Ca²⁺-binding. One possible explanation why the mutated C₂A-domain does not bind to Ca²⁺ lies in the length of top loop 1. As this loop is much shorter in Otof-C₂A than in other C₂-domains which are known to bind Ca²⁺, the appropriate length of this loop might be important to bring the five inserted aspartates in the correct position for Ca²⁺-binding.

5.1.4 Comparison to other proteins: function of Otof-C₂A?

Using *DaliLite*, the closest structural similarities of Otof-C₂A to other proteins were determined: the NMR-solved structure of Myof-C₂A (Nagashima *et al.*, 2DMH on www.pdb.org), another member of the ferlin family present in skeletal and cardiac muscle (Davis *et al.*, 2000), shows the highest structural similarity to Otof-C₂A with a Z-score of 16.0. The function of myoferlin is currently under debate: while some believe it is involved in endocytosis (Bernatchez *et al.*, 2009), others claim a function in muscle development (Doherty *et al.*, 2005) and muscle repair (Demonbreun *et al.*, 2010). Among proteins involved in the presynaptic machinery in the central nervous system, the structure of Munc13-1 C₂B (Tomchick *et al.*, 2010) is most similar to Otof-C₂A with a Z-score of 15.8. Munc13-1 is a synaptic vesicle priming factor (Ashery *et al.*, 2000) containing three C₂-domains. Also the N-terminal C₂-domain of Munc13-1, Munc13-1-C₂A, shows a high similarity to Otof-C₂A with Z=14.4. Munc13-1-C₂A has been shown to either dimerize or to interact with the protein RIM2 (Lu *et al.*, 2006). These similarities between these two C₂-domains suggest a

similar role for both C₂-domains. As Munc13-1-C₂A is a presynaptic priming factor (Augustin *et al.*, 1999), this might support the role of otoferlin in vesicle replenishment at the presynapse, as previously shown in Pangrsic *et al.* (2010). Though Otof-C₂A did not dimerize in size exclusion experiments, it might, like Munc13-1-C₂A, interact with other proteins.

Interestingly, CD-spectra measured with Otof-C₂A look completely different compared to those of Syt1-C₂A. This might be due to more flexible protein folding of Otof-C₂A in aqueous solution like during CD-spectra measurements, while the protein structure is stabilized by polar contacts between the molecules in the crystal packing (contacts of K76 and N105 and T47 and R49). Furthermore, analyzing the similarity of the two with *DaliLite*, the resulting Z-score is only 11.9, meaning Syt1-C₂A is not as similar to Otof-C₂A as Myof-C₂A or Munc13-1-C₂A/B.

To finally clarify the importance of Otof-C₂A, it is planned to inject an otoferlin mutant missing this domain into otocysts of otoferlin knockout mouse embryos and to test the protein function with patch clamp recordings from hair cells.

Moreover, Yeast Two Hybrid experiments with Otof-C₂A are in progress. Currently, a mouse brain cDNA-library and a mouse organ of Corti-library are tested for interaction partners for Otof-C₂A.

5.2 Purification of otoferlin's single C₂-domains besides Otof-C₂A

Manifold problems occurred when working with the Otof-C₂-domains except Otof-C₂A. First, complete insolubility was detected for Otof-C₂D. For the other C₂-domains, only partial solubility could be achieved.

Second, the soluble single C₂-domains, but also tandem- and triple-domains, were aggregated, as indicated by gel filtration. Tandem- and triple-domains also precipitated.

Both problems and also the fact that we could not sufficiently purify any C₂-domain other than Otof-C₂A indicate that the domains were not properly folded and thus could not be crystallized or studied in biochemical assays.

• Discussion •

Thus, it was not possible to compare mutant protein to WT C₂-domains in biochemical assays within this study.

The reason for the purification problems could be that *E. coli* cells were not able to properly fold the C₂-domains. To solve this problem, different expression systems like insect cells or *E. coli* cells specialized on this issue will be used in future experiments.

Table 8: Summary of the progression of the work with the single Otof-C₂-domains.

	C ₂ A His-Tag	C ₂ B GST-Tag	C ₂ C GST-Tag His-Tag	C ₂ D GST-Tag	C ₂ E GST-Tag	C ₂ F GST-Tag His-Tag
Overexpression	😊	😊	😊	😊	😊	😊
Solubility	😊	😊	😊	😞	😊	😊
Monomeric state	😊	😞	😞	😞	No data	😞
Purification	😊	😞	😞	😞	No data	😞
Crystallization	😊	😞	😞	😞	No data	😞
Structure	😊	😞	😞	😞	No data	😞
Biochemistry	😊	😞	😞	😞	No data	😞

Another possibility could be that an optimal construct has not yet been found. Especially for Otof-C₂F, some constructs with differences in starting and ending points of the amino acid sequence were subcloned into different vectors (Table 1&4). To a certain degree, the protein did not accumulate in the exclusion volume of the gel filtration column anymore. However, it also did not appear at the appropriate retention volume corresponding to full length Otof-C₂F, but rather to full length protein plus one degradation product sticking to it. Hence, the protein was probably not correctly folded.

Rare codons that are hard to translate for bacteria could be the reason for degradation products. Again, different organisms like insect cells should be used to bypass this problem. For every organism used for heterologous overexpression, the codon usage will be optimized and synthetic constructs will be subcloned.

Table 7 shows the summary of the achievements concerning the work with the single Otof-C₂-domains.

Interestingly, studies from other laboratories show comprehensive biochemical results with all Otof-C₂-domains. However, as in the studies of Ramakrishnan *et al.* (2009) and Johnson and Chapman (2010) no gel filtration was conducted to assure the monomeric, folded state of the protein, it is unclear whether the C₂-domains in their studies behaved differently than described here. This could concern the results for the interaction studies with all C₂-domains except C₂C in Ramakrishnan *et al.* (2009), and the Ca²⁺- and phospholipid-binding studies with all C₂-domains in Johnson and Chapman (2010). Repeating the purification protocol of Johnson and Chapman (2010) with a construct used in the here presented study, as well as repeating our protocol with the construct used in their study (His₆-8-C₂F, see Table 1), resulted in the same problems: too early elution from gel filtration, indicating that fractions of the domain were sticking to the full domain.

5.3 Expression and purification of Otof-tandem/triple-C₂-domains and full length otoferlin without transmembrane domain

Hoping for better results concerning the purification complex of problems with single C₂-domains, constructs of tandem- and triple-domains and of full length Otof-ΔTM were subcloned and used for expression and purifications. These efforts gave rise to the same set of problems: insolubility and aggregation for the tandem- and triple-domains, lack of overexpression for the full length protein construct. In the future, it will be tried also to overexpress Otof-ΔTM in insect cells, as these cells are known for their ability to produce huge proteins (Otof-ΔTM as GST-fusion-protein: ~250 kDa).

Together, as otoferlin's C₂-domains are hard to express in bacterial cells and difficult to purify and to keep in a folded state, biochemical studies remain are awaiting optimized protocols for producing high quality protein, both regarding the questions whether the C₂-domains of otoferlin bind to Ca²⁺ and to phospholipids, and whether there are changes in mutant C₂-domains. This is important to explain how a single amino acid exchange in this 1997 amino acid protein is able to destroy the whole protein's function, and to build a fundament to help affected people in the future.

6. Summary

Since the necessity of functional otoferlin for normal hearing has been discovered, the role of this protein in inner hair cell exocytosis is subject of intense studies.

In this thesis, the crystal structure of the most N-terminal C₂-domain of otoferlin, Otof-C₂A, was solved and analyzed. Otof-C₂A is a full type II-C₂-domain with eight β-strands and a relatively short top loop one, which in other C₂-domains is part of the Ca²⁺-binding region. Structure-based sequence alignments of Otof-C₂A with other C₂-domains show the absence of four of the five aspartates believed to be necessary for Ca²⁺-binding in C₂-domains. Accordingly, surface charge calculations show a positively charged putative Ca²⁺-binding area. In biochemical and biophysical assays, Otof-C₂A did not bind to Ca²⁺. Together, the results confirm that this domain does not bind Ca²⁺.

As C₂-domains are phospholipid-binding domains, the binding behavior of Otof-C₂A to liposomes with different lipid compositions was tested in floatation assays. Otof-C₂A did not bind to the liposomes under any tested condition.

To test whether the presence of the five mentioned aspartates in a C₂-domain are sufficient for Ca²⁺-binding or Ca²⁺-dependent phospholipid-binding, the mutant Otof-5D-C₂A was created. Four amino acids were replaced by aspartates at the positions where they were missing in the WT protein. In all biochemical experiments performed, the mutant behaved like the WT protein. Probably the shortage of top loop one prohibits Ca²⁺-binding for Otof-C₂A, as the binding “pocket” is incomplete. Together, Otof-C₂A shows the structure of a typical C₂-domain, but does not bind Ca²⁺ or phospholipids. Its function has yet to be revealed.

We aimed to express and purify the other single, tandem- or triple-Otof-C₂-domains as well as full length protein. However, this was not achieved as they were insoluble or aggregated. These problems could not be overcome by more alternative constructs with differing amino acid lengths and different affinity tags, or changing the expression system or the buffers used in purifications, so that no biochemical or structural data could be collected for them.

It will be a challenging task in the future to clarify the exact function and incorporation of otoferlin in the pre-synaptic machinery.

7. References

- Adams, P.D., Afonine, P.V., Bunkóczi, G., Chen, V.B., Davis, I.W., Echols, N., Headd, J.J., Hung, L.-W., Kapral, G.-J., Grosse-Kunstleve R.W., McCoy, A.J., Moriarty, N.W., Oeffner, R., Read, R.J., Richardson, D.C., Richardson, J.S., Terwilliger T.C., Zwart, P.H (2010) a comprehensive Python-based system for macromolecular structure solution. *Acta Crystallogr. D* **66**, 213-221.
- Altschul, S.F., Gish, W., Miller, W., Myers, E.W., Lipman, D.J. (1990) Basic local alignment search tool. *J Mol Biol.* **215**(3), 403-410.
- Ashery, U., Varoqueaux, F., Voets, T., Betz, A., Thakur, P., Koch, H., Neher, E., Brose, N., Rettig, J. (2000) Munc13-1 acts as a priming factor for large dense-core vesicles in bovine chromaffin cells. *EMBO J.* **19**(14), 3586-3596.
- Augustin, I., Rosenmund, C., Südhof, T.C., Brose, N. (1999) Munc13-1 is essential for fusion competence of glutamatergic synaptic vesicles. *Nature* **400**, 457-461.
- Bernatchez, P.N., Sharma, A., Kodaman, P., Sessa, W.C. (2009) Myoferlin is critical for endocytosis in endothelial cells. *Am J Physiol Cell Physiol.* **297**(3), C484-92.
- Berndt, A., Miller, S., Williams, O., Le, D. D., Houseman, B. T., Pacold, J. I., Gorrec, F., Hon, W. C., Liu, Y., Rommel, C., Gaillard, P., Ruckle, T., Schwarz, M. K., Shokat, K. M., Shaw, J. P., and Williams, R. L. (2010) The p110 delta structure: mechanisms for selectivity and potency of new PI(3)K inhibitors. *Nat Chem Biol* **6**, 117-124.
- Bertani, G. (1951) Studies on lysogenesis. I. The mode of phage liberation by lysogenic *Escherichia coli*. *J Bacteriol.* **62**(3), 293-300.
- Beurg, M., Safieddine, S., Roux, I., Bouleau, Y., Petit, C., Dulon, D. (2008) Calcium- and Otoferlin-Dependent Exocytosis by Immature Outer Hair Cells. *J Neurosci.* **28**(8), 1798-1803.
- Böhm, G., Muhr, R., Jaenicke, R. (1992) Quantitative analysis of protein far UV circular dichroism spectra by neural networks. *Protein Eng.* **5**, 191-195.

• References •

- Bragg, W.L. (1913) The Diffraction of Short Electromagnetic Waves by a Crystal. *Proc Cambridge Phil Soc.* **17**, 43-57.
- Brugge, J.F., Howard, M.A. (2002) Hearing. *Encyclopedia of the Human Brain* **2**, 429-448.
- Cho, W., Stahelin, R. V. (2006) Membrane binding and subcellular targeting of C2 domains. *Biochim Biophys Acta* **1761**(8), 838-849.
- Choi, B.Y., Ahmed, Z.M., Riazuddin, S., Bhinder, M.A., Shahzad, M., Husnain, T., Riazuddin, S., Griffith, A.J., Friedman, T.B. (2009) Identities and frequencies of mutations of the otoferlin gene (OTOF) causing DFNB9 deafness in Pakistan. *Clin Genet.* **75**(3), 237-243.
- Corbalán-García, S., Sánchez-Carrillo, S., García-García, J., Gómez-Fernández, J.C. (2003) Characterization of the Membrane Binding Mode of the C2 Domain of PKC ϵ . *Biochemistry* **42**, 11661-11668.
- Dai, H., Shin, O. H., Machius, M., Tomchick, D. R., Sudhof, T. C., and Rizo, J. (2004) Structural basis for the evolutionary inactivation of Ca²⁺ binding to synaptotagmin 4. *Nat Struct Mol Biol.* **11**, 844-849.
- Davis, D.B., Doherty, K.R., Delmonte, A.J., McNally, E.M. (2002) Calcium-sensitive phospholipid binding properties of normal and mutant ferlin C2 domains. *J Biol Chem.* **277**(25), 22883-22888.
- Davis, D.B., Delmonte, A.J., Ly, T.L., McNally, E.M. (2000) Myoferlin, a candidate gene and potential modifier of muscular dystrophy. *Hum Mol Genet.* **9**(2), 217-226.
- DeLano, W.L. The PyMOL Molecular Graphics System, Version 1.2r3pre, Schrödinger, LLC. www.pymol.org.
- Demonbreun, A.R., Lapidos, K.A., Heretis, K., Levin, S., Dale, R., Pytel, P., Svensson, E.C., McNally, E.M. (2010) Myoferlin regulation by NFAT in muscle injury, regeneration and repair. *J Cell Sci.* **123**(14), 2413-2422.
- Doherty K.R., Cave A., Davis D.B., Delmonte A.J., Posey A., Earley J.U., Hadhazy M., McNally E.M. (2005) Normal myoblast fusion requires myoferlin. *Development* **132**(24), 5565-5575.
- Dulon, D., Safieddine, S., Jones, S.M., Petit, C. (2009) Otoferlin is critical for a highly sensitive and linear calcium-dependent exocytosis at vestibular hair cell ribbon synapses. *J Neurosci.* **29**(34), 10474-10487.

• References •

- Emsley, P., Lohkamp, B., Scott, W.G., Cowtan, K. (2010) Features and development of Coot. *Acta Crystallogr D Biol Crystallogr.* 66(4), 486-501.
- Essen, L. O., Perisic, O., Lynch, D. E., Katan, M., and Williams, R. L. (1997) A ternary metal binding site in the C2 domain of phosphoinositide-specific phospholipase C-delta1. *Biochemistry* 36, 2753-2762.
- Eybalin, M., Renard, N., Aure, F., Safieddine, S. (2002) Cysteine-string protein in inner hair cells of the organ of Corti: synaptic expression and upregulation at the onset of hearing. *Eur J Neurosci.* 15, 1409-1420.
- Fettiplace, R., Hackney, C.M. (2006) The sensory and motor roles of auditory hair cells. *Nat Rev Neurosci.* 7(1), 19-29.
- Forge, A., Becker, D., Casalotti, S., Edwards, J., Marziano, N. and Nevill, G. (2003) Gap junctions in the inner ear: comparison of distribution patterns in different vertebrates and assessment of composition in mammals. *J Comp Neurol.* 8, 467-531.
- Fukuda, M., Aruga, J., Niinobe, M., Aimoto, S. Mikoshiba, K. (1994) Inositol-1,3,4,5-tetrakisphosphate binding to C2B domain of IP4BP/synaptotagmin II, *J Biol Chem.* 269, 29206–29211.
- Gaffaney, J.D., Dunning, F.M., Wang, Z., Hui, E., Chapman, E.R. (2008) Synaptotagmin C2B Domain Regulates Ca²⁺-triggered Fusion *in Vitro*. *J Biol Chem.* 283(46), 31763–31775.
- Greenfield, N.J. (2006) Using circular dichroism spectra to estimate protein secondary structure. *Nat Protoc.* 1(6), 2876-2890.
- Heidrych, P., Zimmermann, U., Bress, A., Pusch, C.M., Ruth, P., Pfister, M., Knipper, M., Blin, N. (2008) Rab8b GTPase, a protein transport regulator, is an interacting partner of otoferlin, defective in a human autosomal recessive deafness form. *Hum Mol Genet.* 17(23), 3814-3821.
- Heidrych, P., Zimmermann, U., Kuhn, S., Franz, C., Engel, J., v. Duncker, S., Hirt, B., Pusch, C.M., Ruth, P., Pfister, M., Marcotti, W., Blin, N., Knipper, M. (2009) Otoferlin interacts with myosin VI: implications for maintenance of the basolateral synaptic structure of the inner hair cell. *Hum Mol Genet.* 18(15), 2779-2790.

• References •

- Helfmann, S., Lü, W., Litz, C., Andrade, S.L. (2010) Cooperative binding of MgATP and MgADP in the trimeric P(II) protein GlnK2 from *Archaeoglobus fulgidus*. *J Mol Biol.* **402**(1), 165-177.
- Helfmann, S., Neumann, P., Tittmann, K., Moser, T., Ficner, R., Reisinger, E. (2011) The crystal structure of the C₂A domain of otoferlin reveals an unconventional top loop region. *J Mol Biol.* **406**(3), 479-490.
- Hicks, S. N., Jezyk, M. R., Gershburg, S., Seifert, J. P., Harden, T. K., and Sondek, J. (2008) General and versatile autoinhibition of PLC isozymes. *Mol Cell.* **31**, 383-394.
- Holm, L., Park, J. (2000) DaliLite workbench for protein structure comparison. *Bioinformatics*, **16**(6), 566-567.
- Hutchinson, E.G., Thornton, J.M. (1996) PROMOTIF--a program to identify and analyze structural motifs in proteins. *Protein Sci.* **5**(2), 212-220.
- Jiménez, J. L., and Bashir, R. (2007) In silico functional and structural characterisation of ferlin proteins by mapping disease-causing mutations and evolutionary information onto three-dimensional models of their C2 domains. *J Neurol Sci.* **260**, 114-123.
- Johnson, C. P., Chapman, E. R. (2010) Otoferlin is a calcium sensor that directly regulates SNARE-mediated membrane fusion. *J Cell Biol.* **191**, 187-197.
- Kabsch, W. (2010) XDS. *Acta Cryst. D.* **66**, 125-132.
- Kelley, L.A., Sternberg, M.J.E. (2009) Protein structure prediction on the web: a case study using the Phyre server. *Nat Protoc.* **4**, 363 - 371.
- Khimich, D., Nouvian, R., Pujol, R., Tom Dieck, S., Egner, A., Gundelfinger, E.D., Moser, T. (2005) Hair cell synaptic ribbons are essential for synchronous auditory signalling. *Nature* **434**(7035), 889-894.
- Lee, J.O., Yang, H., Georgescu, M.M., Di, Cristofano A., Maehama, T., Shi, Y., Dixon, J.E., Pandolfi, P., Pavletich, N.P. (1999) Crystal structure of the PTEN tumor suppressor: implications for its phosphoinositide phosphatase activity and membrane association. *Cell* **99**(3), 323-334.
- Littler, D. R., Walker, J. R., She, Y. M., Finerty, P. J., Jr., Newman, E. M., and Dhe-Paganon, S. (2006) Structure of human protein kinase C ϵ (PKC ϵ) C2 domain and identification of phosphorylation sites. *Biochem Biophys Res Commun.* **349**, 1182-1189.

• References •

- López-Bigas, N., Arabonés, M.L., Estivill, X. and Simonneau C. (2002) Expression profiles of the connexin genes, Gjb1 and Gjb3, in the developing mouse cochlea. *Mech Dev.* **119**, 111-115.
- Lu, J., Machius, M., Dulubova, I., Dai, H., Sudhof, T. C., Tomchick, D. R., Rizo, J. (2006) Structural basis for a Munc13-1 homodimer to Munc13-1/RIM heterodimer switch. *PLoS Biol.* **4**(7), e192.
- Magupalli, V. G., Schwarz, K., Alpadi, K., Natarajan, S., Seigel, G. M., Schmitz, F. (2008) Multiple RIBEYE–RIBEYE Interactions Create a Dynamic Scaffold for the Formation of Synaptic Ribbons. *J Neurosci.* **28**(32), 7954-7967.
- Marlin, S., Feldmann, D., Nguyen, Y., Rouillon, I., Loundon, N., Jonard, L., Bonnet, C., Couderc, R., Garabedian, E.N., Petit, C., Denoyelle, F. (2010) Temperature-sensitive auditory neuropathy associated with an otoferlin mutation: Deafening fever! *Biochem Biophys Res Commun.* **394**(3), 737-742.
- Matsunaga, T. (2009) Value of Genetic Testing in the Otological Approach for Sensorineural Hearing Loss. *Keio J Med.* **58**(4), 216-222.
- McCoy, A.J., Grosse-Kunstleve, R.W., Adams, P.D., Winn, M.D., Storoni, L.C., Read, R.J. (2007) *Phaser* crystallographic software. *J Appl Cryst.* **40**, 658-674.
- Morton, N.E. (1991) Genetic Epidemiology of Hearing Impairment. *Ann N Y Acad Sci.* **630**, 16-31.
- Mukherjee, M., Phadke, S.R., Mittal, B. (2003) Connexin 26 and autosomal recessive non-syndromic hearing loss. *Indian J Hum Genet.* **9**(2), 40-50.
- Murshudov, G.N., Vagin, A.A., Dodson, E.J. (1997) Refinement of Macromolecular Structures by the Maximum-Likelihood method. *Acta Crystallogr. D* **35**, 240-255.
- Nalefski, E. A., Falke, J.J. (1996) The C2 domain calcium-binding motif: Structural and functional diversity. *Protein Sci.* **5**(12), 2375-2390.
- Nagashima, T., Hayashi, F., Yokoyama, S. (2006) Solution structure of the first C2 domain of human myoferlin. Deposition as 2DMH at www.pdb.org.
- Nouvian, R., Neef, J., Bulankina, A.V., Reisinger, E., Pangrsic, T., Frank, T., Sikorra, S., Brose, N., Binz, T., Moser, T. (2011) Exocytosis at the hair

• References •

- cell ribbon synapse apparently operates without neuronal SNARE proteins. *Nat Neurosci.* **14**(4), 411-413.
- Ochoa, W. F., Garcia-Garcia, J., Fita, I., Corbalan-Garcia, S., Verdaguer, N., Gomez-Fernandez, J. C. (2001) Structure of the C2 domain from novel protein kinase C[epsilon]. A membrane binding model for Ca²⁺-independent C2 domains. *J Mol Biol.* **311**, 837–849.
- Pangrsic, T., Lasarow, L., Reuter, K., Takago, H., Schwander, M., Riedel, D., Frank, T., Tarantino, L.M., Bailey, J.S., Strenzke, N., Brose, N., Müller, U., Reisinger, E., Moser, T. (2010) Hearing requires otoferlin-dependent efficient replenishment of synaptic vesicles in hair cells. *Nat Neurosci.* **13**(7), 869-876.
- Perisic, O., Fong, S., Lynch, D. E., Bycroft, M., Williams, R. L. (1998) Crystal structure of a calcium–phospholipid binding domain from cytosolic phospholipase A2. *J Biol Chem.* **273**, 1596–1604.
- Petit, C., Levilliers, J., Hardelin, J.P. (2001) Molecular genetics of hearing loss. *Annu Rev Genet.* **35**, 589-646.
- Ramakrishnan, N.A., Drescher, M.J., Drescher, D.G. (2009) Direct Interaction of Otoferlin with Syntaxin 1A, SNAP-25, and the L-type Voltage-gated Calcium Channel Ca_v1.3. *J Biol Chem.* **284**(3), 1364-1372.
- Robertson, N.D., Morton, C.C. (1999) Beginning of a molecular era in hearing and deafness. *Clin Genet.* **55**, 149-159.
- Rodríguez-Ballesteros, M., Reynoso, R., Olarte, M., Villamar, M., Morera, C., Santarelli, R., Arslan, E., Medá, C., Curet, C., Völter, C., Sainz-Quevedo, M., Castorina, P., Ambrosetti, U., Berrettini, S., Frei, K., Tedín, S., Smith, J., Tapia, M. C., Cavallé, L., Gelvez, N., Primignani, P., Gómez-Rosas, E., Martín, M., Moreno-Pelayo, M. A., Tamayo, M., Moreno-Barral, J., Moreno, F., Castillo, I. d. (2008). A multicenter study on the prevalence and spectrum of mutations in the otoferlin gene (OTOF) in subjects with nonsyndromic hearing impairment and auditory neuropathy. *Hum Mutat.* **29**, 823-831.
- Roux, I., Safieddine, S., Nouvian, R., Grati, M. h., Simmler, M.-C., Bahloul, A., Perfettini, I., Le Gall, M., Rostaing, P., Hamard, G., Triller, A., Avan, P., Moser, T. and Petit, C. (2006) *Cell* **127**, 277-289.

• References •

- Roux, I., Hosie, S., Johnson, S.L., Bahloul, A., Cayet, N., Nouaille, S., Kros, C.J., Petit, C., Safieddine, S. (2009) Myosin VI is required for the proper maturation and function of inner hair cell ribbon synapses. *Hum Mol Genet.* **18**(23), 4615-4628.
- Safieddine, S., Wenthold, R.J (1999) SNARE complex at the ribbon synapses of cochlear hair cells: analysis of synaptic vesicle- and synaptic membrane-associated proteins. *Eur J Neurosci.* **11**, 803-812.
- Sambrook, J., Fritsch, E.F., Maniatis, T. (1989) *Molecular Cloning: A Laboratory Manual*, 2nd Edition. Cold Spring Harbor Laboratory Press, Cold Spring Harbor, New York.
- Schiavo, G., Gu, Q.M., Prestwich, G.D., Sollner, T.H., Rothman, J.E. (1996) Calcium-dependent switching of the specificity of phosphoinositide binding to synaptotagmin. *Proc Natl Acad Sci U. S. A.* **93**, 13327–13332.
- Schug, N., Braig, C., Zimmermann, U., Engel, J., Winter, H., Ruth, P., Blin, N., Pfister, M., Kalbacher, H., Knipper, M. (2006) Differential expression of otoferlin in brain, vestibular system, immature and mature cochlea of the rat. *Eur J Neurosci.* **24**(12), 3372-3380.
- Schwander, M., Sczaniecka, A., Grillet, N., Bailey, J.S., Avenarius, M., Najmabadi, H., Steffy, B.M., Federe, G.C., Lagler, E.A., Banan, R., Hice, R., Grabowski-Boase, L., Keithley, E.M., Ryan, A.F., Housley, G.D., Wiltshire, T., Smith, R.J., Tarantino, L.M., Müller, U. (2007) A forward genetics screen in mice identifies recessive deafness traits and reveals that pejvakin is essential for outer hair cell function. *J Neurosci.* **27**(9), 2163-2175.
- Schwarzenbacher, R., Godzik, A., Grzechnik, S.K., Jaroszewski, L. (2004) The importance of alignment accuracy for molecular replacement. *Acta Cryst.* **D60**, 1229-1236.
- Shao, X., Fernandez, I., Sudhof, T. C., Rizo, J. (1998) Solution structures of the Ca²⁺-free and Ca²⁺-bound C2A domain of synaptotagmin I: does Ca²⁺ induce a conformational change? *Biochemistry* **37**, 16106–16115.
- Shin, O. H., Lu, J., Rhee, J. S., Tomchick, D. R., Pang, Z. P., Wojcik, S. M. et al. (2010) Munc13 C(2)B domain is an activity-dependent Ca²⁺ regulator of synaptic exocytosis. *Nat Struct Mol Biol.* **17**, 280–288.

• References •

- Sossin, W.S., Schwartz, J.H. (1993) Ca²⁺-independent protein kinase Cs contain an amino-terminal domain similar to the C2 consensus sequence. *Trends Biochem Sci.* **18**(6), 207-208.
- Stein, N. (2008) CHAINSAW: a program for mutating pdb files used as templates in molecular replacement. *J Appl Cryst.* **41**, 641-643.
- Sterling, P., Matthews, G. (2005) Structure and function of ribbon synapses. *Trends Neurosci.* **28**(1), 20-29.
- Studier, F.W. (2005) Protein production by auto-induction in high-density shaking cultures. *Protein Expr Purif.* **41**(1), 207-234.
- Sutton, R. B., Davletov, B. A., Berghuis, A. M., Sudhof, T. C., and Sprang, S. R. (1995) Structure of the first C2 domain of synaptotagmin I: a novel Ca²⁺/phospholipid-binding fold. *Cell* **80**, 929-938.
- Tomchick, D.R., Rizo, J., Machius, M., Lu, J. (2010) Munc13 C2B domain is an activity-dependent Ca²⁺ regulator of synaptic exocytosis. *Nat Struct Mol Biol.* **17**, 280-288.
- Ubach, J., Lao, Y., Fernandez, I., Arac, D., Südhof, T.C., Rizo, J. (2001) The C2B domain of synaptotagmin I is a Ca²⁺-binding module. *Biochemistry* **40**(20), 5854-5860.
- Varga, R., Avenarius, M.R., Kelley, P.M., Keats, B.J., Berlin, J.I., Hood, L.J., Morlet, T.G., Brashears, S.M., Starr, A., Cohn, E.S. Smith, R.J.H., Kimberling W.J. (2006) OTOF mutations revealed by genetic analysis of hearing loss families including a potential temperature sensitive auditory neuropathy allele. *J Med Genet.* **43**, 576-581.
- Verdaguer, N., Corbalan-Garcia, S., Ochoa, W. F., Fita, I., Gomez-Fernandez, J. C. (1999) Ca²⁺ bridges the C2 membrane-binding domain of protein kinase Ca directly to phosphatidylserine. *EMBO J.* **18**, 6329–6338.
- VP-ITC MicroCalorimeter User's Manual. MicroCal, LLC.; Northampton, MA.
- Wang, D.Y., Wang, Y.C., Weil, D., Zhao, Y.L., Rao, S.Q., Zong, L., Ji, Y.B., Liu, Q., Li, J.Q., Yang, H.M., Shen, Y., Benedict-Alderfer, C., Zheng, Q.Y., Petit, C., Wang, Q.J. (2010) Screening mutations of OTOF gene in Chinese patients with auditory neuropathy, including a familial case of temperature-sensitive auditory neuropathy. *BMC Med Genet.* **11**(79).

• References •

- Wiesner, S., Ogunjimi, A. A., Wang, H. R., Rotin, D., Sicheri, F., Wrana, J. L., and Forman-Kay, J. D. (2007) Autoinhibition of the HECT-type ubiquitin ligase Smurf2 through its C2 domain. *Cell* **130**, 651-662.
- Yasunaga, S., Grati, M., Cohen-Salmon, M., El-Amraoui, A., Mustapha, M., Salem, N., El-Zir, E., Loiselet, J., Petit, C. (1999) A mutation in OTOF, encoding otoferlin, a FER-1-like protein, causes DFNB9, a nonsyndromic form of deafness. *Nat Genet.* **21**(4), 363-369.
- Yasunaga, S. i., Grati, M. h., Chardenoux, S., Smith, T. N., Friedman, T. B., Lalwani, A. K., Wilcox, E. R., Petit, C. (2000). OTOF Encodes Multiple Long and Short Isoforms: Genetic Evidence That the Long Ones Underlie Recessive Deafness DFNB9. *Am J Hum Genet.* **67**, 591-600.

Acknowledgements

Here I would like to thank all the people that supported me in different ways during my PhD time and thus contributed to the successful completion of this thesis.

First I would like to cordially thank Prof. Dr. Tobias Moser for giving me the opportunity to participate in inner ear research and to do my PhD thesis in his laboratories, for constant theoretical and financial support during my work and for writing the expert's report about my thesis. I also thank him for his personal support for my future career.

I warmly thank Dr. Ellen Reisinger for supervision in practical and theoretical experimental work, many fruitful discussions and for intensive care about our joint research paper.

I cordially thank the members of my Thesis Committee (Prof. Dr. Tobias Moser, Prof. Dr. Ralf Ficner, Prof. Dr. Nils Brose) for their constant contributions to improve my protocols and data.

Moreover, I sincerely thank Prof. Dr. Ralf Ficner for providing working space for me in his laboratories in the first time of my thesis. I also thank him for the possibility to use the X-ray diffractometers in the department to analyze protein crystals and for his support and participation in the Otof-C₂A project leading to in our joint research paper. I thank him for writing an expert's report about my thesis.

I would like to cordially thank Prof. Dr. Nils Brose for his permission to perform molecular cloning in his laboratories and for advice/help for solving protein purification problems.

Special thanks go to Dr. Piotr Neumann for solving the mystery of the problematic first crystal. I thank him for helping me solving and improving the structure of otoferlin-C₂A as well as for proof-reading the crystallography-part in my thesis.

• Acknowledgements •

I would like to thank Dr. Achim Dickmanns for advice and help for solving protein purification problems.

I thank Prof. Dr. Kai Tittmann for providing equipment and support in circular dichroism (CD) spectroscopy and for his help with data analysis. In Prof. Tittmann's group, I would also like to thank Dr. Danilo Meyer for his help and discussions about CD-spectroscopy experiments.

Thanks also go to Dr. Dirk Fasshauer and Prof. Dr. Reinhard Jahn for their collaboration concerning the accomplishment of floatation assays in their laboratories. For direct supervision with these experiments I would like to thank Dr. Alexander Stein and Dr. Geert van den Bogaart.

I thank Nina Dankenbrink-Werder and Astrid Zeuch for doing the molecular clonings of His₆-Otof-C₂A and seven GST-Otof-C₂F-constructs.

I would like to thank Anand Radhakrishnan for his contributions in a very early phase of this study, where he purified the Otof-C₂A once and did one ITC on it.

I would like to thank Kirsten Reuter for subcloning four of the five C₂-domains to pGEX-6P-3-vector and for preparing and testing other constructs

I very much thank my colleagues in the InnerEarLab for the very comfortable working climate in the lab, for helpfulness and for their interest in my project. Special thanks go to K. R. for her friendship.

I would like to cordially thank my family for their interest in my research and for their support in every circumstance. Special thanks go to A. S. for SDS-gel-photography, love, support and patience.

Curriculum Vitae

Personal data

Name: Sarah Alexandra Helfmann
Address: Kaakweg 1b, 37077 Goettingen
Date of birth: 07.04.1982
Place of birth: Munich, Germany



Scientific career

Since 03/2008 PhD-student
Laboratory: InnenOhrLabor, Department of
Otorhinolaryngology, University clinical center
Goettingen
Administration: Prof. Dr. Tobias Moser
Title: „Structure and function of Otoferlin C₂-domains“
Graduation 07/2011

05/2007-07/2007 Student assistant
Institute for Microbiology and Genetics, Department
for Molecular Structural Biology, University of
Goettingen

10/2003-12/2003 Student assistant
J.-F. Blumenbach Institute for Zoology und
Anthropology, Department for Neurobiology,
University of Goettingen

University education

Since 04/2011 Human medicine, University of Goettingen

• Curriculum Vitae •

- 08/2006-04/2007 Diploma thesis
Laboratory: Department for Molecular Structural Biology, Institute for Microbiology und Genetics, University of Goettingen
Administration: Prof. Dr. Oliver Einsle
Title: „Function of P_{II}-proteins in Ammonium-Transport of *Archaeoglobus fulgidus*“
- 10/2002-05/2007 Biology (Diploma), University of Goettingen
Degree: Diploma (major subject: Biochemistry, minor subjects: Human genetics and Chemistry); Grade 1.1
- 10/2002-12/2007 Biology and Chemistry (teaching post), University of Goettingen
Degree: First state examination; Grade 1.3

Peer reviewed papers

- **Helfmann, S.**, Lü, W., Litz, C., Andrade, S. L. A. (2010) Cooperative Binding of MgATP and MgADP in the Trimeric P(II) Protein GlnK2 from *Archaeoglobus fulgidus*. *J Mol Biol.* 402(1), 165–177.
- **Helfmann, S.**, Neumann, P., Tittmann, K., Moser, T., Ficner, R., Reisinger, E. (2010) The crystal structure of the C₂A domain of otoferlin reveals an unconventional top loop region. *J Mol Biol.* **406**(3), 479-490.
- Litz, C., **Helfmann, S.**, Gerhardt, S., Andrade, S. L. A. (2010) Structure of GlnK1, a signalling protein from *Archaeoglobus fulgidus*. *Acta Crystallogr Sect F Struct Biol Cryst Commun.* **67**(2), 178-181.

Contributions to conferences

- **Helfmann, S.**, Kirscht, A., Einsle, O., Andrade, S. L. A. (2007) Characterization of GlnK-2 from *Archaeoglobus fulgidus*. Posterpresentation VAAM-Jahrestagung, Osnabrueck, 2007.
- **Helfmann, S.**, Neumann, P., Fasshauer, D., Dickmanns, A., Brose, N., Moser, T., Ficner, R., Reisinger, E. (2009) Structure of the otoferlin C2A domain of *Rattus norvegicus*. Posterpresentation Inner Ear Biology Workshop, Utrecht, 2009.
- Reuter, K., **Helfmann, S.**, Neumann, P., Schwander, M., Fasshauer, D., Brose, N., Jahn, R., Müller, U., Tittmann, K., Ficner, R., Moser, T., Reisinger, E. (2010) Structure of Otoferlin C₂A and Biochemical Analysis of Otoferlin C₂ Domains. Posterpresentation Midwinter Meeting of the Association for Research in Otolaryngology (ARO), 2010.

Göttingen, 19.05.2011